Revista
Portuguesa
de Química

1

**SOCIEDADE
PORTUGUESA
DE QUÍMICA**

DIRECTOR E COORDENADOR DA COMISSÃO EDITORIAL
DIRECTOR AND THE EDITORIAL BOARD COORDINATOR

Fernando Pina
Dep. de Química
Faculdade de Ciências
e Tecnologia
Universidade Nova de Lisboa
2825 Monte da Caparica

COMISSÃO EDITORIAL
EDITORIAL BOARD
Ana Lobo
Dep. de Química
Faculdade de Ciências
e Tecnologia
Universidade Nova de Lisboa
2825 Monte da Caparica

Carlos Crispim Romão
Inst. de Tecnologia
Química e Biológica
Rua da Quinta Grande, 6
Apartado 127, 2780 Oeiras

Carlos F. G. C. Geraldes
Dep. de Bioquímica
Faculdade de Ciências
e Tecnologia
Universidade de Coimbra
3000 Coimbra

Fernanda Madalena A. Costa
Dep. Química
Faculdade de Ciências
Universidade de Lisboa
Rua Ernesto de Vasconcelos,
Bloco 1
1700 Lisboa

Hugh Burrows
Dep. Química
Faculdade de Ciências e
Tecnologia
Universidade de Coimbra
3000 Coimbra

Irene Montenegro
Centro de Química Pura e
Aplicada
Universidade do Minho
Largo do Paço
4700 Braga

José Costa Lima
Dep. Química-Física
Faculdade de Farmácia
Universidade do Porto
Rua Aníbal Cabral, 164
4000 Porto

José Luís Figueiredo
Dep. de Engenharia Química
Faculdade de Engenharia
do Porto
Rua dos Bragas
4099 Porto Codex

José Ferreira Gomes
Dep. de Química
Faculdade de Ciências
Universidade do Porto
4000 Porto

José M. Gaspar Martinho
Dep. Engenharia Química
Instituto Superior Técnico
1096 Lisboa Codex

Lélio Lobo
Dep. de Engenharia Química
Faculdade de Ciências e
Tecnologia
Universidade de Coimbra
3000 Coimbra

Revista Portuguesa de Química

Instruções para os Autores
Instructions for Authors

Tendo em vista um aumento significativo do alcance e impacto da *Rev. Port. Quím.*, os artigos são obrigatoriamente escritos e publicados em inglês, não excedendo as 20-30 páginas dactilografadas (formato A4 a dois espaços, margens de 2,5 cm), incluindo todas as tabelas, esquemas e figuras. As referências e notas *mencionadas no texto do manuscrito* serão ordenadas e numeradas entre parêntesis rectos. No final do manuscrito, antes das tabelas e figuras, essas referências e notas aparecerão numeradas sem parêntesis.

Exemplos:

1. P.R. Kemper, J. Bushnell, von G. Helden, M.T. Bowers, *J. Phys. Chem.* **97** (1993) 52.

2. J.P. Colloman, L.S. Hegedus, J.R. Norton, R.G. Finke, *Principles and Applications of Organotransition Metal Chemistry;* University Science Books: Mill Valey, 1987; pp. 279-354.

3. P.B. Armentrout, in *Gas Phase Inorganic Chemistry;* D.H. Russel, Ed.; Plenum Press: New Tork, 1989; pp 1-42.

As figuras e tabelas aparecerão numeradas em árabe e agrupadas no fim do manuscrito, após as referências e em folhas separadas. As tabelas só deverão ser utilizadas quando representarem uma vantagem para a exposição do texto ou quando não possam ser substituídas por gráficos ou figuras. As figuras devem ser enviadas com grande qualidade gráfica.

No caso de existir mais do que um Autor, deverá ser assinalado com um asterisco (*) o nome daquele a quem toda a correspondência ou comentários deverão ser enviados. Os manuscritos devem ser enviados em **triplicado** ao *Editor da Revista Portuguesa de Química, Sociedade Portuguesa de Química, Av. da República, 37, 4º, 1050 Lisboa, Portugal.*

Do Projecto de Estatuto Editorial da *Revista Portuguesa de Química*

Pretende a Revista Portuguesa de Química (Rev. Port. Quím.) publicar os resultados originais da investigação em Química na forma de revisões críticas concisas e que reflictam a actividade científica levada a cabo por investigadores ou pelas suas equipas.

Os artigos serão predominantemente solicitados através de um **convite** da responsabilidade do *Editor da Rev. Port. Quím.*, e poderão incidir sobre qualquer das áreas e disciplinas da Química, perspectivando a contribuição dos autores no quadro mais geral do seu desenvolvimento internacional e interdisciplinar e referenciando as opiniões e os autores mais relevantes, constantes na literatura.

Pretende-se que pelo seu conteúdo e formato se possa estabelecer um compromisso entre o interesse de uma audiência geral, mas atenta, e uma audiência especialmente ligada ao campo de investigação do(s) Autor(es). A concisão dos artigos submetidos, bem como o esforço de uma boa definição dos conceitos, referência e enquadramento crítico da investigação levada a cabo em torno dos temas propostos da Comissão Editorial ou de avaliadores por ela seleccionados. A inclusão de resultados não publicados deverá ser feita de uma forma moderada e quando significativamente necessária. Pelo contrário, as conclusões finais devem reforçar e perspectivar o significado dos resultados obtidos mais importantes. A submissão de artigos à *Rev. Port. Quím.* implica que o mesmo trabalho não seja ou tenha sido submetido outro Jornal ou Revista.

A Comissão Editorial é nomeada, por um período de três anos, pela Direcção da Sociedade Portuguesa de Química e tem a responsabilidade por todas as decisões editoriais. **A Sociedade Portuguesa de Química** e a **Comissão Editorial** da **Rev. Port. Quím.** não assume, no entanto, qualquer responsabilidade pelas afirmações e opiniões expressas pelos autores dos artigos publicados. Os comentários ou outros textos da responsabilidade dos membros da Comissão Editorial não envolvem a Sociedade ou a própria *Rev. Port. Quím.*

Insulin-Mimetic Vanadium Complexes[†]

Complexos de Vanádio Miméticos da Insulina

KATHERINE H. THOMPSON, JOHN H. MCNEILL AND CHRIS ORVIG*

MEDICINAL INORGANIC CHEMISTRY GROUP, DEPARTMENT OF CHEMISTRY AND FACULTY OF PHARMACEUTICAL SCIENCES,
UNIVERSITY OF BRITISH COLUMBIA,VANCOUVER, BC, V6T 1Z1, CANADA
[†] BASED ON A PLENARY LECTURE DELIVERED BY C.O. AT THE XV ENCONTRO NACIONAL DA SOCIEDADE PORTUGUESA DE QUÍMICA, 22-25 MAY 1996; PORTO, PORTUGAL.

Synthetic design of effective biological mimics requires consideration of thermodynamic and hydrolytic stability, kinetics of complexation/decomplexation, hydrophobic/lipophilic balance, and cell membrane permeability. In the field of medicinal inorganic chemistry, recently developed chelated vanadium complexes illustrate these design principles. In this review, studies undertaken to characterize synthetic inorganic mimics of the hormone, insuline are described in detail. Development and testing of one candidate compound, bis(maltolato)oxovanadium(IV) (BMOV), shows how the requesite biological properties for an orally available insulin mimic were included in its chemical synthesis and design.

No pleaneamento da síntese de compostos bio-miméticos, há vários factores a considerar com vista à sua eficiência, nomeadamente os respeitantes à estabilidade termodinâmica e hidrolítica, à cinética de complexaçãop/descomplexação, ao balanço hidrofóbico/lipofílico e à permeabilidade da membrana celular. Estes princípios são bem evidenciados, no domínio da química inorgânica aplicada à medicina, pelos recém-desenvolvidos complexos de quelatos de vanádio. No presente artigo de revisão são detalhadamente descritos estudos de caracterização de compostos inorgânicos bio-miméticos da hormona insulina. O desenvolvimento e os ensaios levados a cabo com um composto candidato, bis(maltolato) de oxovanádio(IV) (BMOV), vem demonstrar como as propriedades biológicas que são requeridas a um composto bio-mimético de insulina a ser administrado por via oral, podem ser tomadas em conta no processo de síntese química do mesmo.

Medicinal inorganic chemistry has an ancient history but only a very modern science. Inorganic drugs can be categorized into two areas: diagnostic and therapeutic drugs. Two examples of diagnostic drugs incorporating metals are: the ^{99m}Tc, ^{67}Ga, or ^{111}In radiopharmaceuticals, which incorporate radioactive metal nuclei; and the magnetic resonance imaging contrast agents, which utilize the characteristic paramagnetic shift of water molecules bound to a paramagnetic metal ion (*e.g.*, Gd, Dy). For both classes of compounds, a chelating ligand is required to help direct the complex to a site of activity. Therapeutic radiopharmaceuticals can take advantage of the characteristic emission of an α- or β-emitting radionuclide incorporated into a metal complex, wherein a ligand is required to direct the metal complex to a specific site.

This paper focuses on chemotherapeutic metal complexes, those which take advantage of the characteristic chemistry of a particular metal ion (in this case, vanadium). There has been a lot of activity in recent years in the research and development of metal compounds as anti-tumor agents, anti-bacterial compounds, and anti-viral compounds, as well as for treatment of rheumatoid arthritis. Cisplatin (*cis*-diammi-nedichloroplatinum(II)), a therapeutic drug, has been used in the treatment of cancer for close to twenty years, particularly for testicular and ovarian cancers. (Cisplatin can also be considered a prototypical inorganic drug because it contains not one carbon atom, making it truly an inorganic compound!)

To design metal complexes which can be reliably transported to a biological area of interest, both the characteristics of the metal and of the ligand(s) in the metal complex must be considered. Many of the relevant metal ions; e.g., gadolinium, technetium, platinum or gold, are not essential metal ions and therefore there

is no biological mechanism by which these metal ions are actively transported. Since biology is not used to handling them, the biological system may just excrete the metal ions. In order to develop a system to transport a metal ion to its active site, one must consider the biological membrane, which protects the inner contents and the cytoplasm of the cell from the outer contents (water), and which is really a lipid bilayer. In the case of a biologically essential metal ion, there may be an active transport mechanism, such as the ATPase-dependent transport of sodium out of the cell against a gradient, or of potassium into the cell against a gradient. Besides active transport mechanisms, there may also be facilitated transport mechanisms, such as exist for Fe(III) and Cu(II). Various metal ions which are essential are transported by specific molecules. In the case of Fe(III), siderophores are responsible for transporting Fe into a cell (1). However, a lot of the metal ions do not have this kind of specific mechanism like the sodium-potassium ATPase or the siderophores for iron, therefore, a better, and/or simpler, system must be designed for metal complexes to get into the cell by a 'thief mechanism,' *i.e.,* to slip into the cell by passive diffusion. The characteristic properties of the metal complex will allow it to slip through the biological membrane to become available for intracellular processes. Whether the passive diffusion process involves a loss of ligands or binding to an active site is unknown, but from the point of view of complex design for passive diffusion, the ligands should not be too cumbersome or highly charged.

Some characteristic potential ligand properties for passive diffusion which should be considered in the compound design are as follows. First, metal complexes, where the ligand is bound to the metal, should have a high thermodynamic stability (not necessarily the highest) because the metal complex may stay together until it gets to an active site and then fall apart to deliver the metal, but it needs to be controlled to deliver the metal to the active site. A compound should have a very high thermodynamic stability if the metal complex itself has activity. Second, the metal ligand binding should be hydrolytically stable. The metals used in our research group (indium, gallium, aluminum, add; vanadium, lanthanides, technetium and rhenium) are all hydrolysis metals, which undergo hydrolysis, particularly in a biological system, if the metal ligand binding constants are not high enough (2). Third, the kinetics of complexation should be considered. If a chelating agent is developed to remove a metal or to deliver a metal to an active site, then the kinetics with which the metal ion undergoes ligation chemistry are going to be of primary importance. Fourth, the molecular weight of the metal complex is critical because passive diffusion, in many cases, requires metal complexes of a relatively low molecular weight. Hand-in-hand with this is the charge on the metal complex, in order to balance the lipophilicity or fatty-soluble nature of the complex with the

hydrophilicity or water-soluble nature of the complex, where the complexes are of neutral charge. Compounds of low molecular weight with neutral charge and some water solubility are soluble in almost any medium, and may slip through biological membranes by passive diffusion. Lastly, depending on the nature of the project, ligand functionalization should be considered. A biologically directing portion of the molecule such as a steroid, which can bind to tumors in breast cancer, may be used to functionalize the ligand in order to biologically direct the complex.

Over the years (since about the 1960's) a variety of *in vitro* studies have shown that vanadium has many different insulin-like actions (for review, see (3,4,5). Some examples, from a variety of isolated studies, include stimulated transport of hexose sugars in both rat fat cells and skeletal muscle cells, lipogenesis in rat fat cells, and glucose oxidation in muscle and fat cells. Most studies have used added vanadate (vanadium(V)), but some have also examined the effects of vanadyl (vanadium(IV)). These are all activities which are quite characteristic of insulin and suggested to one of us (J. H. McNeill) in the early 1980's that there should be closer specific examination of the insulin-like actions of vanadium, *in vivo* as well as *in vitro* (6).

Three classes of vanadium compounds have been studied for their insulin mimetic effect. These comprise 1) inorganic vanadate (VO_4^{3-}) and vanadyl (VO^{2+}), 2) combinations of vanadate and hydrogen peroxide, called peroxovanadates, and 3) chelated vanadyl complexes. It is interesting to note that in France, in 1899, oral sodium vanadate was reported to have an insulin-like effect in two of three diabetic patients, as shown by lower concentrations of glucose in their urine (7). However, the real pioneering work was done by McNeill and co-workers who showed, in the streptozotocin (STZ)-diabetic rat model, that sodium vanadate actually had insulin-like effects by lowering blood glucose without raising blood insulin levels (6). Posner *et al.* (another Canadian group, at McGill University in Montreal) have recently examined combinations of sodium vanadate and hydrogen peroxide, the peroxovanadates, and have shown that these also have a number of very potent insulin mimetic effects (8). The third category, the chelated vanadyl complexes, are a more recent development (9). In these three categories (the vanadates, the peroxovanadates and the vanadyl complexes) a whole variety of different compounds have been tried. McNeill *et al.* proposed a compound, Naglivan, which has a cysteine backbone with an octyl group attached (10). In addition, a variety of bis(ligand)vanadyl complexes have been reported by Sakurai and co-workers (11) and dihydroxamate vanadyl complexes have been developed by Shechter *et al.* (12). Yale *et al.* have prepared a number of discrete vanadium(V)peroxo compounds with one or two peroxides bound and one organic ligand, usually with a -1 or -2 charge (13).

The candidate list of properties identified above can be applied to the design and preparation of a simple compound: bis(maltolato)oxovanadium(IV), abbreviated BMOV.

BMOV, VO(ma)$_2$
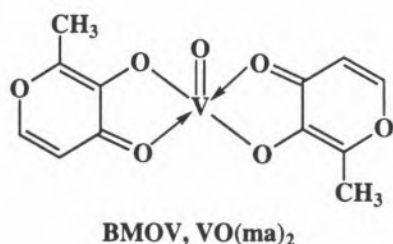
The development of this compound shows quite nicely how the biological properties that need to be incorporated into a complex were included in its chemical synthesis and design. The ligand is maltol, which is very attractive from two major standpoints. Maltol can be used to make neutral metal complexes with appropriate metal ions because it is a bidentate ligand with one ionizable proton. Neutral metal complexes, (for instance, with aluminum) can be made water soluble and neutrally charged with great oral bioavailability. This is presumably because of the ring oxygen. By changing the complex to a pyridinone (wherein a nitrogen replaces the ring O) the water solubility decreases. BMOV can be prepared on a large scale (up to 0.5 kg) simply by combining vanadyl sulphate with maltol at roughly neutral pH, to give a 95% yield, quite pure (14). Some properties of interest include its solubility in water and in organic solvents, and its low molecular weight. With a molecular weight of 317, BMOV is soluble (mM scale) in a fair number of organic solvents and water (15). It has one unpaired electron, characteristic of the vanadyl unit, and a fairly high V=O stretching frequency in the infrared spectrum (995 cm^{-1}), suggesting that there is no ligand (or a weakly bound solvent) in the sixth position. The crystal structure of the compound (Figure 1) shows that the two ligands are oriented trans to one another (15). The vanadium is out of the plane of the four chelating oxygens by about 0.70 Å and the V=O bond length is 1.61 Å (15).

The characterization was consistent with the theoretical structure of the compound, so the question then became did BMOV have the desired insulin mimetic properties? For this, an experimental model of diabetes in the rat was used. In this model, rats are given an injection of STZ, an antibiotic that specifically attacks the insulin secreting β-cells in the pancreas in a dose responsive fashion. This results in greatly reduced insulin secretory capacity of the rat pancreas and hence the development of diabetic characteristics (reduced insulin levels, elevated levels of glucose in blood and urine). A typical experiment examining insulin mimesis involved dividing the animals into four groups: i) control rats that are not diabetic and are not given the vanadium complex in drinking water; ii) control treated rats that are not diabetic but are given BMOV in the drinking water; iii) diabetic animals that are STZ-diabetic but are not given the metal complex and iv) diabetic treated rats that are given the metal complex in their drinking water. The dependent factor is the oral activity because insulin itself is not orally bioavailable and must be taken by injection.

Plasma glucose levels of about 5-7 mM for both the control animals and the control treated animals (5-7 millimolar is average for a rat, and also for a human) were significantly lower than those for the diabetic rats, whose plasma glucose levels were 2-3 times higher than the control levels (16). (Some variation is inherent in this model, because the more diabetic an animal becomes, the less it weighs). However, within one week following BMOV administration, the diabetic treated animals showed a dramatic drop in plasma glucose levels. The plasma glucose levels for the treated diabetic animals were higher than for the control rats, on average, but BMOV had a stark glucose-lowering effect. Data taken from the same animals over the same time period (~1/2 year study) showed that control animals had plasma insulin levels up to about 40 μU/ml in plasma (17). Both the diabetic and the diabetic treated animals had plasma insulin levels that were much lower. The fact that the diabetic, as well as the diabetic treated animals both had low levels demonstrated that, in the diabetic treated animals, production of insulin was not stimulated by the vanadium complex. Possibly, glucose was being handled by some mechanism other than insulin production. Surprisingly, the control treated animals had plasma insulin levels significantly lower than the control untreated animals. These were not diabetic
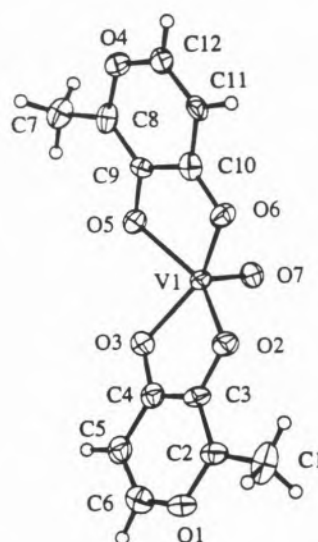

Figure 1 – ORTEP diagram of BMOV (VO(ma)$_2$)

animals but they were taking the vanadium complex in their drinking water. Since insulin is secreted in response to a glucose challenge, the vanadium complex was clearly acting as an insulin mimic. In both intraperitoneal (i.p.) and oral studies (18, 19), a titration of plasma glucose in STZ-diabetic rats *vs*. the dose of BMOV or vanadyl sulphate. showed that plasma glucose levels were lowered to <9 mM by a dose of BMOV that was approximately 2-3 times less than the dose required of vanadyl sulphate, allowing us to come to the conclusion that BMOV is 2-3 times more potent as an insulin mimic than is vanadyl sulphate.

Having established that BMOV is an oral insulin mimic (at least in STZ-diabetic rats) some characteristic chemistry of the metal ion was next elaborated. First, we determined that the stability constants for the binding of 1 and 2 maltols to vanadyl were relatively high; the stepwise constants were log K_1 = 8.80, and log K_2 = 7.51 respectively, to make the bis(ligand) complex, giving an overall log β_2 of 16.31- quite a stable complex. (At pH 2, the mono(ligand) complex is already forming - hence the necessity for spectrophotometric determination of the first stability constant (15)) At a pH of 7.4, (the pH in blood plasma) the complex is completely formed; however, one interesting question is raised by the speciation data. The stomach has a pH of 2-3, depending on its contents (20). At pH 2-3, most of the vanadium is in the form of a mono(ligand) complex and very little (~20%) is in the form of a bis-ligand complex.

Since at pH 2-3 the bis-ligand complex does not predominate, is it necessary to administer the intact complex to see glucose lowering? To answer this question, an experiment was done in STZ-diabetic rats using gavage administration of a single oral dose, followed by monitoring the plasma glucose as a function of time after administration. This is a fairly simple screen that is used to avoid the great expense involved in long term, chronic screens for different complexes. Eight different experiments in STZ-diabetic rats using a variety of combinations of vanadyl, maltol, complex or no complex were tried (15). Only three different groups of experiments showed plasma glucose lowering after administration of the one gavage dose of BMOV to the animals. All three involved intact BMOV being administered. Of these three, one was BMOV only, another was BMOV followed by maltol, the third was maltol followed by BMOV. Several of the other experiments involved administration of vanadyl followed by maltol, maltol followed by vanadyl, vanadyl alone, maltol alone, no vanadyl or maltol. In these cases there was no glucose lowering. It was only when the intact complex was administered that glucose lowering was seen, suggesting that even at pH 3, there was enough of the intact complex to achieve the desired biological activity (15).

A fundamental tenet of vanadium chemistry in aqueous solution is lower pH favours vanadyl (vanadium(IV)oxo, as in BMOV), whereas higher pH favours vanadate, vanadium(V) (21). Clearly redox chemistry between the vanadium(IV) and vanadium(V) oxidation states are going to be of fundamental importance in elucidating the mechanism of action of BMOV. It is known (21) that the standard reduction potential of vanadium(V) to vanadium(IV) falls dramatically as a function of pH. When a methanol/chloroform solution of BMOV is exposed to air, the 8 line pattern (I=7/2, V) falls off dramatically over a period of several days. It is fairly slow but an oxidation of BMOV to a vanadium(V) species does take place (22). In methanol, or in any alcoholic solvent, BMOV oxidizes to form a vanadium(V) alkoxobis(maltolato)oxo complex, VO(OR)(ma)$_2$ (Scheme 1) (22). The crystal structure (Figure 2) of the oxomethoxobis(maltolato) complex shows a six-coordinate vanadium(V) centre with two maltol ligands oriented in a cis fashion and V=O and VOMe in a cis fashion as well. It has a distorted octahedral geometry around the vanadium. The oxidation kinetics in methanol are a function of both complex and molecular oxygen concentrations (22). It is a straightforward reaction between BMOV and molecular oxygen in a 4 : 1 ratio to give the vanadium(V) species, consistent with the fact that BMOV undergoes a 1-electron oxidation and O$_2$ is a 4-electron oxidant. The observed rate constant is directly proportional to the molecular oxygen concentration, consistent with this stoichiometry and the overall rate at 25 °C. It is relatively slow, taking several days for the EPR spectrum to fall off: in the range 0.31 M^{-1} sec^{-1} at 25 °C (22).

In water a similar oxidation was observed, except the oxidation of BMOV is now to a cis-dioxo anion [VO$_2$(ma)$_2$]$^-$ and the observed rate constant for the oxidation has the characteristic S-shape one expects to see for a pH dependent oxidation (due to the fact that molecular oxygen interacts with a vanadium(IV)
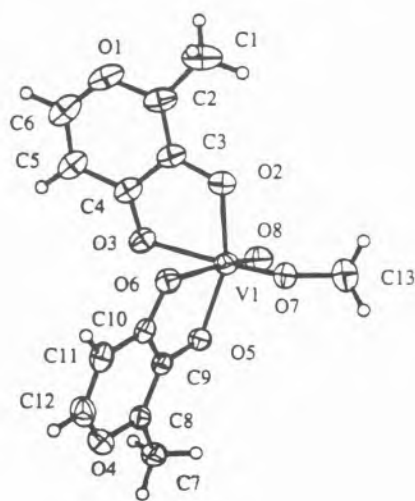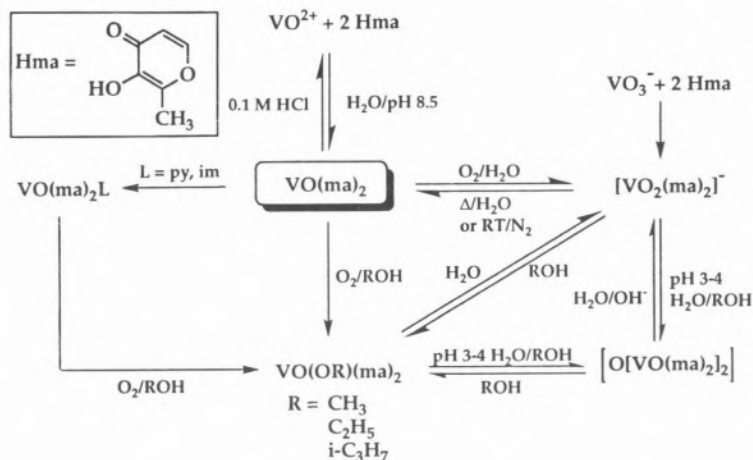

Figure 2 – ORTEP diagram of cis-[VO(OCH$_3$)(ma)$_2$]

Hma = [structure of 3-hydroxy-2-methyl-4-pyranone]

VO²⁺ + 2 Hma

0.1 M HCl | H₂O/pH 8.5

VO₃⁻ + 2 Hma

VO(ma)₂L ← L = py, im | VO(ma)₂ | O₂/H₂O → / Δ/H₂O or RT/N₂ ← | [VO₂(ma)₂]⁻

O₂/ROH | H₂O / ROH | H₂O/OH⁻ | pH 3-4 H₂O/ROH

VO(OR)(ma)₂
R = CH₃
C₂H₅
i-C₃H₇

O₂/ROH →

pH 3-4 H₂O/ROH / ROH → [O[VO(ma)₂]₂]

Scheme 1

bis(ligand)aquo species and a vanadium(IV) bis(ligand)hydroxo species) (22). The pKa for the bound water is 7.2, and this provides two pathways: an aquo pathway and a hydroxo pathway, both giving the cis-dioxo anion. The aquo pathway was considerably slower ($0.08 M^{-1}s^{-1}$ at 25 °C) than the hydroxo pathway ($0.39 M^{-1}s^{-1}$ at 25 °C) and both were relatively slow, appropriate to the situation in which experimental animals are drinking continually in a chronic (long-time) experiment. Since the solutions are changed every 48 hours there must be still a fair amount of vanadium(IV) complex available despite the oxidation.

The cis-dioxo anion was prepared separately from genuine vanadium(V) starting materials (e.g., ammonium metavanadate) and maltol, resulting in the formation of various salts of this dioxo anion, such as $NH_4[VO_2(ma)_2]$ (15). This reaction can also be used to make the potassium or sodium salts; both are easy to prepare in fairly high yield. The crystal structure (15) of the vanadium(V) complex, $K[VO_2(ma)_2] \cdot H_2O$, is a little more complicated than the other vanadium(V) and vanadium(IV) species (Figure 3) because the stoichiometry of one potassium cation to one vanadate anion to one water forms an infinite chain. The vanadium center is in the middle of a distorted octahedron. There are two maltolate ligands cis to one another; the two V=O are cis to one another and are bonded to potassium atoms.

We have studied the variable pH electrochemistry, comparing both BMOV, the genuine vanadium(IV) material, and the cis dioxoanion $[VO_2(ma)_2]^-$, the genuine vanadium(V) material (15). The variable pH electrochemistry indeed shows a genuine conversion between these two species, but it is only reversible at a pH of about 3 (15). There is a reversible cyclic voltammogram at a potential of about 0.45 volts vs. the Ag/AgCl electrode.

What about this oxidation? What about administering solutions to animals whose stomachs are at pH 3? In a series of experiments, the effect of administering a biologically compatible reductant, in this case ascorbate, with BMOV was investigated, to see if the presence of a reducing agent would increase glucose lowering or assist the glucose lowering by keeping more of the vanadium as vanadium(IV) (15). Comparing the administrations of ascorbate, BMOV plus ascorbic acid, and ascorbic acid plus BMOV, it was observed that after about 25 minutes the glucose lowering was not statistically different whether or not ascorbate was added to the BMOV. Thus, adding a biologically compatible reductant did not increase the glucose lowering of BMOV, suggesting again that even at the stomach pH of about 3, there is enough of the intact bis(ligand)vanadyl complex to provide the necessary glucose lowering (15).
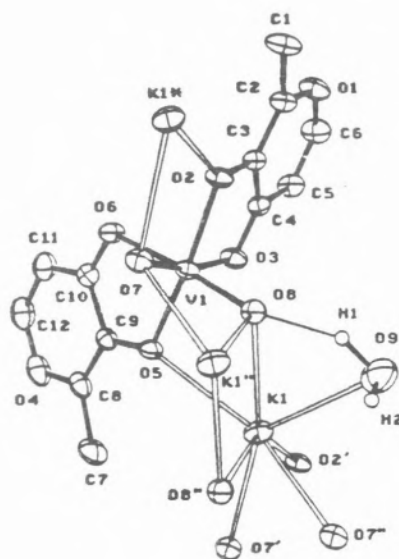
Figure 3 – ORTEP diagram of $K[VO_2(ma)_2] \cdot H_2O$

To summarize, we can prepare biologically relevant vanadium complexes from vanadyl or vanadate to give the vanadium(IV) or vanadium(V) materials (Scheme 1). The vanadium(IV) BMOV will undergo an O_2-dependent oxidation to vanadium(V) $[VO_2(ma)_2]^-$. Substitution reactions of BMOV showed that O_2 must bind for the oxidation to take place. With pyridine or imidazole in the sixth position on BMOV, the six-coordinate vanadium(IV) species undergoes oxidation in alcohols much more slowly than BMOV itself (Scheme 1). In addition to the methoxo species, ethoxo and isopropoxo vanadium(V) complexes can also be prepared, and all these alkoxo species undergo trans esterification reactions (Scheme 1). Dissolving the methoxo complex in ethanol results in formation of the ethoxo complex in 100% yield. Varying the pH conditions (very critically) yields a dimeric vanadium(V)monooxo-bridged analogue $[\mu\text{-}O\text{-}[VO(ma)_2]_2]$ in which there are two vanadium(V) centers bridged by one oxygen (Scheme 1); however, this is only isolable in the pH range 3 - 4 and only in a mixture of alcohols with water. An interesting observation is that $[VO_2(ma)_2]^-$ undergoes esterification to one of the vanadium(V) esters, $[VO(OR)(ma)_2]$, by dissolving in alcohol (ROH), and these revert to the cis-dioxo anion when dissolved in water. This chemistry is analogous to carbon, with carboxylates, esters and even acid anhydrides (23).

Where does the vanadium localize in the rat? The vanadium content of vanadium-treated STZ-diabetic and non-diabetic rats, has been determined by many groups by graphite furnace atomic absorption spectrophotometry (GFAAS) (24). Some were treated with vanadyl, some with vanadate, and some with BMOV. Several factors have become immediately obvious: first, the plasma levels are all between 10 and 15 μM, suggesting that this is the approximate range necessary for an insulin mimetic effect. Second, the biological 'sink' for vanadium is the bone. The highest levels for vanadium in any of these animals were in bone of animals treated with BMOV. Vanadium accumulation in the entire bone structure of the rat, based on a concentration of 26.4 $\mu g/g$ wet weight of tissue (17), is approximately 2 mg of elemental vanadium. Third, the kidney is clearly a target organ for supplemental vanadium. Accumulation in kidney seems appropriate since absorbed vanadium is excreted in the urine, via the kidneys (25). Elevated levels in the liver most likely reflect endogenous excretion of absorbed vanadium via the bile. (Of course this summary is incomplete, because, for instance, it does not take into account the duration of treatment.)

To gain a more accurate picture of vanadium's tissue distribution and curve of disappearance following an acute administration, a collaborative project was undertaken with Tom Ruth and Stephan Zeisler at TRIUMF on the UBC campus (26). A new preparation of ^{48}V was developed to investigate biolocalization of vanadium (27). ^{48}V has a 16 day half-life, and is a high energy gamma emitter with about 50% high energy

gamma and 50% positron emission. This is a very difficult isotope to work with because of its emission profile; however, we could successfully achieve the desired preparation by bombardment of titanium with protons, for a radiochemical yield of about 1 Ci mg^{-1}(26). This new synthesis was required since all the syntheses in the literature pertained to vanadyl chloride, but we needed vanadyl sulphate in order to compare vanadyl sulphate with BMOV, both administered orally. Experiments undertaken involved oral or intraperitoneal (i.p.) administration of ^{48}V in a carrier-added form. From these studies, the absorption of vanadium from an oral dose of ^{48}V-BMOV was determined to be almost twice as high as from ^{48}V-vanadyl sulphate; and bio-localization between the two compounds differed (27). Compartmental analysis of the results showed that the proportion of vanadium taken up by liver following BMOV treatment was almost 4 times higher than with $VOSO_4$ treatment, whereas that taken up by kidney was less than 50% higher, and that by bone (at 24 hours) was almost 3 times higher. The ratio of vanadium predicted by the model in bone:kidney:liver was 8:3:2 for BMOV and 6:4:1 for $VOSO_4$. The increase in uptake averaged over liver, kidney and bone was 2.7 times higher with BMOV compared with $VOSO_4$. Taking into account total tissue weight, the principal uptake of ^{48}V from an oral dose of BMOV vs. $VOSO_4$ was into bone (8.62% vs. 2.99% administered dose, AD), blood (3.55% vs. 2.73% AD), muscle (1.14% vs. 0.67% AD), liver (0.82% vs. 0.21% AD), and kidney (0.23% vs. 0.17% AD), based on model-predicted compartmental masses at 24 hours following gavage (27).

Overall, after 24 hours, giving the same dose of vanadium as BMOV results in about 2-3 times the amount of vanadium in the tissues as does vanadyl sulphate. This correlates well with previous evidence that BMOV was 2-3 times as effective in lowering blood glucose in vivo (16). These two results suggest that BMOV is 2-3 times as effective as vanadyl sulphate because of improved intestinal absorption and tissue uptake. Another kinetic parameter of interest, turnover times, also showed that BMOV differs substantially from $VOSO_4$. Turnover times for vanadium were shortest in blood, and the longest in bone, with intermediate times for liver, kidney and testes. Residence times in blood were 7 minutes for BMOV and 5 minutes for $VOSO_4$; in bone, residence times of 31 days for BMOV and 11 days for $VOSO_4$ were calculated from model simulations (27).

What are the logical next steps in the research? Of major importance is to learn more about the mechanism of action of this vanadium complex. The insulin receptor is a trans membrane protein (28) and the first step of insulin stimulated lipogenesis or glucose oxidation is insulin binding to the insulin receptor which changes its structure on the inside and starts autophosphorylating (29). Vanadium interferes with autophosphorylation reactions because vanadate is a very good phosphate analogue. Vanadate interacts with protein

tyrosine phosphorylation and dephosphorylation both inside and outside the nucleus, and thereby inhibits or stimulates a variety of intracellular signals (30). Unfortunately, in trying to deduce the mechanism of action, there are a whole variety of sites at which vanadium could interact. The intracellular environment is quite reducing and the consensus is that intracellular vanadium exists as vanadium(IV) and extracellular vanadium is vanadium(V). Recent evidence suggests that vanadyl may be acting to stimulate a cytosolic protein tyrosine kinase, distinct from the usual insulin receptor mechanism, and also unlike vanadate's mechanism of action (31).

We have looked at a number of other compounds, some of which are close analogues of BMOV. Kojic acid is commercially available, as is maltol. Instead of having a methyl group at the 2 position on the ring, kojic acid has a hydroxymethyl at the 5 position. We have prepared $VO(ka)_2$ (which is slightly less water soluble than BMOV) and have compared its biological activity with BMOV. BMOV, when administered orally or intraperitoneally, results in a better, sustained decline in plasma glucose *vs.* $VO(ka)_2$ (32). (Vanadyl sulphate and $[VO_2(ma)_2]^-$ were equally ineffective). In a chronic oral study (six weeks in duration), comparing BMOV and $VO(ka)_2$, BMOV lowered blood glucose into the normal (5-7mM) range within a couple of weeks of commencement, whereas $VO(ka)_2$ was considerably less effective (32).

VO(ka)₂
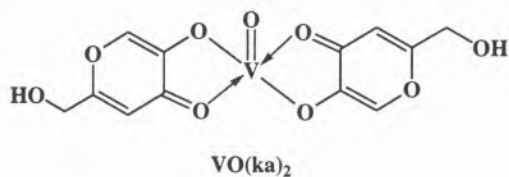
In conclusion, substantial evidence exists that the oral absorption of vanadium can be improved by selecting the right chelating ligand. In this case it is the maltolato ligand which aids the absorption of vanadium. The efficacy of the chelated vanadium compound is increased compared to the inorganic salt, $VOSO_4$. BMOV, bis(maltolato)oxovanadium(IV), is also very stable. We have taken a look at the reaction chemistry, which we have been able to elucidate over the years, and it does undergo aerobic oxidation; however, it is clear from combining the coordination chemistry studies and the biological studies that there is enough intact BMOV in the stomach even at pH 2 - 3 for sufficient activity. The vanadium(V) analogue, $[VO_2(ma)_2]^-$ has no effect. BMOV decreased insulin secretion in the control animals suggesting that there is an alternative mechanism for glucose lowering, and that, if not a substitute for insulin, BMOV may be a good adjuvant for insulin. What happens to BMOV post-absorption is still unknown; however, from the biodistribution study, the vanadium appears to be ultimately redistributed in a somewhat different pattern from that of vanadyl sulphate, with longer turnover times in a variety of organs. The vanadium which is administered as BMOV is redistributed (possibly via transferrin) but further experiments are required. Finally, BMOV clearly is a promising candidate for the oral treatment of diabetes.

References:

1. R. R. Crichton, R.J. Ward *Biochemistry* **31** (1992) 11255.

2. W. O. Nelson, T. B. Karpishin, S. J. Rettig, C. Orvig, *Inorg. Chem.* **27** (1988) 1045.

3. C. Orvig, K. H. Thompson, M. Battell, J. H. McNeill, *Metal Ions Biol. Syst.* **31** (1995) 575.

4. Y. Shechter, A. Shisheva, *Endeavour, New Series* **17** (1993) 27.

5. N. Sekar, J. Li, Y. Shechter, *Crit. Rev. Biochem. Mol. Biol.* **31** (1996) 339.

6. C. E. Heyliger, A. G. Tahiliani, J. H. McNeill, *Science* **227** (1985) 1474.

7. B. M. Lyonnet, E. Martz Martin, *La Presse Medicale* **7** (1899) 191.

8. B. I. Posner, R. Faure, J. W. Burgess, A. P. Bevan, D. Lachance, G. Zhang-Sun, I. G. Fantus, J. B. Ng, D. A. Hall, B. Soo Lum, A. Shaver, *J. Biol. Chem.* **269** (1994) 4596.

9. J. H. McNeill, V. G. Yuen, S. Dai, C. Orvig, *Mol. Cell. Biochem.* **153** (1995) 175.

10. M. C. Cam, G. H. Cros, J.-J. Serrano, R. Lazaro, J. H. McNeill, *Diabetes Res. Clin. Practice.* **20** (1993) 111.

11. H. Sakurai, K. Tsuchiya, M. Nukatsuka, J. Kawada, S. Ishikawa, H. Yoshida, M. Komatsu, *J. Clin. Biochem. Nutr.* **8** (1990) 193.

12. Y. Shechter, A. Shisheva, R. Lazar, J. Libman, A. Shanzer, *Biochemistry* **31** (1992) 2063.

13. J.-F. Yale, D. Lachance, A. P. Bevan, C. Vigeant, A. Shaver, B. I. Posner, *Diabetes* **44** (1995) 1274.

14. J. H. McNeill, V. G. Yuen, H. R. Hoveyda, C. Orvig, *J. Med. Chem* **35** (1992) 1489.

15. P. Caravan, L. Gelmini, N. Glover, F. G. Herring, H. Li, J. H. McNeill, S. J. Rettig, I. A. Setyawati, E. Shuter, Y. Sun, A. S. Tracey, V. G. Yuen, C. Orvig *J. Am. Chem. Soc.* **117** (1995) 12759.

16. V. G. Yuen, C. Orvig, J.H. McNeill, *Can. J. Physiol. Pharmacol.* **71** (1993) 263.

17. V. G. Yuen, C. Orvig, K.H. Thompson, J.H. McNeill, *Can. J. Physiol. Pharmacol.* **71** (1993) 270.

18. V. G. Yuen, C. Orvig, J.H. McNeill, *Can. J. Physiol. Pharmacol.* **73** (1995) 55.

19. V. G. Yuen, R.A. Pederson, S. Dai, C. Orvig, J.H. McNeill, *Can. J. Physiol. Pharmacol.* **74** (1996) 1001.

20. D. Waldron-Edward, in "Intestinal Absorption of Metal Ions, Trace Elements and Radionuclides," S. C. Skoryna, D. Waldron-Edward, eds., Pergamon Press, Toronto, 1971, p. 373.

21. A. Butler, in "Vanadium in Biological Systems," N. D. Chasteen, ed., Kluwer, Dordrecht:, 1990, p. 25.

22. Y. Sun, B. R. James, S. J. Rettig, C. Orvig, *Inorg. Chem.* **35** (1996) 1667.

23. A. Giacomelli, C. Floriani, A. O. d. S. Duarte, A. Chiesi-Villa, C. Guastini, *Inorg. Chem.* **21** (1982) 3310.

24. K. H. Thompson, M. Battell, J.H. McNeill, in "Vanadium in the Environment," Vol. I, J. O. Nriagu, ed., John Wiley & Sons, Ann Arbor, in press.

25. K. H. Thompson, J.H. McNeill, in "Trace Elements in Man and Animals -9: Proceedings of the Ninth International Symposium on Trace Elements in Man and Animals," P. W. F. Fischer, M.R. L'Abbe, K.A. Cockell, R.S. Gibson, eds., NRC Research Press, Ottawa, 1997, p. 349.

26. S. K. Zeisler, T. J. Ruth, *J. Radioanal. Nucl. Chem. Lett.* **200** (1995) 283.

27. I. A. Setyawati, K.H. Thompson, Y. Sun, D.M Lyster, C. Vo, V.G. Yuen, M. Battell, J.H. McNeill, T.J. Ruth, S. Zeisler, C. Orvig, *J. Appl. Physiol.* **84** (1998) 569.

28. G. E. Lienhard, J. W. Slot, D. E. James, M. M. Mueckler, *Sci. Amer.* **267** (1992) 86.

29. M.P. Czech *Ann. Rev. Physiol.* **47** (1985) 357.

30. Y. Shechter, J. Li, J. Meyerovitch, D. Gefel, R. Bruck, G. Elberg, D.S. Miller, A. Shisheva, *Mol. Cell. Biochem.* **153** (1995) 39.

31. J. Li, G. Elberg, D.C.Crans, Y. Shechter *Biochemistry* **35** (1996) 8314.

32. V. G. Yuen, P. Caravan, L. Gelmini, N. Glover, J.H. McNeill, I.A. Setyawati, E. Shuter, Y. Zhou, C. Orvig, *J. Inorg. Biochem.* **68** (1997) 109.

Chemical Reaction Engineering: views and opportunities

Engenharia da Reacção Química: perspectivas e oportunidades

ALÍRIO E. RODRIGUES

LABORATORY OF SEPARATION AND REACTION ENGINEERING, FACULTY OF ENGINEERING, UNIVERSITY OF PORTO – 4099 PORTO CODEX, PORTUGAL

This review addresses four topics. The first deals with the "particle-level problem" in reactor modelling. Transport processes and reaction in catalyst particles are analysed in some detail namely the importance of intraparticle convection in large-pore catalysts for isothermal and non-isothermal situations. The second topic discusses modelling of fixed-bed catalytic reactors with large-pore catalysts, which can be relevant in selective oxidations and steam-reforming processes. The third part illustrates our methodology for studying chemical reactors in various areas of CRE. Two experimental studies are presented: the Merox process for sweetening of gasoline and wastewater denitrification in a biofilm reactor. Finally we discuss the coupling of separation and reaction processes and in particular the case of simulated moving bed adsorptive reactors (SMBAR) for sucrose inversion and glucose/frutose separation.

Este artigo de revisão foca quatro temas. O primeiro tem a ver com o problema ao nível da partícula em reactores modelo. Os processos de transporte e reacção em partículas de catalizado são analisados com algum detalhe, nomeadamente é analisada a importância da convecção ultra-partículas em catalizadores de poros largos em situação isotérmica e não isotérmica.
O segundo tema refere-se à discussão da modelação de reactores catalíticos de leito fixo com catalizadores de poros largos, que podem ser relevantes em oxidações selectivas e processos de "steam-reforming".
A terceira parte ilustra a nossa metodologia para o estudo dos reactores químicos em várias áreas do "OCRE". São apresentados os dois estudos experimentais: os processos Merox para o "sweeting" da gasolina e a desnitração das águas de despejo num reactor de biofilme. Finalmente é discutido o acoplamento dos processos de separação e reacção e em particular o caso da simulação de reactores de absorção de leito móvel (SMBAR) para a inversão da sacarose e separação da glucose/frutose.

Introduction

Levenspiel says in the Third P.V.Danckwerts Memorial Lecture [1] that "the raison d'être of chemical engineering is to search for and the creation and development of new processes to make materials wanted by man". Chemical Reaction Engineering (CRE) has greatly contributed to that goal and, although "engineers know little about the roots of their profession" [2], one should mention two reference points in the history of CRE corresponding to different philosophies and approaches of CRE: 1947 - Hougen and Watson published "Chemical Process Principles, Part 3 - Kinetics and Catalysis" [3] and 1957 - First Symposium on CRE, Amsterdam [4] .

CRE is today a well recognized discipline. It builts a common structure of reaction systems, organizing knowledge in a systematized way. Nevertheless, the application of the strategy of CRE to a particular industrial process should be used with care since every process is unique [5, 6]. CRE methodology permeates through various areas of knowledge such as biochemical engineering, environmental engineering, fabrication of electronic devices, polymer engineering, hidrology, etc. This shows the strength of CRE and at the same time carries some danger, according to pessimistic views, of breakage of a well organized body of knowledge into pieces. Knowledge about reaction engineering was accumulated and refined based on work of many researchers [7] carried out in "laboratories in the cellars where kinetic results were said to be catalysed by cigarette smoke" [8] or in sophisticated laboratories with computer-controlled experiments (we are not following here Danckwerts' comment "Computers, those killers of creative thinking, had not been developed at that time"[8] although one should try to extract a positive message from such point of view).

The particle-level problem

The analysis of transport and reaction in catalyst pellets usually considers diffusion as the only mechanism for mass transfer inside particles. However, in some cases large-pore catalysts are used (e.g., selective oxidations) and then intraparticle convection should be taken into consideration. The importance of intraparticle convection on the catalyst effectiveness factor has been discussed by Nir and Pismen [9] for isothermal catalysts and first order irreversible reactions. The analysis was later extended to the case of sequential reactions by Nir [10], Cresswell [11] and Rodrigues *et al.* [12] to zero-order reactions. However, the problem was tackled many years ago by Hawtin and Murdoch [13] in an experimental paper related with the air oxidation of large tubes of graphite.

Isothermal catalysts. Let me review the main result obtained by Nir and Pismen for isothermal catalysts. Model equations in dimensionless form are shown in Table I for a slab catalyst of thickness 2 ℓ where f=c/c$_s$ and x=z/2 ℓ are the reduced fluid phase concentration inside the catalyst pores and the reduced space coordinate, respectively.

Table I - Diffusion, reaction and convection in isothermal catalysts (slab geometry; first order irreversible reaction)

Model Equations

Steady-state mass balance for reactant species:

$$\frac{d^2f}{dx^2} - 2\lambda_m \frac{df}{dx} - 4\phi_s^2 f = 0$$

Boundary conditions:

x=0 , f=1 and x=1 , f=1

Model Parameters:

$\phi_s = \ell \sqrt{k(T_s)/D_e}$	Thiele modulus
$\lambda_m = v_o \ell /D_e$	Mass intraparticle Peclet number

The effectiveness factor of the catalyst is defined as the ratio between observed reaction rate and reaction rate at surface conditions, i.e., $\eta_{dc} = <\Re(c)>/ \Re(c_s)$ and so:

$$\eta_{dc} = [1/r_1 - 1/r_2]/[\coth r_1 - \coth r_2]$$

where $r_1, r_2 = [\lambda_m \pm \sqrt{\lambda_m^2 + 4\phi_s^2}]/2$. In the limiting case of no convection ($\lambda_m = 0$) we recover the effectiveness factor of slab catlalyst for the reaction/diffusion problem,i.e., $\eta_d = [\tanh \phi_s]/\phi_s$. Figure 1 shows the effectiveness factor η_{dc} as a function of the Thiele modulus ϕ_s and the mass intraparticle Peclet number λ_m. The message which comes out from the theoretical analysis is that in the intermediate regime there is an enhancement of the catalyst effectiveness due to intraparticle convection.
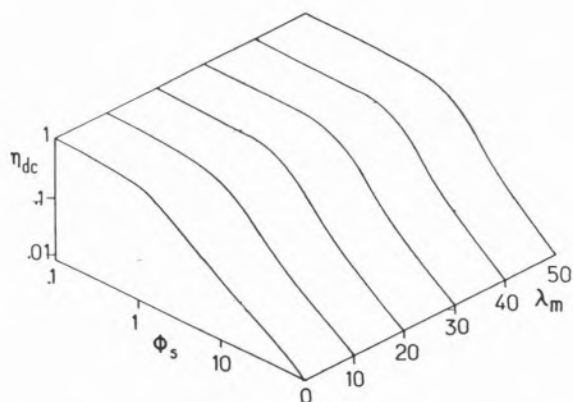

Figure 1 – Effectiveness factor of a slab isothermal catalyst for first order reaction, diffusion and convection, η_{dc} as a function of Thiele modulus, ϕ_s for various values of mass intraparticle Peclet numbers, λ_m.

Measurement of effective diffusivity using passive tracers. There are other aspects to be looked at when dealing with intraparticle convection in large-pore supports. One is related with the measurement of effective diffusivities by using chromatographic techniques. Experiments are usually carried out in fixed-beds, either "wide-body" or "single pellet string reactor" (SPSR) [14]. A pulse of tracer is injected and the concentration signal measured at two different points in the system. The effective diffusivity is obtained via a system model. I became interested in this problem when analyzing some results obtained by Ahn [15] at the Université de Technologie de Compiègne. He found that the "apparent" effective diffusivity increases with flowrate. The experimental conditions used are reported in Table II and results are shown in Figure 2 . It happens that I had read the paper by Nir and Pismen so I suggested that intraparticle convection could be a possible explanation of those results [16].
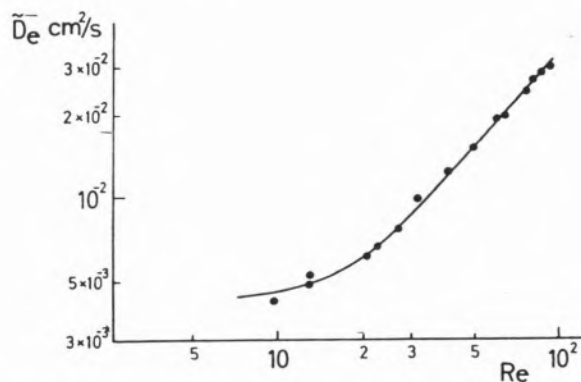

Figure 2 – Apparent effective diffusivity, $\tilde{D}_e$ as a function of Reynolds number , *Re*.

Table II - Experimental conditions used by Ahn [15] for the measurement of effective diffusivities by chromatographic technique

Reactor:

Length	$L=30$ cm	
Diameter	$d_t=2.12$ cm	
Porosity	$\varepsilon=0.676$	

Tracer : Hydrogen

Carrier gas : air

Temperature : 293 K

Catalyst:

Rhone Poulenc BM329 (vanadium and phosphorus oxides stabilized by copper for partial oxidation of butene to maleic anhydride).

Particle diameter	$d_p=0.45$ cm
Solid density	$\rho_s=2.84$ g/cm^3
Apparent density	$\rho_a=1.31$ g/cm^3
Specific surface area	$S_{BET}=4.3$ m^2/g
Pore volume	$V_{pore}=0.41$ cm^3/g
Particle porosity	$\varepsilon_p=0.537$
Pore diameter	$d_{pore}=10^4$ Å

The analysis of chromatographic experiments carried out with inert, passive or nonadsorbable, nonreactive tracers with a model which includes only an "apparent" effective diffusivity $\tilde{D}_e$ (which in fact disguises diffusion and convection), leads to an "apparent" effective diffusivity which changes with flowrate. In fact, $\tilde{D}_e$ is related with the "true" effective diffusivity D_e (which comes out from a model which includes both diffusion and convection of the tracer inside pores) by the relationship: $\tilde{D}_e = D_e/f(\lambda_m)$ where $f(\lambda_m) =(3/\lambda_m)$ [$1/\tanh \lambda_m -1/\lambda_m$]. This result can be obtained by just considering particle models regardless the type of equipment used [17]. At low flowrates and so low λ_m we have $\tilde{D}_e =D_e$; at high flowrates (high λ_m), $\tilde{D}_e =D_e \lambda_m /3=v_o \ell /3$ and convection dominates. The consequences of using $\tilde{D}_e$ instead of D_e on reactor design can be now easily understood. In summary: for a passive tracer $\tilde{D}_e/D_e=1/f(\lambda_m)$. This result is the key to understand Perfusion Chromatography, a process patented by PerSeptive Biosystems [18] for the separation of proteins using permeable particles [19] and illustrates cross fertilization between Reaction and Separation Engineering.

A difficulty still remains regarding the estimation of the intraparticle convective velocity v_o used for the calculation of the parameter λ_m. The simplest way is to write the equality of pressure drop across the particle and along the bed, *i.e.*, $\Delta p/2\ell = \Delta P/L$; using Ergun's equation for the bed pressure drop, $\Delta P/L=au_o+bu_o^2$ and Darcy's law for the pressure drop across the particle, i.e., $\Delta p/2\ell = \mu v_o/B$ where B is the permeability of the catalyst we get v_o as a function of the superficial velocity in the bed u_o. Figure 2 compares model and experimental results. Similar observations were made by Cheng [20, 21] working with α-alumina particles.

Reactive tracer. When the tracer is <u>reactive</u>, following first order reaction, model equivalence between steady-state models including "apparent" diffusivity and reaction (Model I) and "true" diffusivity, convection and reaction (Model II), leads to $\tilde{\eta}_d = \eta_{dc}$ or

$$\frac{\tanh \tilde{\phi}_s}{\phi_s} = \sqrt{\lambda_m^2+4\phi_s^2} \ \{\cosh\sqrt{\lambda_m^2+4\phi_s^2} - \cosh\lambda_m\}/2\phi_s^2$$
$$\sinh \sqrt{\lambda_m^2+4\phi_s^2}$$

Figure 3 shows $D_e/\tilde{D}_e = \tilde{\phi}_s^2/\phi_s^2$ as a function of ϕ_s and λ_m. The situation is now more complex. The interesting point is that in the case of absence of reaction, i. e., $\phi_s \rightarrow$ 0 we obtain the result already known for inert tracers. In fact an asymptotic development of both sides of the previous equation leads to $\tilde{\eta}_d \approx 1- \frac{\phi_s^2}{3}$ and $\eta_{dc} \approx 1 \frac{\phi_s^2}{\lambda_m}$ [$1/\tanh \lambda_m -1/\lambda_m$] and thus from $\tilde{\eta}_d = \eta_{dc}$ we get $D_e/\tilde{D}_e = f(\lambda_m)$.

Nonisothermal catalysts. Let us now look at the effect of intraparticle convection on the effectiveness factor of <u>non-isothermal catalysts.</u> The classical approach involving mass diffusion, heat conduction and reaction finds its roots on the work of Damkohler [22]. He looked at the steady-state equality between heat generated by reaction and heat removed by conduction arriving at the Damkohler equation $T-T_s= [(-\Delta H)D_e/\lambda_e] (c_s-c)$. The maximum temperature inside the pellet is $T_{max}=T_s(1 + \beta)$ where $\beta=(-\Delta H)D_e c_s/\lambda_e T_s$ is the Prater thermicity factor.

When convection is included such simple analysis is not so easy since it requires the use of numerical methods for solving the model equations shown in Table III. For gas/solid catalytic reactions we expect $\beta = 10^{-5}-10^{-1}$, $\gamma_s =5-30$ and $\lambda_h/\lambda_m=10^{-3} - 10^{-1}$.
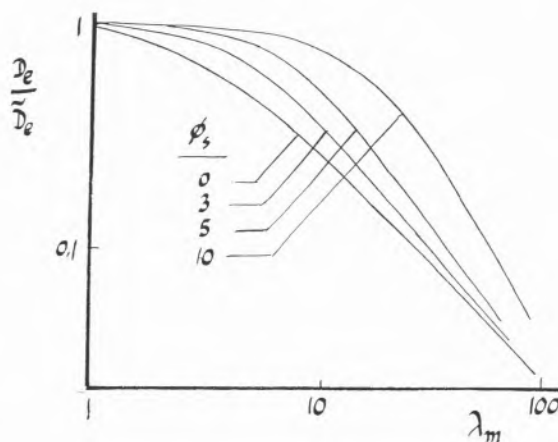

Figure 3 – $\dfrac{D_e}{\tilde{D}_e}$ as a function of mass intraparticle Peclet numbers, λ_m f for various values of Thiele modulus, ϕ_s for reactive tracers.

Table III -Diffusion/Conduction,Convection and Reaction in Nonisothermal Catalysts (slab geometry, first order exothermic reaction)

Model Equations

Steady-state mass balance for reactant species:

$$\frac{d^2f}{dx^2} - 2\lambda_m \frac{df}{dx} - 4\phi_s^2 \exp[-\gamma_s(1/T^*-1)]\, f = 0$$

Energy balance

$$\frac{d^2T^*}{dx^2} - 2\lambda_h \frac{dT^*}{dx} - 4\phi_s^2 \beta \exp[-\gamma_s(1/T^*-1)]\, f = 0$$

Boundary conditions:

x=0 , f=l ,T*=l

x=2 , f=l , T*=l

Model parameters are: Thiele modulus, $\phi_s = \sqrt{k(T_s)/D_e}$; mass intraparticle Peclet number, $\lambda_m = v_o\ell/D_e$; Arrhenius number, $\gamma_s = E/RT_s$; Prater thermicity factor $\beta = (-\Delta H)D_e c_s/\lambda_e T_s$; and Heat intraparticle Peclet number $\lambda_h = v_o\ell/[\lambda_e/\rho_f c_{pf}]$. The numerical solution of model equations enables us to calculate concentration and temperature profiles inside the catalyst, which are now asymetric, as well as catalyst effectiveness factors (Figure 4) and the maximum temperature inside the catalyst [17, 23-25]. Some refinements are still open concerning: i) the stability analysis for the convection /diffusion/reaction problem; ii) "complete" solution of the nonisothermal problem including the momentum equation [26]; iii) measurement of permeabilities of catalysts; and iv) extension to membrane-type reactors.
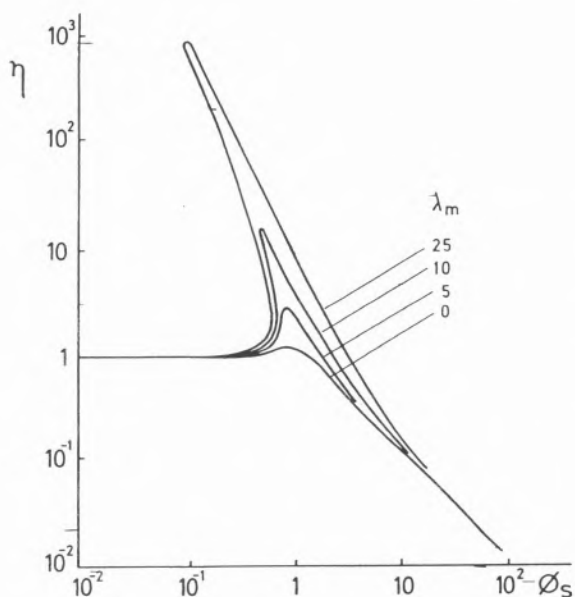

Figure 4 – Effectiveness factor of a nonisothermal catalyst. Effect of λ_m.

Fixed-bed catalytic reactors with large-pore catalysts

The effect of intraparticle convection on the fixed-bed behavior was studied both for steady-state and transient regimes.The reaction chosen was the oxidation of o-xylene to produce phthalic anhydride. Three models were compared: pseudohomogeneous (PH), heterogeneous diffusion (HT_d) and heterogeneous diffusion/ convection model (HT_{dc}).

The first goal was to construct runaway diagrams by using these models. Using the "maxima curve" method, it is interesting to notice that two maxima appear in the curve of the partial pressure of solute in the bulk p_b as a function of the bulk temperature T_b for the hot spot conditions when the HT_{dc} model is used (Figure 5); this is not the case when dealing with pseudohomogeneous or HT_d models. Alternatively we looked at the method of isoclines although the generalized sensitivity functions [27] seems to be the most convenient. The runaway diagram is displayed in Figure 6.
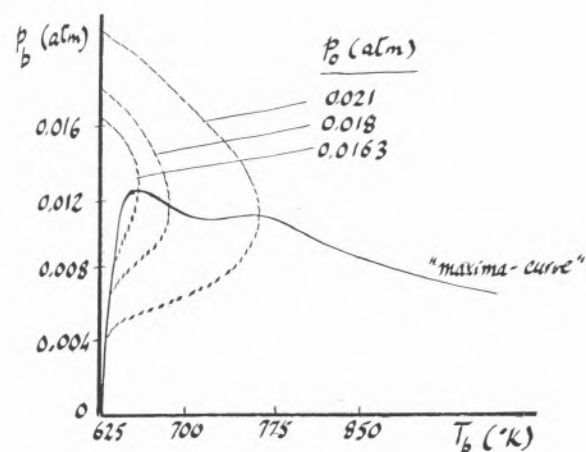
Figure 5 – "Maxima-curve" for HT_{dc} model.

Several comments should be made: i) in the low temperature region there is a difference between the PH model and HT models due to the inclusion of film resistances in HT models; ii) above 600 K the PH leads to more conservative results (lower region of stable operation; iii) predictions by the HT_{dc} model are those of the HT_d model in the limits of low temperature and high temperature; iv) in the intermediate region the stable region is lower for thr HT_{dc} model.

The transient behavior (response of a clean bed to a step function in concentration at the inlet) for HT_{dc} model was also addressed [28]. The temperature wave travels much faster than the concentration wave. Until the normalized time t*=1 the bed is about the feed temperature whilst the steep concentration profiles

Figure 6 – Runaway diagram for the selective oxidation of o-xylene: PH, HT_d and HT_{dc} models.

Figure 7 – Bed-to-wall heat transfer coefficient, h_w as a function of d_t/d_p for various Reynolds number, Re_p.

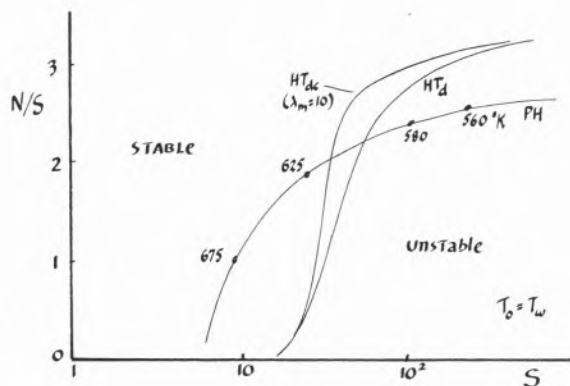travel along the bed. This part of the numerical solution is the one which takes the big share of the total computing time; however, it is just a short real time compared with the time needed to reach the final steady-state (t*=2500). At time t*=1 the concentration profile corresponds to the isothermal situation (the bed is at T_o). The idea coming to mind is to say that the initial condition is that corresponding to the "isothermal" profile of concentration; this strategy reduces the computing time. Moreover, this is most appropriate for control purposes. All this work needed numerical methods such as collocation on finite elements or moving finite element method [29].

Comments on model parameters. Some considerations about modeling should be made. The first is about model parameters. Ideally we would like to have independent measurements of all parameters! We have already seen how sophisticated can be the analysis of a chromatographic experiment to get the effective diffusivity. Other parameters are often estimated from correlations. How reliable are they? Heat transfer coefficients, film mass transfer coefficients, etc. are obtained from a given set of experiments but are model dependent.

Let us look at experiments done in a fixed bed heat exchanger of α-alumina particles (d_p=3.1 cm) through which air at ambient temperature is flowing. Bed wall is heated at constant temperature. Temperature measurements are made at various axial and radial positions in the bed [30]. Now we are going to analyse the results with the unidimensional pseudohomogeneous model so we will get a bed-to-wall heat transfer coefficient h_w= $Gc_{pf}(d_t/4z)$ $\ln[(T_w-T_o)/(T_w-T_z)]$ where T_z is the average temperature over the cross section at the axial position z. If we plot h_w as a function of d_t/d_p at different particle Reynolds numbers Re_p (Figure 7) we find a maximum in the curves around the ratio $d_t/d_p \approx 5$ to 6! This is about the value used in multitubular reactors. This maximum was also found by Wellauer *et al.*[31].
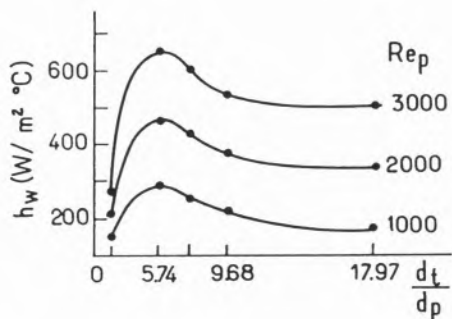
If we analyse the same results with the bidimensional pseudohomogeneous model described by the model equations presented below:

$$Gc_p \frac{\partial T}{\partial z} = k_{er} \left(\frac{\partial^2 T}{\partial r^2} + \frac{1}{r} \frac{\partial T}{\partial r} \right)$$

$$z=z_o, 0 < r < R \qquad T(z_0,r) = T_0(r),$$

$$z > z_o, r=0 \qquad \frac{\partial T}{\partial r} = 0,$$

$$r=R \qquad k_{er} \frac{\partial T}{\partial r} = \alpha_w (T_w-T_o)$$

we have now two parameters: the radial bed thermal conductivity k_{er} and the fluid-to-wall heat transfer coefficient α_w. Model equivalence will suggest that $\frac{1}{h_w} = \frac{1}{\alpha_w} + \frac{dt}{4k_{er}}$

Now let's look at some data (Figures 8 a,b). All profiles were considered simultaneously for a given Reynolds number in view of the estimation technique. We finally got for d_t/d_p=17.47 the correlations α_w (W/m^2.C)=α_w^0 + a Re_p with a=0.438 and α_w^0=7.153 and k_{er} (W/m.C) =k_{er}^0 + b Re_p with b=2.413x10^{-3} and k_{er}^0=0.139. When collecting and using heat transfer correlations, one should know in which models they were based. Only a few authors looked at angular variations of temperature at a given z and r (Cresswell [32]). This fact explains why we can only get heat transfer coefficients with 30% confidence range. Nevertheless, the angular-smoothed radial temperature profiles look nice. I am convinced that detailed analysis of this question should be done before we start the discussion on "heat transfer coefficients changing under reaction conditions ".

As far as film mass transfer coefficients are concerned it has been recognized that surface roughness affects film mass transfer. Van Vliet and Young [33]
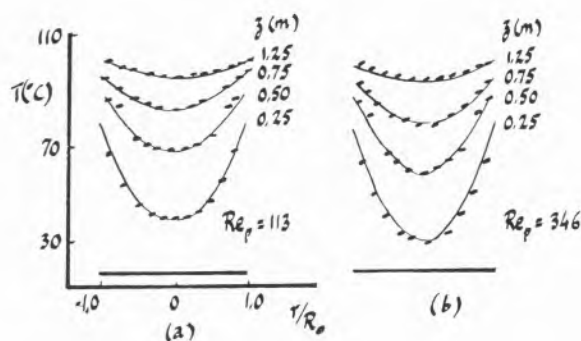
Figure 8 – Radial temperature profiles at various bed axial positions.
a) $Re_p = 113$; b) $Re_p = 346$
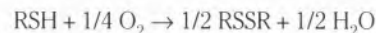(ooo experimental; - - - bidimensional model).

suggest that the fractal dimension of the rough profile is the parameter required to characterize rough surfaces. They looked at smooth particles (polymeric adsorbents; fractal dimension D=1.1) and rough particles (activated carbon; D=1.35). The message to be retained is that film mass transfer coefficients in rough surfaces can be one order of magnitude higher than those for smooth surfaces.

Some final comments should be made at this point: i) development on modeling and simulation of catalytic reactors depends strongly on progress on numerical techniques and computers (Sargent [34]); ii) there is a conflict between sophisticated or detailed models used for learning and control purposes; iii) the last objective requires reduced models; iv) large-pore catalysts can contribute to energy savings since one needs lower temperatures than in the case of catalysts with no convection; v) new concepts are permeating the reaction engineering field (fractal, percolation, network pore models [35-37]) helping in the understanding of physical phenomena (mass transfer, coking); vi) new CFD tools are becoming popular in understanding reactor fluid dynamics [38]; vii) axial dispersed models and boundary conditions are being reconsidered [39]; viii) recently available dynamic simulators such as gPROMS [40] move the effort to the engineering side instead of spending much time in programming and numerical techniques.
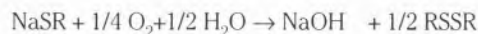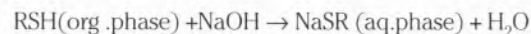
Laboratory studies of reaction processes

Gasoline sweetening. The methodology of CRE is going to be illustrated with cases already studied in our laboratory. The first is an example of an industrial process which operates at moderate pressure (6 atm) and mild temperature (38° C) used to convert mercaptans from gasoline into disulphides by oxidation with air in the presence of caustic solution. The catalyst is based on cobalt phthalocyanine supported in activated carbon. The process was developed by UOP in 1959 for gasoline sweetening (Merox process). The overall reaction is:

$$RSH + 1/4\ O_2 \rightarrow 1/2\ RSSR + 1/2\ H_2O$$

The sequence of reaction steps is:

$$RSH(org.phase) + NaOH \rightarrow NaSR\ (aq.phase) + H_2O$$

$$NaSR + 1/4\ O_2 + 1/2\ H_2O \rightarrow NaOH\ + 1/2\ RSSR$$
(aq.phase)   (aq.phase) (insoluble in the aq.phase)

Typical operating conditions of a Merox process are: reactor volume 20 m^3, gasoline flowrate 600 ton/day with mercaptans concentration in the feed of 290 ppm, excess oxygen of 120-200% above the stoichiometric air (13.4 N m^3/h), caustic soda flowrate 30 l/h. The process runs at 38° C and 6 Kg/cm^2 with a space time of 30 min. The amount of catalyst is 25 Kg. The impregnation of the activated carbon with the catalyst is made *in situ*. A solvent (methanol or ammonia) passes through a catalyst pot and the solution goes through the fixed bed of activated carbon.

Several objectives were aimed to be achieved with this study [41-44]: i) to obtain the basic experimental information for understanding the impregnation step; ii) to simulate the impregnation as it is actually carried out in industry; iii) to study the kinetics of n-butylmercaptan oxidation and heavier mercaptans in presence of Merox catalyst alone, activated carbon alone and supported catalyst; iv) to simulate the industrial reactor.

First of all we measured adsorption equilibrium isotherms for the system Merox in methanol/activated carbon. The results are shown in Figure 9 and were fitted with the Toth equation $q = Qc/(b+c^M)^{1/M}$. The next step was to obtain the intraparticle effective diffusivity. A fixed bed experiment in a small column (10 cm long, ID=1.1 cm, space time 30 s) was carried out and a breakthrough curve was obtained and fitted by a pore-diffusion model (axial dispersion and film mass transfer were also included). Since the stoichiometric time is $t_{st} = \tau(1+\xi)$ and the capacity factor $\xi = 3800$ we get $t_{st} = 1900$ min! Finally a value for the pore diffusivity was found $D_{pe} = 1.7 \times 10^{-6}$ cm^2/s and checked by CSTR experiments. Now we can simulate the industrial impregnation with the operating conditions: $c_o = 85$ mg/l (Merox concentration in methanol), $\rho_a = 270$ g/l, $\varepsilon_p = 0.85$, $\tau = 25.6$ min. The model includes axial dispersion for the bulk fluid phase, external diffusion, pore diffusion and adsorption in the particles. Model parameters are: Pe=1900 , N_d =1.74, N_f =478, ξ=429. What can we learn from the model solution? Figure 10 shows the average adsorbed concentration $\tilde{q}$ (x,t) as a function of the reduced distance x along the bed. Only 10% of the bed contains the Merox catalyst. However, we should be aware that the activated carbon is also a catalyst.
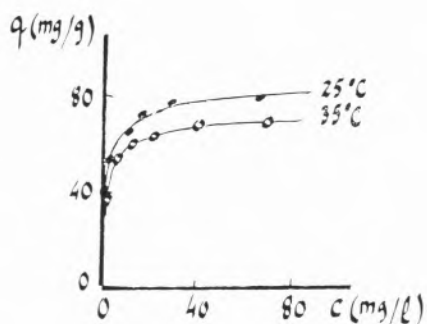
Figure 9 – Adsorption equilibrium isotherm, q *versus* c, for the system Merox in methanol/activated carbon.
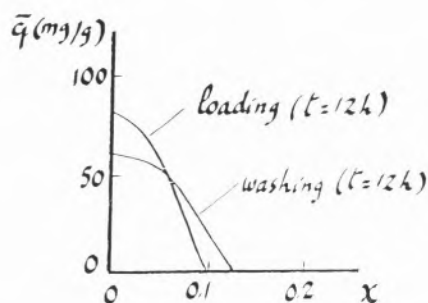

Figure 10 – Simulation of the industrial impregnation of activated carbon with Merox in methanol: axial profiles of the average adsorbed concentration of Merox.

Then we looked at the kinetics of mercaptans oxidation in a laboratory reactor Buchi BEP 280. The main results are:

a) with Merox catalyst alone: The reaction was found to be first order relative to mercaptan species and the activation energy of 25.8 Kcal/mole. In the range 2 to 9 atm the reaction is zero order relative to oxygen.

b) with activated carbon alone: The reaction was found to be 2nd order relative to mercaptan species and zero order relative to oxygen in the range 4 to 9 atm. The activation energy was found to be 19.4 kcal/mole.

c) with supported catalyst: The idea was to predict the activity of a supported catalyst (5.4 mg of Merox per gram of activated carbon) from the knowledge of the isolated kinetics for Merox alone and carbon alone according to $\Re = k_{mM} X_M c_m + k_{mC}(1-X_M)c_m^2$

The fitting is good with $k_{mC} = 2.58 \times 10^{-2} m^6 kg_{cat}^{-1} s^{-1} mol^{-1}$ and $k_{mM} = 5.95 m^3 kg_{cat}^{-1} s^{-1}$ but k_{mM} had to be changed. In the experiment reported in the Figure 11 the Thiele modulus is 32.7 at t=0 and 20.2 at 168 min so the process is diffusion limited.

On the basis of the kinetic information also obtained for heavier mercaptans and gasoline, simulation of

the fixed-bed reactor was carried out. Model equations were solved either by collocation method (PDECOL package) or by the numerical method of characteristics. The operating conditions of the industrial reactor are : T=38° C, P=6 atm, gasoline flowrate =10 m³/h, sodium hydroxide =10 l/h , mercaptans concentration =290 ppm, excess oxygen 125%, particle diameter d_p=1.1 mm, mass of activated carbon =840 kg, mass of Merox = 4.5 kg, reactor length L=4.27 m and Reactor diameter d_t=1.22 m.
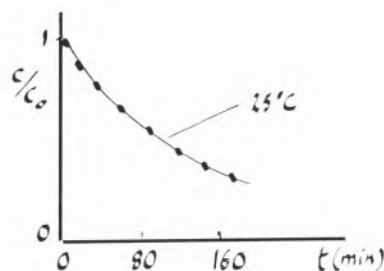
Figure 11 – Kinetics of n-butyl mercaptan oxidation in a supported catalyst.

The laboratory study of the Merox process opened several possibilities of further research, namely: i) modeling and experimental investigation of catalyst impregnation; ii) kinetics of catalytic reactions on bidisperse catalysts, *e.g.*, the synthesis of MTBE catalysed by macroreticular ion exchange resins on H^+ form [45]; iii) the development of computer-controlled experiments for kinetic studies, *e.g.*, vanillin production from kraft lignin [46].

Biofilm reactors. The second problem I want to discuss comes from the area of biofilm reactors: wastewater denitrification in a biological fluidized-bed reactor [47,48]. Experiments were carried out using either sand or activated carbon particles as support for the biomass. The methodology for the study of a catalytic reactor still applies to bioreactors. We first looked at biomass growth in a batch reactor (Figure 12). In a rotating disk biofilm reactor (CSTR) we grew biofilms of different thicknesses. Biofilm density decreases when biofilm thickness increases and the rate of reaction for each biofilm was measured (Figure 13). A simple model, developed some years ago for biofilm reactors of CSTR type, was tested. The model is based on the analogy between a catalyst particle and a biofilm [49]. For a zero order reaction it is shown that the reactor efficiency (conversion) is $E = N_r$ (biofilm working in kinetic-controlled regime) or $E = \sqrt{\alpha(\alpha+2)}$ biofilm working in diffusion-controlled regime) where N_r is the number of reaction units and $\alpha = N_r N_d$.

Figure 12 – Biomass growth in a batch reactor.

Figure 13 – Observed reaction rate r_a, in a rotating disk bioreactor as a function of nitrate concentration, N in the solution.

Now we can look at the biological fluidized bed reactor which is 3 m high and d_t=3.6 cm. Biofilm grows around particles. With sand particles (d_p=400 μm) those with thicker biofilms go to the top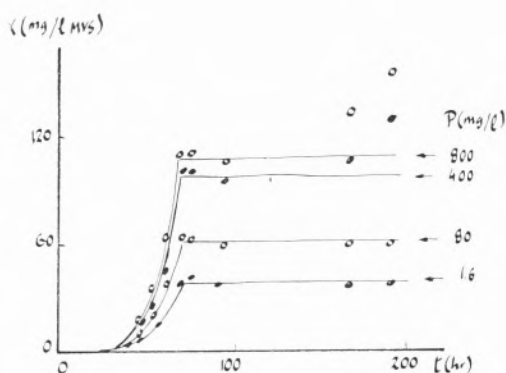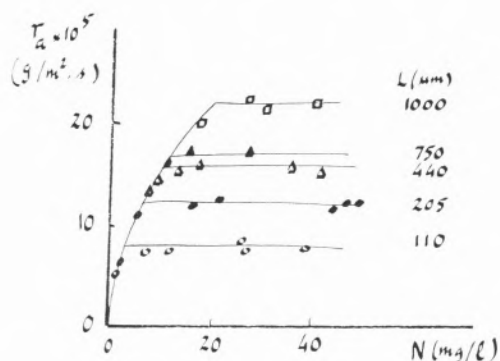 of the bed and there is bed stratification. With activated carbon particles as support the bed is homogeneous with regard to biofilm thickness. The consecutive reactions are both zero-order $NO_3^- \xrightarrow{K_1} NO_2^- \xrightarrow{K_2} N_2$. Three cases can be considered: i) the biofilm is fully penetrated by the nitrate and nitrite species; ii) the biofilm is partially penetrated by the nitrate alone; iii) the biofilm is partially penetrated by nitrate and nitrite. The reaction/diffusion analysis of the biofilm leads to the following results: i) When $\phi_1 < \sqrt{2}$, the effectiveness factors for the consumption of nitrates η_1=1 and the effectiveness factor for the net removal of nitrites is η_2=1; ii) for $\sqrt{2} < \phi_1 < \sqrt{2}$ $(1+\sqrt{sf^*_2/\delta})$ then $\eta_1 = \sqrt{2}/\phi_1$ and η_2=1 since f_1=0 at x^*=1-$\sqrt{2}/\phi_1$; and iii) For $\phi_1 > \sqrt{2}(1+\sqrt{sf^*_2/\delta})$ we get $\eta_1 = \sqrt{2}/\phi_1$ and $\eta_2 = (\sqrt{2}/\phi_1)$ $(1+\sqrt{sf^*_2/\delta})$ where f_1=0 at x^* and f_2=0 at x'=1- $(\sqrt{2}$ $/\phi_1)(1+\sqrt{sf^*_2/\delta})$. In the previous results δ=D_1/D_2 and s=k_1/k_2.

Concentration profiles along the reactor were measured for species 1 (nitrates) and species 2 (nitrites) and pseudo steady-state operation. The reactor model is a simple one: in fact from tracer experiments it was observed that Peclet number is around 150 and thus plug flow was assumed. Typical profiles are shown in Figures 14 and 15 for the cases of sand and activated carbon supports, respectively.
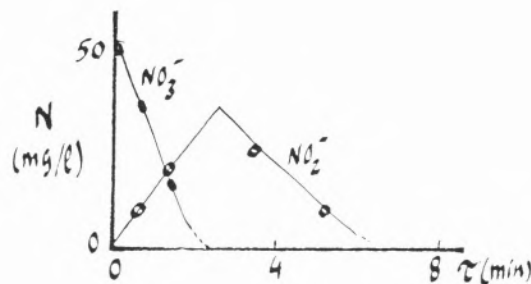
Figure 14 – Axial profiles of nitrate and nitrite species in a fluidized bed biological reactor for wastewater denitrification with sand as a support.
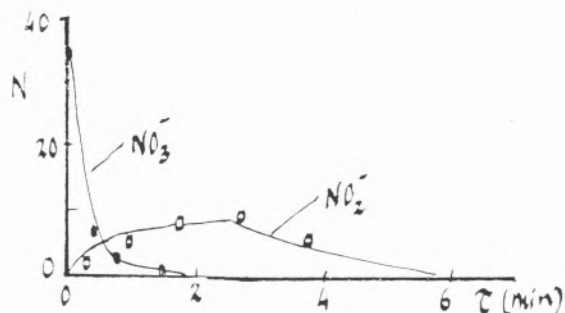
Figure 15 – Axial profiles of nitrate and nitrite species in a fluidized bed biological reactor for wastewater denitrification with activated carbon as a support.

Some points arise from this project: i) The fact that biofilm density changes with biofilm thickness can probably carry some analogy with catalysts with nonuniform activity profile and should be investigated further; ii) Further knowledge about the internal structure of the biofilm is needed which requires the use of microsensors; iii) Competing fermentation reaction of molasses which influences pH and so denitrification should be carefully analysed; iv) Unsteady-state modeling of biofilm reactors is of paramount importance [50].

Separation and reaction processes in a single unit

The last topic I want to address briefly is the coupling of adsorption and reaction in chemical engineering. This is an area which has been encountered by people working on adsorption with the objective of increasing the useful operation time of a fixed-bed column[51, 52]; it has also been of interest to reaction engineering people involved with reversible reactions as a way of achieving conversions higher than those obtained under equilibrium [53].

A nice example of adsorptive reactor is the carbon mask [54]. A fixed bed of activated carbon impregnated with a metal salt is used to convert toxic gases. The solute is nonlinearly adsorbed on the carbon whilst the reaction takes place in the adsorbed phase. Model equations include film mass transfer resistances in the fluid and inside particles; the mass balances for the solute A and the impregnant M are:

$$u_o \frac{\partial c}{\partial z} + \varepsilon \frac{\partial c}{\partial t} + k_v a (c-c^*)=0$$

$$\rho_b \frac{\partial M}{\partial t} = - \alpha \Re (q, M)$$

$$\rho_b \frac{\partial q}{\partial t} = k_v a(c-c^*) - \Re (q, M) = \rho_b k_p a(q^*-q) - \Re (q,M)$$

$$\Re (q,M) = k \rho_b{}^2 q M \quad \text{(kinetic law of reaction)}$$

$$q^* = Q K_L c^*/(1+K_L c^*) \quad \text{(adsorption equilibrium isotherm)}$$

$$t = 0 \qquad z > 0 \qquad c=q=c^*=q^*=0 , M=M_o$$

$$z = 0 \qquad t > 0 \qquad c=c_o$$

where c is the solute concentration in the fluid phase, q is the solute concentration in the adsorbed phase, M is the impregnant concentration, c^* and q^* are the solute concentrations in equilibrium at the interface, k is the kinetic constant, k_v and k_p are the film mass transfer coefficients in the film and in the particle, respectively. The important information here is the breakthrough time.

This problem of practical interest is quite different from the one in which the solute is adsorbed in the support and at the same time reacts on the active sites of the catalytic species. The main point to be retained is that the breakthrough time increases relatively to the case of adsorption alone provided that the adsorption equilibrium isotherm is nonlinear.

On the other hand one can look at problems from the reaction engineering side as it is the case of chromatographic reactors. There is obviously the incentive to achieve conversions higher than the equilibrium ones but also the possibility of process intensification by doing in a piece of equipment what is actually done in a reactor and an adsorber separately [55].

The idea of coupling reaction and separation in a single unit has been tested recently in our laboratory using the Simulated Moving Bed (SMB) technology (UOP). We used the SMB pilot plant with 12 columns packed with ion exchange resin in calcium form (Figure 16). The feed was a stream of sucrose solution with invertase enzyme. The reaction products are frutose and glucose which can be separated with the adsorbent resin. Results were recently presented at the "Process Intensification" conference [56].
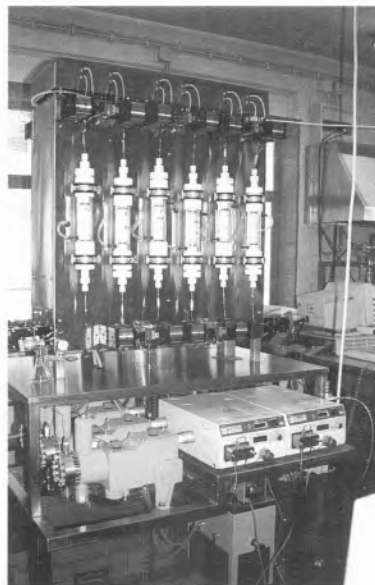
Figure 16 – Simulated Moving Bed laboratory unit at the LSRE.

Conclusion

Chemical engineering is faced today with many problems common to a changing world. Chemical industry is highly diversified with large-scale processes for the production of bulk chemicals and small-scale processes for the production of specialty chemicals.

Energy savings can nevertheless be achieved when: i) the reaction either consumes (steam-reforming) or produces (partial oxidation of hydrocarbons) large amounts of heat, ii) the feedstock represents an important amount of energy and iii) there are equilibrium restrictions .

These developments can be achieved through new reactor technologies, the design of new catalysts and new ideas combining separation and reaction. One example is the exhaust converter which uses monoliths giving a low pressure drop and using low active material/volume ratio; other examples are in the area of cyclic separation /reaction processes as SMBR and PSAR (pressure swing adsorptive reactors).

Computers offer new perspectives for modeling and simulation of chemical reactors involving kinetics, heat and mass transfer and hydrodynamics information. Also it helps laboratory work through automated data acquisition, graphics display , process control and scheduling.

New concepts from physics and mathematics are also permeating the chemical engineering field, *e.g.*, fractal and percolation concepts. New experimental techniques as well as the availability of new sensors contribute greatly to the understanding of fundamental phenomena arising in chemical reaction engineering.

Notation

B	permeability
c	fluid phase concentration
c_{pf}	fluid heat capacity
d	diameter
D	fractal dimension
D_e	true effective diffusivity
$\tilde{D}_e$	apparent effective diffusivity
E	activation energy
f	reduced solute concentration in the fluid phase or in the particle
G	mass flow
h_w	bed-to-wall heat transfer coefficient
ΔH	heat of reaction
k	kinetic constant
k_{er}	radial thermal conductivity
K_L	Langmuir constant
L	bed length
M	metal concentration
N	ratio of number of heat transfer units (based on the wall heat transfer coefficient)
N_f	number of film mass transfer units
N_d	number of pore diffusion units
N_r	number of reaction units
p	partial pressure of solute
P	pressure
Pe	Peclet number
q	adsorbed phase concentration
Q	maximum adsorbed phase concentration
R	ideal gas constant; radius of the reactor
r	radial coordinate
S	abcissae in the runaway diagram (dimensionless adiabatic temperature rise x Arrhenius number)
t	time
T	temperature
T^*	reduced temperature
u	normalized radial variable $(=r/R)^2$
u_o	superficial velocity
u_i	intersticial velocity
v_o	intraparticle convective velocity
x	reduced spacial coordinate for the particle or fixed bed
z	spacial coordinate

Symbols

ℓ	half thickness of the catalyst
ϕ	Thiele modulus
τ	time constant
λ_m	mass intraparticle Peclet number
λ_h	heat intraparticle Peclet number
λ_e	effective thermal conductivity
θ	reduced time
η	effectiveness factor
β	Prater thermicity factor
γ	Arrhenius number
ρ	fluid density
α_w	fluid-to-wall heat transfer coefficient
ε	bed porosity
α	universal parameter for biofilm in diffusional regime

Subscripts and superscripts

o	inlet
w	wall
s	surface; solid
b	bulk
~	apparent
*	equilibrium conditions
a	apparent
m	mass
h	heat
p	particle
d	diffusion
c	convection
r	reaction

References

1. O.Levenspiel, *Chem. Eng. Sci.*, **43** (1988)1427.

2. N. Amundson, *Chem. Eng. Educ.*, **168** Fall 1986.

3. Hougen, O. and K.Watson, *Chemical Process Principles*, Part 3 - Kinetics and Catalysis, J.Wiley (1947).

4. *First Symposium on CRE*, in *Chem. Eng. Sci.*, **8** (1958).

5. O.Levenspiel, *Chem.Eng.Sci.*, **35** (1980) 1821.

6. *Frontiers in Chemical Engineering: Research Needs and Opportunities*, National Research Council, Washington, D.C. (1988).

7. N.Amundson, *Chem. Eng. Res. Dev.*, 64 (1986) 233.

8. P.V. Danckwerts,"The challenges of chemical engineering science" in *Research and Innovation for the 1990's*, The Institution of Chemical Engineers, London (1986).

9. A.Nir and L.Pismen, *Chem. Eng. Sci.*, **32** (1977) 35.

10.A.Nir, *Chem.Eng.Sci.*, **32** (1977) 925.

11.D.Cresswell, *Applied Catalysis* ,**15** (1985) 103.

12.A.Rodrigues, J.Orfão and A. Zoulalian, *Chem. Eng. Comm.*, **27** (1984) 327.

13.P.Hawtin and R.Murdoch, *Chem. Eng. Sci.*, **19** (1964) 819.

14.D.Cresswell and N.Orr,"Measurement of binary gaseous diffusion coefficients within porous catalysts" in *Residence Time Distribution in Chemical Engineering*, ed. A. Petho and R. Noble, Verlag (1982).

15. B.Ahn, Ph.D. Thesis, Univ.Tech. Compiègne (1980).

16. A. Rodrigues, B.Ahn and A.Zoulalian, *AIChEJ*, **28** (1982) 541.

17. A. Rodrigues and R.Ferreira, *AIChE Symp.Series* 266, **84** (1988) 80.

18. N. Afeyan, F.Regnier and R.Dean jr., USPat 5019270, May **28** (1991).

19. A. Rodrigues, LC-GC (1993) 20.

20. S. Cheng, Ph.D.Thesis, Univ. Tech. Compiègne (1986).

21. S. Cheng and A.Zoulalian, *The Chem. Eng. J.*, **41** (1989) 91.

22. G. Damkohler, *Z.Phys.Chem.*, A **193** (1943) 16.

23. A. Rodrigues, "Mass transfer and reaction in fixed-bed heterogeneous systems: application to sorption operations and catalytic reactors" in *Disorder and Mixing*, ed. E.Guyon *et al.*, Kluwer (1988).

24. R. Ferreira, Ph.D. Thesis, Univ. Porto (1988).

25. A. Rodrigues and R. Quinta-Ferreira, *Chem. Eng. Sci.*, **45** (1990) 2653.

26.J. Lopes, M.Dias, V.Mata and A.Rodrigues, *Ind.Eng.Chem.Res.*, **34** (1995) 148.

27. M. Morbidelli and A.Varma, *Chem. Eng. Sci.*, **44** (1989) 1675.

28. R. Quinta-Ferreira, C. A. A. Costa and A. Rodrigues, *Comp. Chem. Engn.*, **30** (1996) 1201.

29. C. Sereno, PhD Thesis, Univ. Porto, (1990).

30. M. Chalbi, J.Castro, A.Rodrigues and A. Zoulalian, *The Chem. Eng. J.*, **34** (1987) 89.

31. Wellauer,T.,D.Cresswell and E.Newson, *ACS Symp. Series* **196** (1982) 528.

32. D.Cresswell, "Heat transfer in packed bed reactors" in *Chemical Reactor Design and Technology*, ed. H.de Lasa, Kluwer (1986).

33. B.Van Vliet and B.Young, *Chem. Eng. Comm.*, **69** (1988) 81.

34. R.Sargent,"Computing and Chemical Engineering", Proc. Chempor 89, Lisbon.

35. M. Steintuch and S.Brandon, *Chem. Eng. Sci.*, **44** (1989) 69.

36. Reyes, S. and K. Jensen, *Chem. Eng. Sci.* I, **41** (1986) 333.

37. Sharratt,P. and R.Mann, *Chem. Eng. Sci.*, **42** (1987) 1565.

38. P.Trambouze, Revue de L'Institut Français du Petrole, **48** (1993) 595.

39. K.Westerterp, V. Dil'man, A.Kronberg and A. Benneker, *AIChEJ*, **41** (1995) 2029.

40. M.Oh and C. Pantelides, *Comp. Chem. Eng.* **20** (1996) 611.

41. A. Leitão,"Estudo do processo Merox", Ph.D. Thesis, Univ. Porto (1987)

42. A. Leitão, C.Costa and A.Rodrigues, *Chem. Eng. Sci.*, **42** (1987) 2291.

43. A. Leitão and A. Rodrigues, *Chem. Eng Sci.*, **44** (1989) 1245.

44. A. Leitão and A. Rodrigues, *Comp. Chem. Eng.*, **15** (1991) 287.

45. N. Caetano, J. Loureiro and A. Rodrigues, *Chem. Eng. Sci.*, **49** (1994) 4589.

46. C. Fargues, A. Mathias and A. Rodrigues, *Ind.Eng.Chem.Res.*, **35** (1996) 123.

47. R.Boaventura and A. Rodrigues, *Chem. Eng. Sci.*, **43** (1988) 2715.

48. I.Coelhoso, MSc Thesis, Univ. Porto (1987).

49. A.Rodrigues, A.Grasmick and S.Elmaleh, *The Chem. Eng. J.*, **27** (1983) B39.

50. A. Leitão and A. Rodrigues, *Chem. Eng. Sci.*, **51** (1996) 4595.

51. D.Friday, *AIChE Symp Series*, **84** (1988) 89.

52. J. Loureiro, C. Costa and A.Rodrigues, *The Chem Eng.J.*, **27** (1983)135.

53. Westertep,K. and M.Kuczynski, *Chem. Eng. Sci.*, **42** (1987) 1871.

54. R. Soares, J. Loureiro, C. Sereno and A. Rodrigues, *Ind. Eng. Chem. Res.*, **34** (1995) 2762.

55. P.Plehiers, "Chemical reactors" in *Energy efficiency in industrial processes: future R&D requirements*, Report EUR 12046 EN, CEE (1988).

56. C. Leão, L. Pais, M. Santos and A. Rodrigues, "Simulated Moving Bed Adsorptive Reactors" in *Process Intensification*, ed., BHR Press (1997).

Dihydrogen activation by nickel containing hydrogenases
Biological inspiration for new organometallic catalysts

Activação do hidrogénio por hidrogenases contendo níquel
Inspiração biológica para novos catalizadores organometálicos

JOSÉ J. G. MOURA*, ANA PAMPLONA, MARTA CAREPO AND RICARDO FRANCO

DEPARTAMENTO DE QUÍMICA AND CENTRO DE QUÍMICA FINA E BIOTECNOLOGIA, FACULDADE DE CIÊNCIAS E TECNOLOGIA, UNIVERSIDADE NOVA DE LISBOA
2825 MONTE DE CAPARICA, email jose.moura@dq.fct.unl.pt
* CORRESPONDING AUTHOR

This article reviews very recent results on a novel heterodinuclear site containing nickel and iron found in the active site of hydrogenase, a key enzyme in bioenergetics. These results represent a stimulating challenge to the researchers involved in Inorganic Chemistry and Catalysis. Most of the efforts will aim to the study of novel catalysts and new reaction possibilities. Model systems should assist on the development of simple structural models and the interpretation of activity performances (H_2 production/uptake and H/D exchange).

O presente artigo de revisão apresenta estudos estruturais recentes num novo agregado heterodinuclear contendo níquel e ferro caracterizado no centro catalítico da hidrogenase, enzima chave em processos bioenergéticos. Estes resultados representam um importante estímulo para investigadores com interesses em Química Inorgânica e em Catálise em geral. Tal abordagem pode conduzir à proposta de novos catalisadores e a sistemas modelo que permitam analisar os desempenhos reaccionais da enzima (produção e consumo de hidrogénio e permuta H/D).

Abstract

Hydrogen production and uptake are important topics since dihydrogen is believed to become the fuel of the future. Since the discovery of the involvement of nickel in the biocatalysis of the dihydrogen molecule, a large attention has been devoted, from many complementary skills, to the characterization of the oxidation states and coordination sphere of the metal sites in the native and in the substrate reacted states of the hydrogenase enzyme. This multiple information has been used to hypothesize the mechanism of enzyme action. Different spectroscopic tools (in certain cases coupled to adequate isotopic metal substitutions) have contributed to probe the oxidation states of nickel and to reveal the structural features of the catalytic site. These spectroscopic techniques include EPR (and related ENDOR and ESSEM methods), EXAFS and UV-Visible-IR-Raman in parallel with oxidation-reduction studies and molecular biology approaches. Recently, the first tridimensional structure of a nickel containing hydrogenase was solved by Volbeda *et al.* (1). The enzyme has a complex structure and contains multiple centers. The analysis supports the previously proposed [Fe-S] cluster arrangement (one tri and two tetranuclear iron-sulfur clusters located in the small subunit of the

enzyme) and introduces a challenge observation: besides the nickel atom, buried in the larger subunit, a second metal (iron) can be found forming a new heterodinuclear Ni-Fe site. This iron atom is bridged by cysteine-sulfur atoms to the nickel site and contains three additional ligands, most probably diatomic molecules – most surprisingly identified as one carbon monoxide and two cyanide molecules (2-4).

Excellent reviews on spectroscopic studies of hydrogenases can be found in the literature (5-9). The present article will focus mainly on the dinuclear active center recently discovered in [Ni-Fe] hydrogenases and its implication at structural and catalytic levels.

Introduction

Molecular hydrogen plays a major role on the oxidation-reduction processes involved in bacterial energetics, as well as in the degradation and conversion of biomass related with all major elemental cycles. Hydrogenase has a key role on this process and catalyzes the reversible oxidation of dihydrogen (the simplest known oxidation-reduction reaction), which is important in bacterial anaerobic metabolism:

$$2\,H^+ + 2\,e^- \leftrightarrow H_2$$
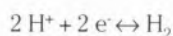
Unsolved structures are present at the active sites and unexpected features have been revealed. Most of the efforts undertaken have been oriented to the purification of [NiFe] hydrogenases and to the characterization of the metal centers involved, using biochemical and spectroscopic methods (EPR, Mössbauer, MCD, EXAFS and mass spectrometry) (5,6,9).

Sulfate Reducing Bacteria (SRB) are found in many different environments. Their economic and ecological impact is well documented. These organisms are involved in the microbial metal corrosion that occurs in anaerobic environments at neutral pH, with production of large amounts of sulfide (10). The classical mechanism proposed by Kühr and van der Vlugt suggests the involvement of hydrogenase in this process. A cathodic depolarization of the metal surfaces occurs upon hydrogen consumption by SRB. Hydrogenase would accelerate anode dissolution of iron by using cathodically formed elemental hydrogen for the dissimilatory reduction of sulfate (11). The industrial relevance of these biocorrosion processes along with the fact that H_2 can be used as an alternative energy source encouraged studies of possible ways to increase or inhibit hydrogen production by hydrogenase.

Sulfate reducing bacteria (SRB) of the genus *Desulfovibrio* (*D.*) have been until now one of the main sources of the enzyme. Extension of these studies to thermophiles is of great interest in particular to the hydrogen metabolism in respect to anaerobic bacterial corrosion (12). The utilization of SRB capable of doing the respiration of alternative substrates (i.e., nitrate instead of sulfate) enabled the study of the hydrogen metabolism in a situation with a wider environmental impact (13). Hydrogenases can be found in different sites in the bacterial cell: periplasm, cytoplasm and membrane. A given species may have hydrogenases only in one or in several of this cell sites. The hydrogenases isolated from SRB of the *Desulfovibrio* genus, can be broadly classified as *[iron-sulfur]-only* and *nickel--[iron-sulfur]-containing hydrogenases* (Table I):

[Iron-sulfur]-only or [Fe] hydrogenases are rare, lack nickel, and contain [4Fe-4S] clusters and, in addition, a catalytic iron cluster (designated as *H-cluster*) of unknown structure (14). *Nickel-[iron-sulfur]-containing hydrogenases* or [NiFe] hydrogenases are the most common and contain two [4Fe-4S] clusters, one [3Fe-4S] cluster and a nickel site. A sub-division under this class can be made for *nickel-selenium-[iron-sulfur]-containing hydrogenases* that lack the [3Fe-4S] cluster and exhibit seleno-cysteine coordination to the nickel site (14,15).

Specially for this latter class of hydrogenases, a large effort has been devoted to the purification and the characterization of the metal centers involved, using biochemical, genetic, spectroscopic and crystallographic techniques. Relevant questions have been addressed on the nickel chemistry in the context of its biological function: role of nickel during the oxidation-reduction cycle of the enzyme, nickel oxidation states involved, coordination mode and preferred ligands, assignment of nickel by different spectroscopic methods and interaction between the nickel and other metallic centers.

Nickel and Biology

Nickel is a transition metal required for a wide range of biological functions, namely hydrogen activation, CO transformation, urea processing and can also be found as part of unique cofactors in methanogenic organisms (16,17). The metal can be stabilized in different oxidation-reduction states (0 to +4). Ni(IV), d^6, is diamagnetic and prefers an octahedral coordination. Ni(III) is EPR active (d^7) and generally found in a distorted six coordinated environment. Ni(II), the most common oxidation state is a diamagnetic d^8 system, mostly found in square planar geometry and Ni(I), d^9, is again EPR active, preferring a lower coordination number, i.e., tetrahedral. Ni(III), Ni(II) and Ni(I) are considered to participate in biological reactions (18). The [61]Ni isotope (2% natural abundance, with a non-zero nuclear magnetic moment, I = 3/2) has been a most valuable tool for the assignment of EPR active species (8). The most abundant isotopes ([59]Ni and [60]Ni) have I = 0. [63]Ni is often used as radioactive marker in biochemical analysis.

D.gigas Hydrogenase – a model system

D.gigas hydrogenase has been used as a prototype of the [NiFe] hydrogenases and detailed data on active site composition, oxidation-reduction and catalytic properties has been obtained. The enzyme is an heterodimer and contains four oxidation-reduction centers: one nickel site, one [3Fe-4S] and two [4Fe-4S] clusters, as proven by electron paramagnetic resonance (EPR) and Mössbauer spectroscopic studies (19).

The nickel site was recently described as a heterodinuclear complex containing nickel and iron (1), as

Table I Physico-Chemical Properties of [Fe] and [Ni(Se)Fe] Hydrogenases

	Fe «only» hydrogenase	[NiFe] hydrogenase	[NiSeFe] hydrogenase
Molecular Mass (kDa)	57	89	87
Subunits (kDa)	46,11	63,26	53,34
Clusters	2 [4Fe-4S]	2 [4Fe-4S]	2 [4Fe-4S]
	H Center	1 [3Fe-4S]	
Specific Activity (μmolH$_2$/min.mg)	4800	440	526

will be extensively presented below. The EPR data analysis discussed below uses a terminology established prior to the detection of the additional iron atom, but should be considered through the text as referring to the Ni-Fe site.

D.gigas hydrogenase has been isolated with different isotopic enrichments (^{61}Ni (I=3/2), ^{59,60}Ni (I=0), ^{56}Fe (I=0) and ^{57}Fe (I=1/2)) and studied after reaction with hydrogen (H$_2$ and D$_2$ labeled). Isotopic substitutions are valuable tools for spectroscopic assignments and catalytic studies. The effect of these isotopic substitutions on the EPR signals is described in Table II, and will also be discussed later.

Table II Isotopic substitution effects on the EPR signals of [NiFe] hydrogenases

	^{57}Fe(I=1/2)	H/D	^{61}Ni (I=3/2)
Ni-A	—	—	X
Ni-B	—	—	X
Ni-C	—	X	X
[Fe-S]	X	—	—

X – observed
— – not detected

Most of the [NiFe] hydrogenases are inactive, as isolated, and the nickel center exhibits an intense rhombic EPR signal termed Ni-A (g = 2.31, 2.23 and 2.01) with variable amounts of another nickel species, termed Ni-B (g = 2.33, 2.16 and 2.01), with slightly different rhombicity (8) (Figure 1). Some hydrogenases may contain only Ni-B type EPR signals (13). Upon reaction with hydrogen, the natural substrate, and after a reductive activation step (lag phase), these signals disappear and are replaced by a transient nickel EPR signal termed Ni-C (g = 2.19, 2.14 and 2.01). Ni-C species is considered a *key intermediate* (detected in all [NiFe] hydrogenases). These signals can be observed up to 100 K without noticeable line broadening. All these signals are extensively affected by ^{61}Ni substitution (Table II), supporting that most of the spin density is located at the nickel atom (20).

Ni-A EPR signals in hydrogenases have been related to an unready state of the enzyme and to the reversible inactivation of hydrogenases. The minor amount of Ni-B species that are observed in the oxidized state, can be enhanced by recycling the enzyme in the absence of oxygen (21). This increase in the amount of Ni-B has been pointed out to represent an enzyme state that is easy to activate and that does not require deoxygenating steps but just a reductive one (21,22). Oxidation-reduction titrations revealed the existence of two other EPR silent oxidation-reduction states, designated as Ni-Si (Ni-Silent) and Ni-R (Ni-Reduced) (19, 23). The oxidation-reduction pattern can be described by the following sequence of events (on the oxidation direction):

$$\text{Ni-R} \rightarrow \text{Ni-C} \rightarrow \text{Ni-Si} \rightarrow \text{Ni-B} \rightarrow (+ O_2) \rightarrow \text{Ni-A}$$
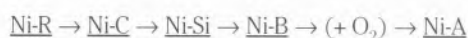
The assignment of the oxidation states involved in the catalytic cycle of the enzyme is still under debate. EPR spectroscopy cannot distinguish in a straightforward manner between Ni(I) and Ni(III) (6,8), but as discussed below, reduction steps involving Ni(III) and Ni(II) states are favored by us, since the oxidation-reduction potentials of Ni(I)/Ni(0) are quite low. It has been proposed that the Ni-C state is related to a Ni(I) or Ni(III) species (5-9). Support for the first suggestion comes from oxidation-reduction titrations and the interpretation of the nickel EPR spectra having H$_2$ and ^{13}CO as ligands (24). However, a more rhombic signal is expected in the case of a Ni(III) species, as proved by the study of various model compounds. The Ni(II) state is suggested for the EPR silent state of [NiFe] hydrogenases (8) or for the as-isolated state of [NiSeFe] hydrogenases (25), in a low-spin state (S=0).

The Mössbauer data on the native state of [NiFe] hydrogenase revealed the presence of a [3Fe-4S] and two [4Fe-4S] clusters. As prepared, the [NiFe] hydrogenase is described as containing four non-interacting oxidation-reduction centers, i.e., the three [Fe-S] clusters and the Ni site (19,21). A complete Mössbauer study was performed on the iron-sulfur clusters of the enzyme at different oxidation-reduction potentials indicating that no cluster conversion occurs (19). The metallic centers interact magnetically after substrate reaction: a broadening of the EPR signal of the reduced 3Fe center can be detected and there is conversion of the Ni-C species into a fastrelaxing EPR species due to its interaction with the reduced 4Fe cores [(19), see Figure 1].
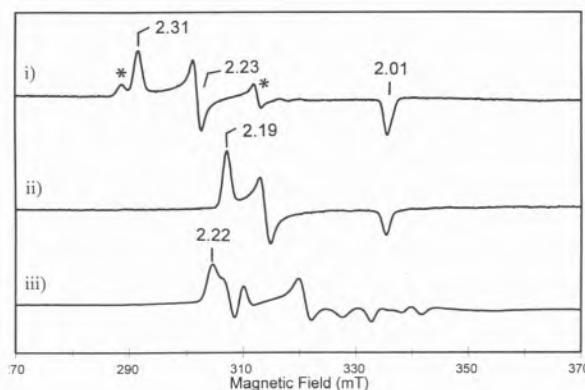

Figure 1 – Typical EPR signals observed in [NiFe] Hydrogenases
i) as isolated enzyme: Ni-A and Ni-B (* denotes the features associated with Ni-B) (100 K)
ii) hydrogen reacted state: Ni-C (40 K)
iii) hydrogen reacted state: fast relaxing species (6 K).

Chemical models that mimic hydrogenase

Although not extremely relevant at this stage, since the nickel containing active site is heterodinuclear, results on mononuclear Ni(II) complexes containing aromatic nitrogen and thiolate sulfur coordinating ligands, readily afford Ni(I) and Ni(III) analogues which lead to interesting speculation on the oxidation-reduction behavior of the nickel site (26,27). Nickel synthetic compounds are known to display widely separated Ni(III)/Ni(II) and Ni(II)/Ni(I) oxidation-reduction couples with oxidation-reduction potentials which are much more positive than those found in hydrogenase (-100 mV to -450 mV). Krüger and Holm (26) have addressed the problem of lowering the Ni(III)/Ni(II) oxidation-reduction potentials by using ligands with polarizable, electron-rich donor atoms. Such a ligand is $(Et_4N)[Ni(pdtc)_2]$ (pdtc= pyridine-2,6-bis(monothiocarboxylate)), which affords a thiolate-rich coordination to the metal, yielding a complex with an oxidation-reduction potential of -85 mV. Alteration of the coordination sphere through the activation steps and reaction with substrate would be a requirement for making the active site available for the binding and processing of the dihydrogen molecule.

Ni(II) is difficult to stabilize in tetrahedral coordination geometry. Also sulfur predominant coordination is difficult to model. Rubredoxin (Rd) is a small electron transfer protein that contains in its active center an iron atom with four cysteinyl residues coordinated on a tetrahedral distorted geometry. The active center iron has been replaced by nickel (28-31), providing this latter metal with a sulfur-rich coordination environment. Ni(III) oxidation state studies were generated on the oxidized nickel-substituted rubredoxin. This nickel derivative (Ni-Rd), mimics in certain aspects the catalytic activity of hydrogenases: H_2 production, D/H exchange and inhibition by CO (29). However, the catalytic activity is 10^4-fold lower in Ni-Rd, indicating fundamental differences between the two nickel-containing sites. Furthermore it has been postulated that tetragonal distortion of the tetrahedral coordination in Ni-Rd leads to a Ni(II) S=1 (30). The CN^--bound form of the oxidized Ni-Rd (Ni(III)) prepared from *Pyrococcus furiosus* Rd, gives EPR signals which are very similar to the Ni-C and its photolytic product, Ni-C*, in hydrogenases (32). This result supports a Ni(III) character for the Ni-C EPR signal.

From the inorganic chemistry point of view, a few monomeric nickel thiolates have been synthesized and inorganic model compounds are emerging in the optics of oxidation-reduction and coordination models for the nickel site in hydrogenases. They will be valuable tools for the study of parameters controlling spectral and reaction properties in these biological altered systems. The introduction of nickel in a ferredoxin cluster like in the mixed metal core $[NiFe_3S_4]$ is also the great interest in biological modeling (33), as models for CO dehydrogenase.

Interaction of the Nickel site with substrate

The interaction of the substrate molecule with the enzyme has been observed with great interest from a mechanistic point of view. The involvement of a hydride species has been much searched in consequence of the heterolytic cleavage mechanism put in evidence by the isotopic exchange reactions (34). D_2/D_2O and H_2/H_2O reactions were used to probe the substrate binding at the nickel site. A narrowing of 0.5 mT at the g_{max} feature associated with the Ni-C EPR signals was observed upon exchanging with deuterium and attributed to a weak interaction with one or more protons from the solvent (13, 35). In this context it is important to refer the isotopic effect detected in the light induced alteration observed in Ni-C EPR signal of *Chromatium vinosum* hydrogenase (36). In fact, the rate of the photochemical reaction proved to be about six times slower in D_2O than in H_2O. These results strongly suggested that an hydride-nickel species is involved. In favor of the existence of this intermediate, ENDOR studies on the *D. gigas* hydrogenase Ni-C form revealed that this site is accessible to solvent protons and/or gaseous dihydrogen, as opposite to Ni-A. It was also concluded that two different types of exchangeable protons are bound to the former form of nickel: i) one type characterized by a small hyperfine coupling (~ 4.4 MHz), which is consistent with the proton being associated with H_2O (or OH^-) bound to Ni-C and ii) another with a larger hyperfine coupling (16.8 MHz), identified as an in-plane hydride or an X-H proton involved in an agostic interaction with nickel or even as H_2 (37).

3D Structure of *D.gigas* [NiFe] Hydrogenase

Crystallographic studies of the Ni-Fe hydrogenase from *D.gigas* (2.8 Å) have shown that the active site is a new heterodinuclear site, containing nickel and another transition metal (probably iron) (1). This unexpected result challenges previous reported spectroscopic studies that failed to predict the existence of this second metal ion. [Ni-Fe] hydrogenase is a heterodimer containing two subunits: a small subunit, 26 kDa, and a large subunit, 63 kDa. The small subunit has two [4Fe-4S] centers and a [3Fe-4S] center, while the catalytic center, that contains nickel, is buried in the large subunit (Figure 2). The [4Fe-4S] clusters are classified as distal or proximal, based on their distance to the Ni center. An histidinyl residue was detected as coordinating ligand of the distal [4Fe-4S] cluster which represents the first time that such an observation is made in a protein structure.

The Novel Heterodinuclear Site
$(Cys)_2$-Ni-$\mu(Cys)_2$-$\mu("O")$-Fe(CO)(CN)$_2$
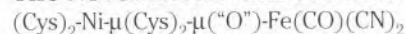
The crystallographic analyses of the native *D.gigas* hydrogenase have shown that this center is an heterodi-

Figure 2 – 3D structure of *D.gigas* Hydrogenase (coordinates provided by M.Frey).

nuclear center, consisting of nickel and a second metal ion, that by anomalous dispersion effects, EXAFS and Q-band ENDOR studies, has been assigned to an iron atom (38,39). The nickel atom is coordinated by four cysteine residues, Cys 65, Cys 68, Cys 530, and Cys 533. Two of this four coordinating cysteins (Cys 533, Cys 68) serve as
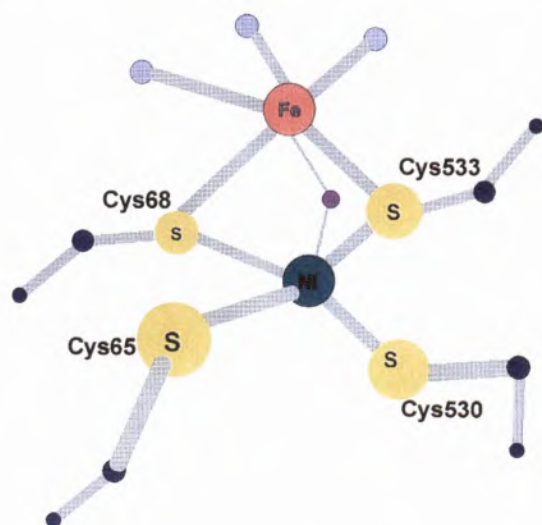

Figure 3 – Structural details on the heterodinuclear NiFe catalytic site of *D.gigas* Hydrogenase. Blue circles indicate the iron-coordinated CN⁻ and CO molecules and the purple circle represents the bridging oxygen species.

bridging ligands between nickel and iron. Cys530 is replaced by seleno-cysteine in the [NiSeFe] hydrogenases. Iron is also coordinated by three non-protein ligands (diatomic molecules), that recently have been proposed, by FTIR measurements and elemental analysis as being one CO and two CN⁻ molecules (2-4). A fourth non-protein ligand, probably involving oxygen, could bridge Ni and Fe (1,4) (Figure 3). The surprising nature of these three diatomic ligands puts hydrogenase in the small group of biological systems that use organometallic compounds, along with vitamin B_{12} and carbon monoxide dehydrogenase (40,41).

Spectroscopic Evidence for the novel Heterometal Cluster

⁵⁷Fe ENDOR Studies on the Nickel EPR signals

X-ray crystallographic analysis of native *D.gigas* hydrogenase has shown a novel heterodinuclear cluster containing nickel and a second transition metal proposed to be iron (1). A careful analysis of the linewidths of the Ni-A EPR signals obtained from both natural-abundance and ⁵⁷Fe-enriched hydrogenase shows no evidence of hyperfine broadening from ⁵⁷Fe. However, Q-band pulsed ENDOR spectra indicate, at the frequency range around the ⁵⁷Fe nuclear Larmor frequency (v_{Fe} = 1.51 MHz at 11000 G), that ⁵⁷Fe-enriched native *D.gigas* Hase (Ni-A EPR signals) shows a sharp doublet, not seen in the ⁵⁶Fe sample, and therefore assigned to hyperfine-coupled ⁵⁷Fe to the nickel site [A(⁵⁷Fe) ~ 1 MHz at g₁=2.31] (Figure 4) (39). The hyperfine tensor components measured in different field positions differ little from the isotropic coupling of ~ 1 MHz. This value is consistent with both the absence of any broadening in the EPR spectrum and the inability of Mössbauer spectroscopy to detect the site. This result completes the identification of the active site of the Ni-containing hydrogenases as a novel heterodinuclear [Ni-Fe] cluster.

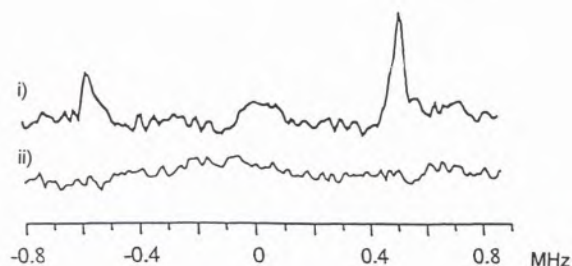Figure 4 – Q-band ENDOR spectrum of *D.gigas* hydrogenase obtained from bacteria grown in: i) ⁵⁷Fe enriched medium and ii) natural abundance ⁵⁶Fe medium. Both spectra were obtained in the Ni-A, native form of the enzyme, at g₁=2.31. Other experimental conditions: temperature, 2 K; microwave power, 34.7 GHz.

Table III Predicted values for the global spin of the heterodinuclear [NiFe] cluster

		Ni^{III}(3d^7)		Ni^{II}(3d^8)	
		$S_1= 3/2$	$S_1= 1/2$	$S_1= 1$	$S_1= 0$
Fe^{III} (3d^5)	$S_2= 5/2$	S=1; 4	S= 2; 3	S= 3/2; 7/2	S= 5/2
	$S_2= 1/2$	S=1; 2	S= 0; 1	S= 1/2; 3/2	S= 1/2
Fe^{II} (3d^6)	$S_2= 2$	S=1/2; 7/2	S= 3/5; 5/2	S= 1; 3	S= 2
	$S_2= 0$	S=3/2	S= 1/2	S= 1	S= 0

Proposal of a Mechanism for the Catalytic Cycle

The discovery of a new heterodinuclear active site in hydrogenases opens new avenues for the proposal of a catalytic cycle. Based on the available spectroscopic data obtained in different oxidation-reduction states, a few clues are put forward as follows:

1) recent EXAFS studies reveal that the Ni-edge energy upon reduction of the enzyme is altered, supporting an increase in the charge density of the nickel (38).

2) sulfur as coordinating atoms are generally considered as "non-innocent" ligands, and may delocalize part of the spin density at the site (8,26);

3) the large value of the ^{61}Ni hyperfine coupling associated with the Ni-A EPR signal (20) is consistent with Ni in a paramagnetic Ni(III) state; the small value of A(^{57}Fe) for Ni-A is consistent with the iron ion being low-spin (diamagnetic) ferrous, with the observed coupling stemming from a small degree of delocalization from Ni(III) within the [NiS$_2$Fe] core. The cluster in Ni-A, as pictured in Figure 3, thus is best described as a trapped-valence, heterodinuclear [Ni(III)-Fe(II)] center, with a global S = 1/2. Table III shows the wide range of possible values that can be obtained for the global spin value of a heterometal core as described, assigning different oxidation and spin states to the metals.

4) several pieces of evidence indicate that the nickel site is involved with substrate handling (see before and ref. 8).

These observations and considerations led us to propose a catalytic oxidation-reduction cycle for the enzyme that involves a nickel-based redox chemistry (Figure 5a). This scheme is an alternative proposal to the one presented by Fontecilla-Camps (42), that suggested a possible alteration of iron oxidation-reduction state keeping nickel unchanged during enzyme turnover (Figure 5b). The cycle shown in Figure 5a is also an extension of our previous reported proposals (8,9).

Electron Transfer

The knowledge of the 3D structure of hydrogenase gave important information about protein structural aspects and provided interesting mechanistic hints. To elaborate on enzyme catalytic mechanisms it is necessary to consider many factors specially protein metal ligands, geometry and distortions imposed by the protein around the active site, and the protein catalytic site exposure to substrate and solvent. The study of hydrogenase in different oxidation states and in interaction with substrate and inhibitors will also help to clarify mechanistic aspects.
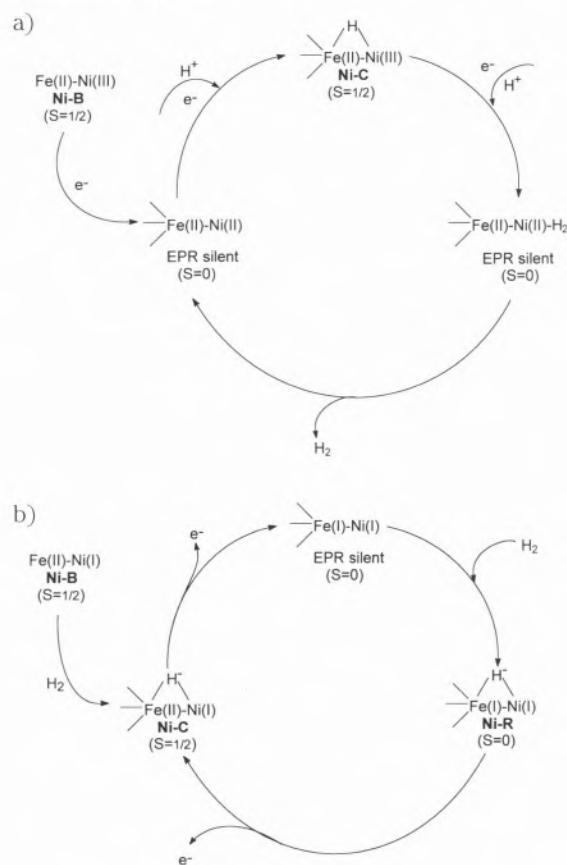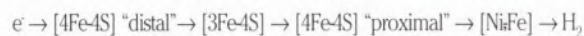

Figure 5 – Catalytic cycles proposed for *D.gigas* Hydrogenase
a) Nickel based redox chemistry
b) Iron based redox chemistry

The *D.gigas* hydrogenase 3D structure was solved on the native state and not on the active state of the enzyme, so a required step will be the transformation of the "unready" into the "ready" form of the enzyme. Protein conformational changes may induce modifications on the coordination sphere of the metal during enzyme catalysis so that the substrate interacts with the catalytic site. The spatial arrangement presented by the iron-sulfur clusters: one [4Fe-4S] cluster proximal to the nickel center and the other [4Fe-4S] cluster near the protein surface (called distal), with the [3Fe-4S] cluster located half-way between these two centers, may provide an electron channel to transfer electrons between hydrogenase and its redox partners (Figure 6). The fact that one iron in the distal [4Fe-4S] cluster is coordinated to a histidine instead of a cysteine residue (a new observation in biological systems) suggests a direct involvement of the imidazole ring from the histidine in the electronic transfer. The 3D structure clearly points to the definition of the substrate interacting and the electron transfer sites (1). An electron transfer pathway was proposed based on the hydrogenase structure:

$$e^- \rightarrow [4Fe\text{-}4S] \text{ "distal"} \rightarrow [3Fe\text{-}4S] \rightarrow [4Fe\text{-}4S] \text{ "proximal"} \rightarrow [NiFe] \rightarrow H_2$$

The conjunction of spectroscopy and crystallography is a powerful mean for the study of hydrogenase. Nickel and iron coordination motifs found in *D.gigas* hydrogenase are very innovating and challenging. The crystallographic study of hydrogenase samples in defined oxidation-reduction states and in interaction with dihydrogen are anticipated with major interest. The proposed bridging oxygen atom can be the key for the
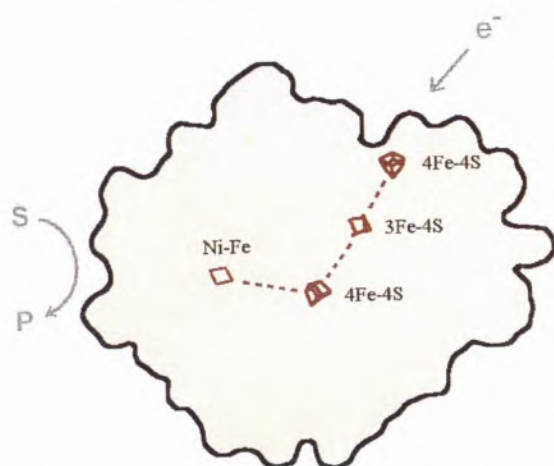
change of unready to ready state of the enzyme. The coordination of dihydrogen to the heterodinuclear site possibly in a bridging position, is a very tempting proposal to be demonstrated.

Acknowledgments

Note Added in Proof

Recently, the crystal structure of *D. vulgaris* Miyazaki [NiFe] hydrogenase has been solved at 1.8 Å resolution by Higuchi, Y., Yagi, T., and Yasuoka, N.. Unusual ligand structure in Ni-Fe active center and an additional Mg site in hydrogenase were revealed by high resolution X-ray structure analysis, *Structure, 5,* 1671 (1997). The overall folding pattern and the spatial arrangement of the iron clusters are very similar to the *D. gigas* hydrogenase, as described. The main difference is the fact that the ligands of the heterodinuclear NiFe center have been proposed to be diatomic S=O, C≡O, and C≡N molecules instead of the two C≡N and one C≡O found in the *D. gigas* enzyme. The authors suggest that such unusual ligands could be involved in the electron transfer from the hydrogenase active site to its biological redox partners or, could stabilize the redox state of the Fe(II) during the catalytical cycle of the enzyme.

Figure 6 – Postulated electron pathway in *D.gigas* Hydrogenase. The route indicates a connection between the surface [4Fe-4S] center (histidinyl ligated) and the Ni-Fe cluster (substrate binding site).

References

1. Volbeda, A., Charon, M-H, Piras, C., Hatchikian, E.C., Frey, M. and Fontecilla-Camps, J.C. (1995) *Nature* **373**, 580-587.

2. Bagley, K.A., Duin, E.C., Roseboom, W., Albracht, S.P.J. and Woodruff, W.H. (1995) *Biochemistry* **34**, 5527-5535.

3. Van der Spek, T.M., Arendsen, A.F., Happe, R.P., Yun, S., Bagley, K.A., Stufkens, D.J., Hagen, W.R. and Albracht, S.P.J. (1996) *Eur.J.Biochem.* **237**, 629-634.

4. Happe, R.P., Roseboom, W., Bagley, K.A., Pierik, A.J., and Albracht, S.P.J. (1996) *Nature* **385**, 126.

5. Cammack, R., Fernandez, V.M., Hatchikian, E.C. (1994) "Microbial Sulfur Metabolism" Methods in Enzymology (Peck,Jr., H.D. & LeGall, J., eds.) **243**, 43-68.

6. Albracht,S.P.J.(1994) *Biochim.Biophys.Acta* **1188**, 167-204.

7. Cammack, R. (1992) in "Bioinorganic Catalysis" (Reedijk, J., ed.) Marcel Dekker, New York.

8. Moura, J.J.G., Teixeira, M., Moura, I. and LeGall, J. (1988) in "The Bioinorganic Chemistry of Nickel" (Lancaster, Jr. ed.), pp. 191-226, VCH, New York.

9. J.J.G.Moura, I.Moura, M.Teixeira, A.V.Xavier, G.D.Fauque and J.LeGall (1988) in "Metal ions in biological systems", vol. 23 (Sigel, H. & Sigel, A., eds.), pp. 285-314, Marcel Dekker, Inc., New York and Basel.

10. Postgate, J.R. (1982) *Phil. Trans. R. Soc. Lond. B* **298**, 583-600.

11. Hamilton, W.A. (1985) *A. Rev. Microbiol.*, **39**, 195-217

12. G.Fauque, M.Czechowski, Y.M.Berlier, P.A.Lespinat, J.LeGall and J.J.G.Moura (1992) *Biochem. Biophys.Res.Comm.* **184** 1256-1260.

13. Franco, R., Moura, I., LeGall, J., Peck, H.D., Jr., Huynh, B.H. and Moura, J.J.G. (1993) *Biochim. Biophys. Acta* **1144**, 302-308.

14. Fauque, G., Peck, H.D., Jr., Moura, J.J.G., Huynh, B.H., Berlier, Y., DerVartanian, D.V., Teixeira, M., Przybyla, A.E., Lespinat, P.A., Moura, I. and LeGall, J. (1988) *FEMS Microbiol. Rev.* **54**, 299-344.

15. Prickril, B.C., He, S.H., Li., C., Menon, N.,Choi, E.S., Przybyla, A.E., DerVartian, D.V., Peck, H.D. Jr., Fauque, G., LeGall, J.,Teixeira, M., Moura, I., Moura, J.J.G., Patil, D. and Huynh, B.H. (1987) *Biochem.Biophys.Res.Commun.* **149**, 369-377.

16. Diekert, G. (1988) in "The Bioinorganic Chemistry of Nickel" (Lancaster, Jr., J.R., ed.), 299-309, VCH, New York

17. "Metal ions in biological systems", vol. 23 (Sigel, H. & Sigel, A., eds.), Marcel Dekker, Inc., New York and Basel.

18. Cammack, R. and Hughes, M.N. (1994) Encyclopedia of Inorganic Chemistry (King, R.B., ed.) vol.5, pp. 2384-2391, John Wiley & Sons, Ltd.

19. Teixeira, M., Moura, I., Xavier, A.V., Moura, J.J.G., LeGall, J., DerVartanian, D.V., Peck, H.D., Jr. and Huynh, B.H. (1989) *J. Biol. Chem.* **264**, 16435-16450.

20. Moura, J.J.G., Moura, I., Huynh, B.H., Krüger, H.-J., Teixeira, M., DuVarney, R.C., DerVartanian, D.V., Xavier, A.V., Peck, H.D., Jr. and LeGall, J. (1982) *Biochem.Biophys.Res.Commun.* **108**, 1388-1393.

21. Teixeira, M., Moura, I., Xavier, A.V., Huynh, B.H., DerVartanian, D.V., Peck, H.D., Jr., LeGall, J. and Moura, J.J.G. (1985) *J. Biol. Chem.* **260**, 8942-8950.

22. Fernandez, V.M., Hatchikian, E.C. and Cammack, R. (1985) *Biochim. Biophys. Acta* **832**, 69-79

23. Lindhal, P.A., Kojima, N., Hausinger, R.P., Fox, J.A., Teo, B.K., Walsh, C.T. and Orme-Johnson, W.H. (1984) *J. Am. Chem. Soc.* **106**, 3062-3064

24. Coremans, J.M.C.C., Van Garderen, C.J., Albracht, S.P.J. (1991) *Biochem. Biophys. Acta*, **1119**, 148-156.

25. C.-P. Wang, R.Franco, J.J.G.Moura, I.Moura and E.P.Day (1992) *J.Biol. Chem.*, **267**, 7378-7380.

26. Krüger, H.J. and Holm, R.H. (1990) *J. Am. Chem. Soc.* **112**, 2955-2963.

27. Baidya, N., Olmstead, M.M., Mascharak, P.K. (1992) *J. Am. Chem. Soc.*, **114**, 9666-9668.

28. Moura, I., Teixeira, M., Le Gall, J. and Moura, J.J.G. (1991) *J. Inorg. Biochem.* **44**, 127-139.

29. P.Saint-Martin, P.A.Lespinat, G.Fauque, Y.Berlier, J.LeGall, I.Moura, M.Teixeira, A.V.Xavier and J.J.G.Moura (1988) *Proc. Natl. Acad. Sci. USA* **85**, 9378-9380.

30. Huang, Y.H., Park, J.B., Adams, M.W.W. and Johnson, M.K. (1993) *Inorg. Chem.* **32**, 375-376.

31. Kowal, A.T., Zambrano, I.C., Moura, I., Moura, J.J.G., Le Gall, J. and Johnson, M.K. (1988) *Inorg.Chem.* **27**, 1162-1166.

32. Elp, J. van, Peng, G., Searle, B.G., Mitra-Kirtley, S., Huang, Y.H., Johnson, M.K., Zhouu, Z.H., Adams, M.W.W., Maroney, M.H. and Cramer, S.P. (1994) *J. Am. Chem. Soc.* **116**, 1918-1923.

33. Moreno, C., Macedo, A.L., I.Moura, LeGall J. and J.J.G.Moura (1994) *J. Inorg. Biochem.* **53**, 219-234.

34. Lespinat, P.A., Berlier, Y., Fauque, G., Czechowski, M., Dimon, B. and LeGall, J. (1986) *Biochimie* **68**, 55-61

35. Cammack, R., Fernandez, V.M., Schneider, K. (1988) in "The Bioinorganic Chemistry of Nickel" (Lancaster, Jr., J.R., ed.) pp.167-190, VCH, New York

36. Van der Zwaan, J.W., Albracht, S.P.J., Fontijn, R.D., Slater, E.C. (1985) FEBS Lett., 179, 271-277.

37. Fan, C., Teixeira, M., Moura, J.J.G., Moura, I., Huynh, B.H., Le Gall, J., Peck, Jr., H.D. and Hoffman, B.M. (1991) *J.Am.Chem. Soc.* **113**, 20-24.

38. Gu, Z., Dong, J., Choudhury, S.B., Franco, R., Moura, J.J.G., Moura, I., LeGall,J., Przybyla, A.E., Roseboom, W., Albracht, S.P.J, Axley, M.J., Scott, R.A. and Maroney, M.J. (1996) *J.Am.Chem.Soc.* **118**, 11155-11165

39. Huyett, J., Carepo, M., Pamplona, A., Franco, R., Moura, I., Moura, J.J.G. and Hoffman, B. (1997) *J.Am.Chem.Soc.* **119**, 9291-9292.

40. Pratt, J.M. (1972) in "Inorganic Chemistry of Vitamin B$_{12}$" Academic Press, New York.

41. Ragsdale, S.W., Bauer, J.R., Gorst, C.M., Harder, S.R., Lu, W.P., Roberts, D.L., Runquist, J.A. and Schiau, I. (1990) *FEMS Microbiol. Rev.* **87**, 397-421

42. Fontecilla-Camps, J.C. (1996) *J. Biol. Inorg. Chem.* **1**, 91-98.

The biological membrane viewed as a heterogenous chemical system

As membranas biológicas analisadas como um sistema químico heterogéneo

WINCHIL L. C. VAZ [1] AND EURICO MELO[2]

[1] UNIVERSIDADE DO ALGARVE, 8000 FARO, PORTUGAL, AND
2 INSTITUTO DE TECNOLOGIA QUÍMICA E BIOLÓGICA AND INSTITUTO SUPERIOR TÉCNICO,
APARTADO 127, P-2780 OEIRAS, PORTUGAL.

The biological membrane, a cellular structure that separates the cell from its environment and intracellular compartments from each other, is composed principally of a so-called "lipid bilayer" that is made up of two apposed monomolecular layers of amphiphilic lipids, generally phospholipids but also glycolipids and cholesterol. The lipid bilayer, a thin quasi-two-dimensional fluid film with two polar surfaces and an apolar core and a thickness of approximately 10 nm, acts as a solvent system for several proteins which may be dissolved in it or adsorbed to its surface. The chemical composition of the lipid bilayer is known to be complex, generally containing three or four lipid classes known to be not ideally miscible among themselves. This creates the conditions for a probable heterogeneity of the system in the physical-chemical sense. In fact, it is known that the two monomolecular layers of the lipid bilayer in many biological membranes have different chemical compositions, what corresponds to a transmembrane heterogeneity of the system. Microscopic (molecular scale) and macroscopic (cellular scale) in-plane heterogeneities are known to exist. Although to a chemist it is quite clear that between these two extremes (microscopic and macroscopic scales) a mesoscopic heterogeneity must also exist, this has not been clearly shown, to be the case for biological membranes primarily because of the non-existence of suitable techniques with the necessary spatial resolution for this sort of system. It must be emphasized, however, that the existence of mesoscopic heterogeneities in artificial lipid bilayers is today a generally accepted phenomenon.

Mesoscopic heterogeneity raises interesting questions with regard to phase topology which in its turn has important consequences for component distribution, percolation and chemical kinetics in the system. Here we shall address ourselves primarily to the questions of percolation and chemical kinetics emphasizing experimental and Monte Carlo simulations on model systems and the extrapolation of these results and their consequences for biological membranes.

A membrana biológica, a estrutura celular que separa a célula do seu ambiente exterior e também os compartimentos intracelulares uns dos outros, é composta essencialmente por aquilo a que se convencionou chamar "bicamada lipídica" que é constituída por duas monocamadas moleculares adjacentes formadas por lípidos anfifílicos, geralmente fosfolípidos, mas também glicolípidos e colesterol. A bicamada lipídica, um filme fluido quase-bidimensional de superfícies polares e centro apolar, com uma espessura de cerca de 10 nm, faz o papel de solvente para muitas proteínas que nela se incorporam ou se adsorvem à superfície. Esta bicamada lipídica natural tem uma composição química complexa, geralmente contendo três ou quatro classes de lípidos que se sabe não formarem misturas ideais. É, portanto, de prever que estas misturas apresentem heterogeneidade química-física. De facto, em muitas membranas biológicas as duas monocamadas constituintes da bicamada lipídica têm composição diferente, donde resulta uma heterogeneidade transmembranar. Porém, também se sabe existirem heterogeneidades, quer microscópicas (à escala molecular) quer macroscópicas (à escala celular) no plano da membrana. De um ponto de vista estritamente químico não pode deixar de existir também, entre estes dois extremos (heterogeneidade microscópica e macroscópica), uma heterogeneidade mesoscópica, embora esta nunca tenha sido evidenciada de uma forma indubitável no caso de membranas biológicas. Não podemos esquecer que não existem, actualmente, técnicas com a resolução espacial necessária para a observação destes sistemas sem criar perturbações que ponham em dúvida os resultados. Em bicamadas lipídicas artificiais a existência de heterogeneidade mesoscópica está actualmente experimentalmente provada.

Reconhecida a existência de heterogeneidade mesoscópica, fica em aberto a sua topologia que, por sua vez, condiciona a distribuição de solutos e componentes, e, em consequência, a difusão/percolação e cinética das reacções químicas no sistema. No presente trabalho abordamos os problemas levantados pela percolação e compartimentalização de reagentes em sistemas modelo, analisados quer experimentalmente quer por simulação e discutimos as consequências da extrapolação dos resultados obtidos ao caso de membranas biológicas.

Introduction

Our current understanding of the biological membrane has its origin in a report by Gorter and Grendel [1], that was subsequently developed by reports from various researchers of which the landmark papers of Danielli and Davson [2], Robertson [3] and Singer and Nicolson [4] merit special mention. Today, the generally accepted working hypothesis is that the biological membrane is a "fluid mosaic" composed basically of a mostly, if not completely, fluid lipid bimolecular layer as its basal structure with proteins "extrinsically" adsorbed to the polar surfaces of the layer or "intrinsically" dissolved in the fluid sheet. The crucial point that is made in this model is that the membrane is a quasi-two dimensional fluid sheet and all its components (lipids and proteins) are, in principle, free to diffuse (rotationally and translationally) in the plane of the sheet. A homogeneous state, in the physical-chemical sense, is generally assumed for the lipid bimolecular fluid layer. While this model has helped advance our understanding of the structure and dynamics of biological membranes and their physiological role in the cell, in that it has stimulated a considerable amount of research in the area, it leaves many questions of a more quantitative nature unanswered.

Very early studies [5] showed that under certain conditions lipids in bilayers showed immiscibility both in the solid and fluid phases. These studies have been since confirmed and extended by several workers (for a collection of data see [6]) and, from the several phase diagrams for lipid bilayers formed from binary lipid mixtures that are available now, the conclusion can be drawn that lipid immiscibility in bilayers is more the rule than the exception. This would lead us to expect that the biological membrane or, more particularly, its lipid bilayer is more probably a heterogenous system rather than a homogenous one. This has, in fact, been observed to be the case at several levels. Macroscopic heterogeneities (over dimensions that are more comparable with those of the cell than of the molecular constituents) in biological membranes have now been quite well established. Careful analysis of the chemical composition of the inner and outer leaflets of several cellular membranes shows that the two halves of these membranes have distinct compositions. Besides this inside-outside heterogeneity, a clearly defined macroscopic lateral heterogeneity, often termed "functional polarity", has been clearly shown in some cell types, epithelial cells [7] and hepatocytes [8] being some of the best studied cases from this point of view. Another form of membrane heterogeneity is observed at the microscopic level (comparable to molecular dimensions) and arises from the specific interaction of membrane components among themselves as is the case in the so-called "boundary lipid" layer around integral membrane proteins.

If immiscibility is assumed, the two-dimensional nature of the membrane should also permit heterogeneity at a mesoscopic (several 10^2 to 10^4 times molecular dimensions) level [9, 10]. Such a mesoscopic heterogeneity, while being extremely difficult to clearly demonstrate due to unavailability of experimental methods with an adequate resolution, would explain a large number of observations with regard to the dynamics of membrane constituents [9]. Jain [11] has proposed that the lipid bilayer in the fluid mosaic model should include a phase heterogeneity that results in an overall non-random distribution of components in the system. We have subscribed this point of view [12, 13] and discussed some of the consequences of this refinement of the fluid mosaic model [9, 14].

In the present paper we propose to briefly review some concepts on biological membrane heterogeneity, discuss its causes and consequences and attempt to propose new lines of research that may be important for our understanding of the complex functions of this important cellular structure.

Phase Behaviour in Lipid Bilayers

Artificial lipid bilayers, which form spontaneously when certain phospholipids are hydrated, have provided many important insights into the structural and dynamic properties of the biological membrane. While the results of studies on these systems are not always directly translatable to the lipid bilayer in a biological membrane, they do provide excellent points of reference for the understanding of these. Model lipid bilayers prepared from most of the classes of lipids commonly encountered in biological membranes are lyotropic, thermotropic and barotropic smectic liquid crystal systems that undergo specific phase transitions between one or several ordered phases and disordered phases [15]. The ordered phases typically occur at low (<40 weight %) water content, low temperatures and/or very high pressures, all of which are not very significant from the biological point of view. They are characterized by a high degree of conformational order in the lipid acyl chains and positional order of the lipid chains and of the lipids themselves over long ranges in the plane of the bilayer. The disordered (often called fluid, liquid or liquid crystalline) phases are of more biological relevance in that these are the phases found in most biological membranes under normal conditions. These phases are characterized by low conformational order in the chains and lack of long range positional order in the plane of the bilayer. A characteristic example of lipid bilayer polymorphism in a single-component lipid bilayer under constant pressure and in excess water is shown in Figure 1 in which the transitions between different phases is thermally triggered. The temperatures at which these transitions occur are dependent on the nature of the phospholipid "head groups" (polar parts that are expo-

LAMELLAR ORGANIZATION · LAYER STRUCTURE · CHAIN PACKING

Disordered Phase

L_α
Liquid, Fluid or Liquid Crystalline

Ordered Phases

$P_{\beta'}$
Rippled

L_β
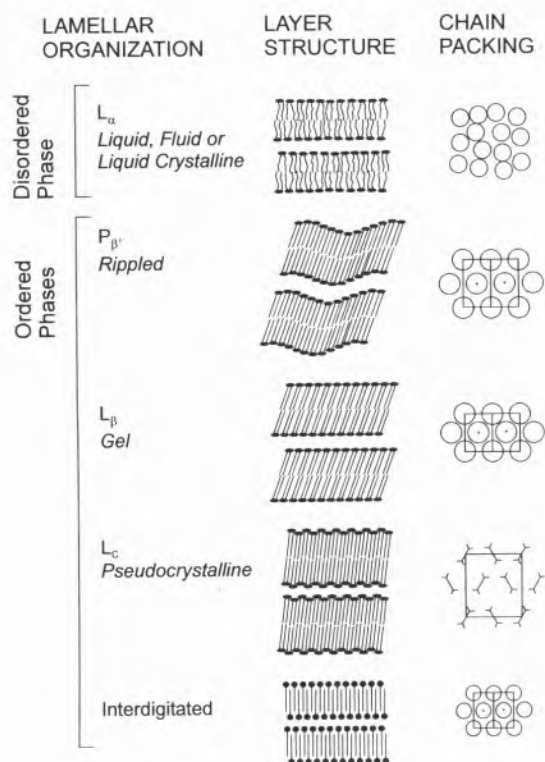Gel

L_c
Pseudocrystalline

Interdigitated

Figure 1 – Diagrams showing the layer structures and chain packing arrangements for the thermotropic phases found for pure phospholipids at constant pressure in excess water.

sed to water in the bilayer) as well as the lengths and degree and position of unsaturation of the acyl chains. When ionizable lipids are involved, the local pH and ionic strength of the aqueous phase in contact with the bilayer must also be specified since these also influence the bilayer polymorphism [16]. It is important to bear the complexity of this polymorphism in mind when considering bilayers that are composed of several constituent lipids as is the case in biological membranes.

We shall not address ourselves here to a consideration of the complexity of phase behaviour in the biological membrane. The problem is probably not addressable with the level of information we are presently capable of obtaining and processing. Rather, it is our intention to exemplify the consequences of phase separations in the lipid bilayers, as models for the far more complicated biological membranes, using simple two-phase bilayers prepared from binary lipid mixtures in which the phase diagrams have been reasonably well studied and understood. Figure 2 shows a few temperature-composition phase diagrams for lipid bilayers formed in excess water under isobaric conditions from binary lipid mixtures. It is of interest to note that the only mixture that shows complete miscibility of the chemical components in both ordered and disordered phases is one in which the two components are identical in all

respects except for a difference of two carbon atoms in their acyl chain lengths. All other systems show some degree of immiscibility either in the ordered phases and in some cases, particularly where the head groups are different, in the disordered phases as well. It is probably safe to state that in most biological membranes immiscibility in the disordered phases is more relevant since these membranes are known to be mostly fluid. The principles we shall be discussing, however, are more easily demonstrable in systems with solid-fluid phase coexistence and the lessons drawn from such models are probably equally applicable to liquid-liquid phase coexistence as well.

What causes phase coexistence in a lipid bilayer? Gibbs [17, 18] was the first to describe the conditions of chemical composition, temperature and pressure that permit phase coexistence in heterogeneous systems. Heterogeneity is a consequence of component immiscibility and the causes for this are primarily thermodynamic: the intermolecular interaction energy between two molecules in a system causes them either to associate or repel each other and entropy drives the system towards a homogenous state. This is true for any system at equilibrium. Perturbations of such systems through chemical (addition of new molecules) or physical (temperature, pressure or electrical) stresses, will cause the system to relax to a new equilibrium state at a rate that is dependent upon several processes, the kinetics of some of which may be extremely slow. It is important to remember that the biological membrane is a dynamic system, being continuously subjected to chemical and physical stresses which derive from the environment or from physiological processes such as metabolic activity of the cell and protein and lipid biogenesis, insertion and sorting [19, 20]. Hindered lateral transport [21 - 24] within the bilayer plane can make the kinetics of membrane response to these perturbations quite slow. Thus, it is very probable that the biological membrane is not a system at equilibrium and that heterogeneity in it is probably more determined by kinetic rather than by thermodynamic considerations alone.

Having accepted that heterogeneity is a fact in the biological membrane, phase disposition becomes an important consideration. Typically, in a three-dimensional fluid, phase coexistence at equilibrium is characterized by a bulk separation of the coexisting phases with a minimal interfacial area between them. The driving force for this is the interfacial surface tension which tends to reduce the interfacial area to a minimum. Reduction of the interfacial surface tension, for example by addition of surfactants to an oil-in-water or water-in-oil dispersion, reduces the tendency for bulk phase separation. In a two-dimensional system, such as the lipid bilayer, the reduction in interfacial tension is a consequence of reduced dimensionality (a two-dimensional system with an interfacial line tension as opposed to a three-dimensional system with an interfacial surface tension). Thus, one might expect microscopic to mesos-
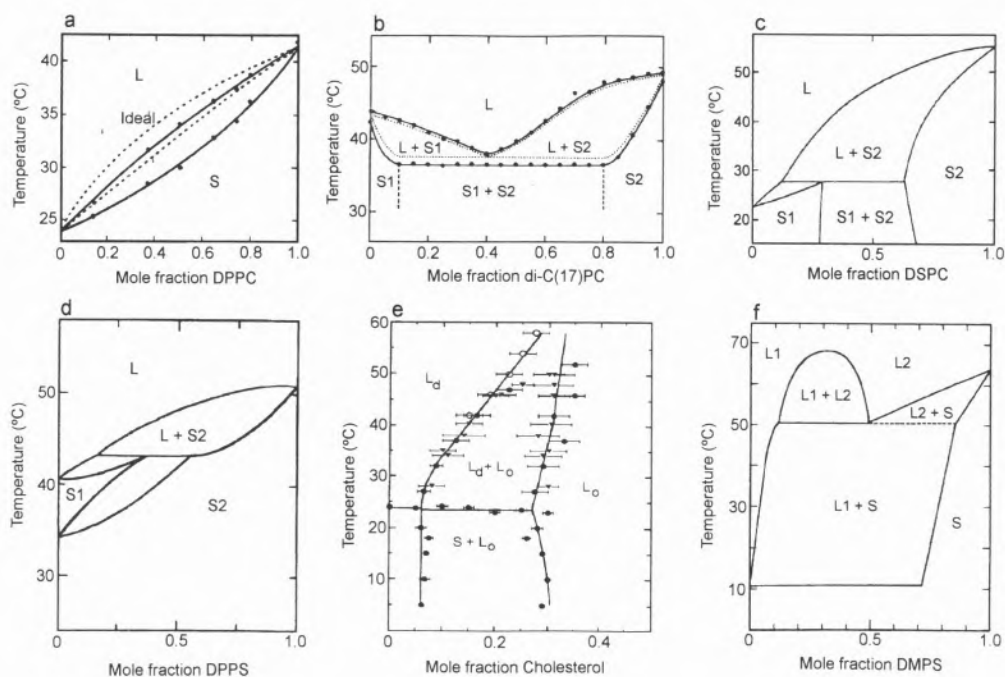
Figure 2 – Examples of temperature-composition phase diagrams for lipid bilayers in excess water under isobaric conditions. The phase diagrams are shown for: (a) isomorphous mixture of di-C(14)PC and di-C(16)PC; (b) eutectic mixture of di-C(17)PC and C(12)C(22)PC; (c) peritectic mixture of di-C(14)PC and di-C(18)PC; (d) peritectic mixture of di-C(16)PC and di-C(16)PS; (e) monotectic mixture of di-C(14)PC and cholesterol; (f) monotectic mixture of di-C(18:1, trans)PC and di-C(16)PE.

copic dispersions of coexistent phases in lipid bilayers, whether of thermodynamic or kinetic origin, to intrinsically have sufficiently long lifetimes to become physiologically relevant.

Component Distribution

From the previous section it should have become clear that we visualize the biological membrane as a heterogeneous quasi-two dimensional liquid system. The various protein species that are associated with the membrane must, strictly speaking, be viewed as chemical constituents of the system so that there is no distinction between "lipid domains" and "protein domains". Thus, under a given compositional definition of the membrane, the protein distribution in the coexistent phases will be determined by the same rules that govern lipid distribution which have been discussed earlier. An alternative view is to consider the proteins and other minor constituents of the membrane as a very small molar fraction of the system and view them as solutes in a heterogeneous solvent. From this point of view their preferential presence in one or the other of coexistent phases in a membrane is a consequence of preferential solubility in those phases. This solubility preference can be absolute so that it becomes conceivable that a given protein species is encountered exclusively in (or totally

excluded from) one or some of several coexisting phases in the membrane.

There are several examples in the literature for solubility preferences of lipid probes and proteins in lipid bilayer membranes, the most common cases being the observed preferences of lipid-like molecules for solid or fluid phases [25 - 27]. Freeze-fracture electron microscopy studies [28] clearly show that some proteins were excluded from solid phase lipid domains in bilayers with coexisting solid and fluid phases. More recently, there has been a report [29] on the phase partitioning of gramicidin between solid and fluid phases. Fluid-fluid partitioning of lipid-like molecules and proteins has never been experimentally shown but some proteins are known to show a higher affinity for certain lipids in their boundary lipid layer [30, 31] so that it may be concluded that these proteins would necessarily show a preferential solubility in phases rich in these lipids if such phases existed in the membranes. The "hydrophobic mismatch" of an integral membrane protein in a heterogeneous fluid lipid bilayer could also be a driving force for a preferential protein solubility among the coexisting phases. We [32] have recently shown that the insertion of α-hemolysin, a protein with a membrane-inserting hydrophobic sequence, into ordered liquid phase bilayers (formed from phosphatidylcholines with a high cholesterol content) is considerably more difficult than its insertion into disordered

liquid phase bilayers (formed from pure phosphatidyl-cholines or binary mixtures of these with a low choleste-rol content). While this in itself is not direct evidence for a preferential solubility of this protein in disordered liquid phases as compared to ordered liquid phases, it clearly indicates that such may be the case. Considerable work needs to be done in this regard before clear rules emerge for solubility preferences of lipid-like or protein molecules in lipid bilayers.

Another aspect of the heterogeneity of membrane protein distribution has to do with the way in which proteins are added to biological membranes in the process of membrane biogenesis. This process probably occurs via the intracellular fusion of vesicles with the target membrane [33]. In this case the newly inserted material must diffuse freely to become homogeneously distributed in the membrane. Hindrances to diffusion due to lack of percolation (see below) caused by intra-membranous or extra-membranous (cytoskeletal or glycocalyx) structure will cause a kinetic trapping of components that may lead to physiologically significant heterogeneities.

Finally, we may imagine a protein component of a membrane which, though constrained to be integrally associated with the membrane due to its hydrophobic nature, finds no ideal solvent phase among the domains available and is forced to "precipitate" or to form homologous aggregates within the bilayer plane. Several membrane protein aggregation phenomena associated with important physiological processes are known.

Percolation

The ability of membrane components to laterally diffuse in the membrane plane is an important consequence of the fluid mosaic model for biological membrane structure and dynamics. It makes interaction between the membrane components possible, thereby permitting bi- (or higher-) molecular reactions, that are important for membrane physiology, to occur. Fluorescence Recovery After Photobleaching (FRAP) is a well established technique for the study of the lateral diffusion coefficient in two dimensional samples [24,34] (see Figure 3 for a short explanation of the method and experimental setup). This method permits observation of lateral diffusion in membranes over distances of several tens to hundreds of micrometers and is useful in studies with artificial lipid bilayers as well as with cellular membranes. In the case of synthetic bilayers the experiment is performed on a stack of a few hundred fully hydrated planar bilayers deposited on a microscope slide. These bilayers are doped with a fluorescent and photobleachable tracer molecule, which in our case is a phospholipid marked with N-(7-nitro-2,1,3-benzoxadiazol-4-yl), NBD, at a fractional molar concentration of $\leq 10^{-3}$. The general recovery behavior in homogeneous fluid bilayers is presented in Figure 4A. The

fluorescence intensity, maximum before bleaching, $F(t<0)$, is reduced upon bleaching to $F(t=0)$. Then, the fluorescence intensity slowly recovers due to the diffusion of neighboring tracer molecules into the bleached spot, see Figures 3a and 4. If the reservoir of unbleached molecules is infinite, as is generally the case for fluid
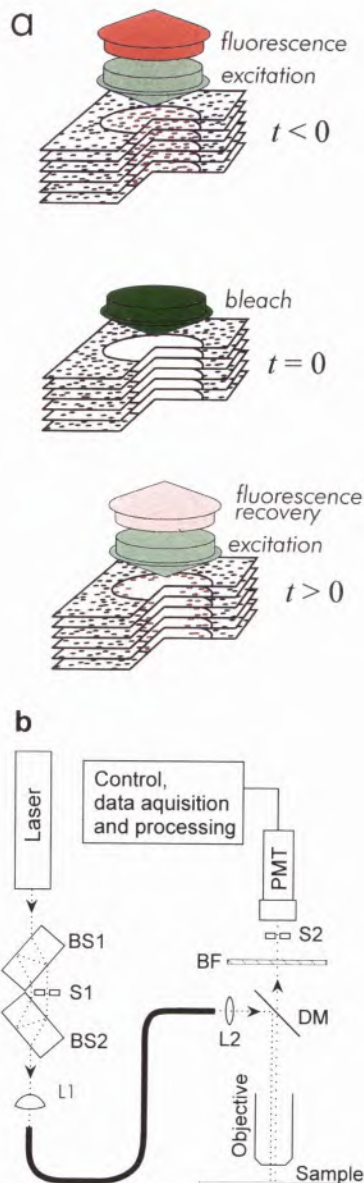

Figure 3 – Schematic description of *a)* a FRAP experiment performed on a stack of lipid bilayers, and b), the scheme of the FRAP apparatus where BS1 and BS2 are beam splitters, S1 the shutter that opens to bleach the sample with the intense pulse of light. Both analyzing and bleach beams are focused by L1 in an optical fiber whose output is focused by L2 through a dicroic mirror, DM, on the sample. The fluorescence is observed by a photomultiplier, PMT, protected from the intense bleaching pulse by the shutter S2, after being filtered by a cut-off filer BF.

homogeneous bilayers, the final fluorescence intensity attains the initial value $F(t=\infty)=F(t<0)$, that is, the fraction of recovery, R, defined by equation (1) is 1.0.

$$R = \frac{F(\infty) - F(0)}{F(t<0) - F(0)} \qquad (1)$$

The time dependent recovery curve, is parametrized by the translational diffusion coefficient of the tracer, D, and the radius of the circular bleaching spot, ω, according to equation (2) [35], where $\tau_D = \omega^2/4D$, and I represent Bessel functions. We may, therefore, obtain the diffusion coefficient of the tracer in the lipid matrix from the best fit between experimental data and equation (2), as shown in Figure 4.

$$F(t) = F(\infty) - \left[F(t<0) - F(0)\right]\left\{1 - \exp\left(-\frac{2\tau_D}{t}\right)\left[I_0\left(\frac{2\tau_D}{t}\right) + I_1\left(\frac{2\tau_D}{t}\right)\right]\right\} \qquad (2)$$

Depending on temperature, and tracer and lipid characteristics, diffusion coefficients that vary between $\approx 10^{-8}$ and $\approx 10^{-16}$ cm^2 sec^{-1} have been observed. Below the ordered-disordered phase transition temperature, when the bilayer is in the so-called gel phase, the fluorescence recovery is usually very slow and incomplete over reasonable measurement times. These experimental curves, when analyzed using equation (2) often give poor fits and, if a diffusion coefficient is to be derived, values between $\approx 10^{-10}$ and as low as $[10^{-16}]$ cm^2 sec^{-1} have been reported [36, 37], Figure 4B. In the rigid phase, part of the diffusion observed has been attributed to the mobility of the probe molecules in the grain boundaries of the two-dimensional crystals. In fact, the probe molecules, even if phospholipids of a very similar structure to those forming the bilayer, having the fluorescent probe attached to them, will always behave as impurities in the system with a high degree of order. In this way, some of the molecules will be retained in the crystals as point defects while other are forced into the grain boundary defects. The first group of tracer molecules is responsible for the incomplete and very slow recovery, and the second results in a recovery process that is not, in principle, described by equation (2).

In our work over the past decade we have attempted to describe the lateral diffusion of membrane components in phase-separated lipid bilayers in the phase coexistence region using the FRAP technique. While we are aware that ideally such studies, which serve as models for the biological system, should probably examine liquid-liquid phase coexistence, it is very difficult to encounter tracer molecules that partition exclusively in one of the coexisting phases with the consequence that data analysis becomes a very complex matter. For the purposes of percolation the principles governing diffusion are similar whether we examine liquid-liquid or solid-liquid phase coexistence. Our attention has, therefore, been mostly limited to bila-
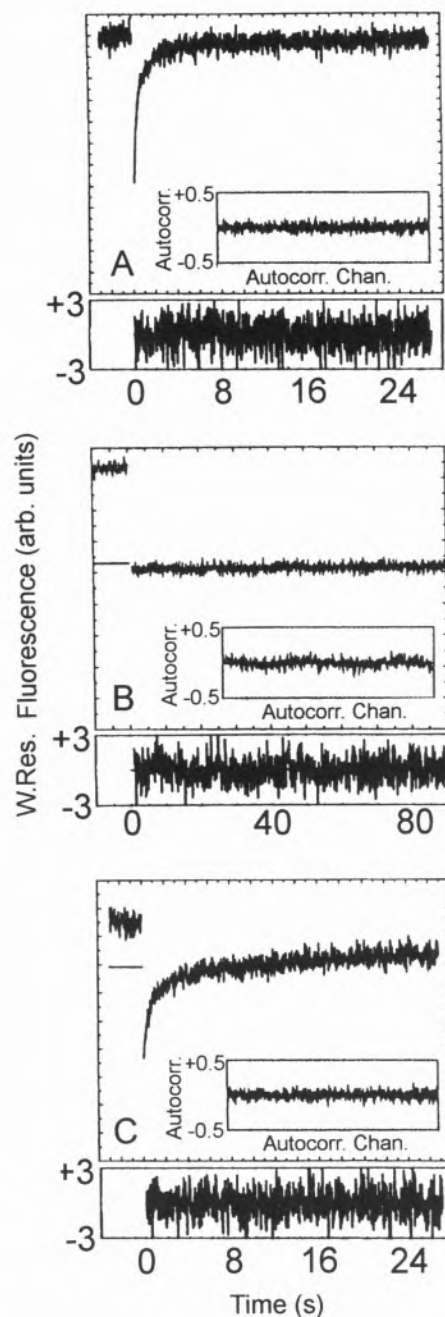

Figure 4 – Typical FRAP curves obtained for the system di-$C_{17.0}$PC / $C_{22.0}C_{12.0}$PC in multibilayers. Diagram A presents the recovery of pure di-$C_{17.0}$PC in the fluid phase, T=52.3°C for which 99% of recovery is observed and τ_D=0.21 s (corresponding to D=1.1×10^{-7} cm^2 s^{-1}); diagram B is for pure $C_{22.0}C_{12.0}$PC bellow phase transition, T=30.1°C, for which a τ_D ca. 200 s obtained corresponds to D=1.1×10^{-10} cm^2 s^{-1} and a recovery of only 3%; and diagram C is for the mixture of di-$C_{17.0}$PC with $C_{22.0}C_{12.0}$PC (80/20, mol/mol) in the phase coexistence region, T=43.2°C. The analysis of the curves A and B were performed with equation (2) and for curve 3 an additional slope had to be used in order to obtain fit to the experimental data.

yers formed from binary lipid mixtures, in which there is a clearly defined solid-liquid phase coexistence, using probes that partition almost exclusively into the fluid phase which is the case of a short chain phospholipid in a longer chain matrix or an unsaturated phospholipid in a mixture of saturated ones. Depending on the fraction of the rigid phase, obtained from the phase diagram for the mixture, a variety of behaviors are observed [26, 38 - 41] as seen in Figure 4 for the system constituted by 1-docosanoyl-2-dodecanoyl-*sn*-gycero-3-phosphocholine ($C_{22:0}C_{12:0}PC$) and 1,2-diheptadecanoyl-*sn*-gycero-3-phosphocholine (di-$C_{17:0}PC$) [40]. For small solid fractions, the recovery of fluorescence after photobleaching is slower than what is to be expected for an equivalent fluid bilayer, but the recovery is still complete, $R \cong 1.0$. On increasing the solid fraction only a partial recovery is obtained and the recovery, fast at the beginning becomes slower for long times displaying a long tail, Figure 4C. The experimental data in this last case can no more be fitted with equation (2). It is intuitive that such behavior can be ascribed to the hindrance of diffusion by the solid domains, and to the reservoir of tracer molecules accessible to the FRAP spot being no more infinite [42].

The question arises as to what the topology of a bilayer in this phase coexisting region is, and how it relates to the experimentally observed FRAP result. It has been observed that in Langmuir-Blodget monolayers with the same composition the phase-separation is visible with an optical fluorescence microscope and the rigid domains have a characteristic elliptical shape at the beginning, growing in spiral-like formations [43]. However, in bilayers it has not been possible to observe the domain geometry probably because, in this case, at least one of the linear dimensions of the objects is submicroscopic (smaller than the Abbé limit of $\sim\lambda/2$). Electron microscopy is not of much help because the sample preparation procedure disturbs the system, and the recent microscopic techniques with nanometer resolution, adequate for this type of samples, are yet under development. Therefore we are left with indirect methods to model the geometry of the separated phases and of the topology of the membrane. The results obtained by FRAP are, for this purpose, the most adequate because what is in fact observed is the arrival to the central spot (the photobleached area) of tracer molecules that have, on their way, sampled the intricacies of the membrane topology, i.e., we observe the result of the two-dimensional lateral molecular percolation through the system.

Percolation is a general phenomenon well known to the chemists, the percolation filter being very common in chemical industry. In the last two decades, however, a new body of theory for percolation in lattices has developed which results from the need to mathematically describe phenomena such as forest fire propagation, diffusion of small atoms in solid structures, or electrical conductivity of composite materials. All these processes fall within the area of discrete percola-

tion and are, in themselves, quite difficult to formalize mathematically. As a consequence, and given that problems in two spatial dimensions (plus time) are some of the more relevant cases of percolation, most of the practical cases are studied using straightforward Monte-Carlo techniques. Diffusion with percolation, or continuum percolation, is formally much more complicated than discrete percolation and has not yet received much attention from theoreticians. This lack of tools to deal with continuum percolation has been circumvented by the modeling of the continuum system as a discrete matrix with a lattice resolution such that the phenomena which are monitored are still described with sufficient approximation. In our study of percolation with diffusion in phase-separated synthetic bilayers we follow this approach.

The general case of diffusion in a plane in the presence of obstacles has been studied by Saxton using Monte-Carlo techniques [44]. In the diffusion in a homogeneous bilayer the mean-square displacement, $<r^2>$, of a molecule is proportional to the molecular diffusion coefficient, D, and to time. In obstructed diffusion the mean square displacement is still proportional to D but depends upon a fractional power of time, equation (3).

$$<r^2> = 4Dt \ (t/\tau)^{2/d_w - 1} \tag{3}$$

While for normal diffusion $d_w = 2$, in the presence of obstacles $d_w > 2$. The time constant τ is the time necessary for the probe to diffuse through the unit mean square distance. When viewed with a macroscopic technique the observed diffusion coefficient, D^*, is time dependent because the tracer molecules near the region of observation do not have to traverse the same complicated path as the more distant ones.

In a two-dimensional infinite plane of which a given fraction, p, is fluid, it has been shown that for a given geometry of the solid obstacles, randomly distributed in the plane, there is a fixed fluid fraction above which there is at least one continuous fluid cluster that connects one side of the plane with the other. This fluid fraction, characteristic of the system, is called the percolation threshold, p_c. It is important to realize that above this percolation threshold isolated finite regions of fluid do exist, but there is at least one infinite fluid cluster. Since p_c is highly dependent on the system topology we could, in principle, derive this topology from the experimental value of p_c obtained from the FRAP experiments. However, for this to be possible we first need a precise value of the percolation threshold experimentally obtained from FRAP and then need to know the shape of the elemental forms that combine to build the solid network.

To simplify the analysis of FRAP results obtained from experiments performed on systems with phase coexistence, the recovery curves were analyzed using the superposition of a fast recovery, given by equation (2), and a slow recovery, simulated by a linear ramp. The fast component describes the hindered diffusion in

an archipelago while the linear ramp models, in the experimental time range, the slow diffusion due to the defects in the gel phase. With this strategy we were able to analyze the non-conventional recovery of the fluorescence of many phospholipid systems in the region of solid-fluid phase coexistence [38-41]. In Figure 4C we present an example of the extremely good fits obtained and the data obtained from such analysis. The total recovery due only to the fast component is related to the connective fluid region that crosses the bleaching spot. At a first glance it could be suggested that since the system is either percolative or non-percolative, there should be either no recovery of fluorescence below the percolation threshold and near complete fluorescence recovery above it. However, the experimental results do not confirm these expectations as presented in Figure 5 for the system 1,2-dimyristoyl-*sn*-glycero-3-phosphocholine (DMPC) and 1,2-distearoyl-*sn*-glycero-3-phosphocholine (DSPC), 50/50 mole fraction. The sigmoid shape of the curves indicate that below p_c some flow of the tracer probe is still existent and above p_c recovery is still observed. This behavior is characteristic of percolating systems where the observation area, spot area, is of a dimension comparable with the linear dimension of the fluid regions. In figure 6 we show the theoretical variation of the fractional recovery for different relative linear dimension of the fluid areas and spot radius [45]. We may therefore conclude that whatever the geometry of the phases the dimension of the fluid phase must be of the order of magnitude of the spot radius (μm). To further define the topological characteristics of the system we have to postulate the geometric characteristics of the elements that constitute the rigid phase and verify if the resulting structure is coherent with the existing experimental data. This verification has been done by Monte-Carlo simulation of the FRAP experiments.
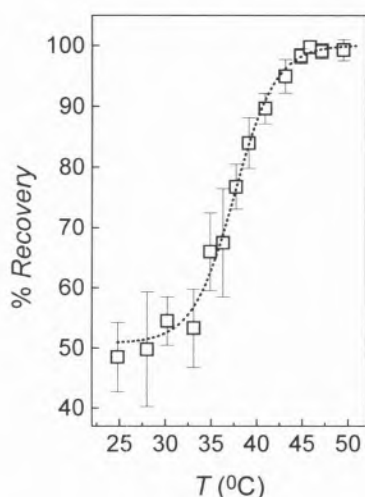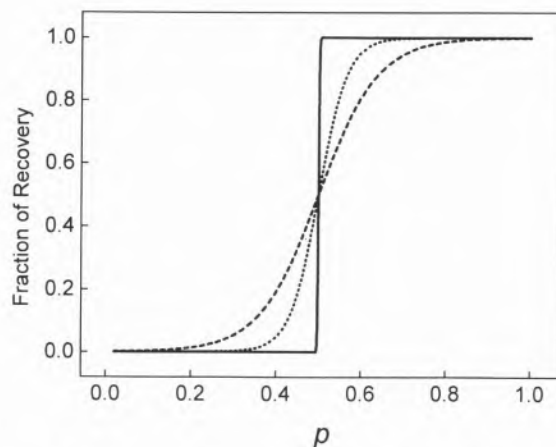

Figure 6 – Percolation theory prediction of the fraction of recovery obtained in a FRAP experiment in a system for which the percolation threshold is 0.5 for three different characteristic linear dimensions of the fluid region, L, (whatever it means in our particular case). When L is much smaller than the dimension of the spot a nearly step function is obtained, solid line, but when the observation is done with a spot similar in dimension to the characteristic dimension of the fluid there is not a well defined percolation point: dotted and dashed lines respectively for L=20 and 7.5 times the spot radius.

The simulation of the rigid phase as randomly distributed superimposable ellipses with aspect ratio b/a is convenient from the view point of percolation theory and reasonable with regard to two-dimensional phospholipid crystal shape. Percolation in 2D with randomly distributed ellipses has been thoroughly studied by Thorpe and coworkers [46,47] and, at least in monolayers, phospholipid crystals grow initially with a well known elliptical shape [43]. Based on this ellipse model we simulated the fractional fluorescence recovery as a function of the fluid fraction for the system DMPC:DSPC 50:50 [42]. The best fit to the high fluid fraction range was obtained for an ellipse major semi-axis of 1.0 μm and aspect ratio equal to 0.2 near the percolation threshold.

Using the same topological model, the FRAP curves simulated by Monte-Carlo in the time regime for the same system resulted in a not much different geometry of 1.0 μm and 0.3 for the major semi-axis and ellipse aspect ratio, respectively, near the percolation threshold [42]. The agreement between simulation and experiment is quite good except for fluid fractions below 0.4, Figure 7. The results from these simulations lead to a picture of the phase separated bilayer as represented in Figure 8. For large fluid fractions, Figure 8a, all the fluid is continuous but, near the percolation threshold, Figure 8b, many small regions are isolated, and for a fluid fraction of 0.2 all the fluid domains are very small, Figure 8c. In fact, the histograms of Figure 9 demonstrate that large fluid pools become highly improbable below the percolation threshold, p_c=0.47, and dominate immediately above it.

Figure 5 – Percent recovery for a DMPC / DSPC 1:1 molar fraction as a function of temperature.
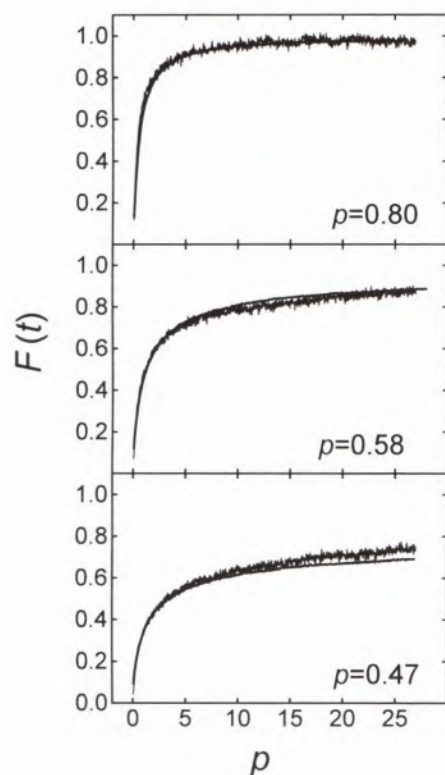
Figure 7 – Time dependent experimental fluorescence recovery curves obtained for DMPC/DSPC (1/1 mol/mol) system at three different fluid area fractions, p, and the corresponding Monte-Carlo simulations. The rigid domains were simulated as a fixed number of random ellipses that, for p=0.80, have semi-axes a=0.42 and b=0.18 μm; for p=0.58, a=0.88 and b=0.29 μm, for p=0.47, a=1.12 and b=0.30 μm.

It is to be expected that molecules of reactant proteins or any other membrane components with a structure different from the lipid matrix will be more soluble in the fluid bilayer than in the more structured rigid region. Even if it is not the case those molecules that stay in the rigid phase do not have much chance to interact because of the small diffusion coefficients. In this way the compartmentalization observed results necessarily in an inhibition of bimolecular reactions taking place between membrane components.

Reactions in heterogeneous systems

When dealing with reactions in microdispersed systems two kinds of special effects have to be taken into account: dimensional, and distributional effects. The reduced dimensionality of such systems, two-dimensional, nearly-two-dimensional, or any other case where the reactants are not free to diffuse to infinite distances, do not directly affect reaction controlled processes but, in the case of diffusion controlled or nearly diffusion controlled reactions, a quite different
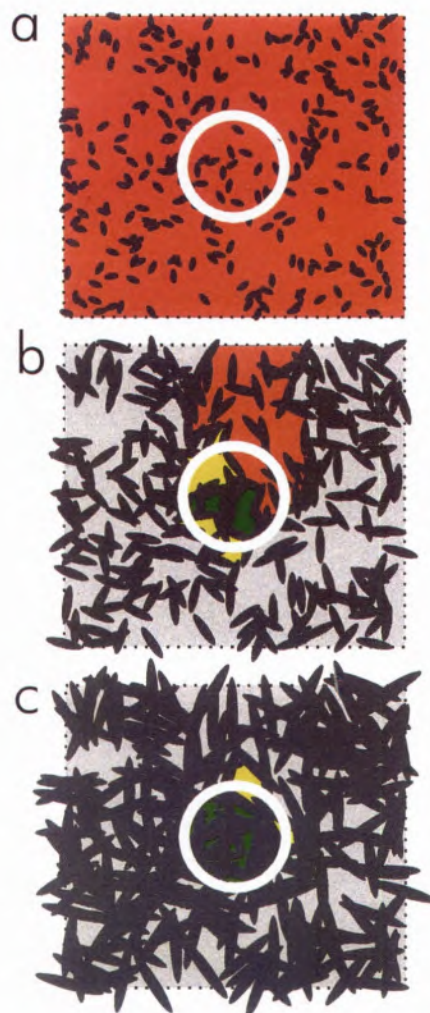

Figure 8 – Simulation of a FRAP experiment in a single bilayer plane for the DMPC/DSPC (1/1 mol/mol) system having p_c=0.47 for p=0.80 (a), 0.50 (b), and 0.20 (c). Red areas represent reservoirs that extend out of the plane (considered as completely recoverable), yellow areas partially recoverable bleached areas and those in green are unrecoverable because they are entirely closed and inside the spot.

kinetics from that expected for the equivalent 3D system is observed [48]. In what concerns the yield of the reactions, the dimensional effects will only affect those reactions for which one of the reactants is short lived. Distributional effects, however, have a marked impact upon both, the kinetics and the yield of bimolecular reactions. The consequences of distributional effects upon the yield and kinetics of reactions are better illustrated for a dimerization reaction. Consider a reaction micro-vessel where one single monomer is isolated: in this case dimerization will never take place. If, instead, two monomers are present, they dimerize, if there are three the reaction will be faster but one monomer is left unreacted. The consequences on the yield are evident,
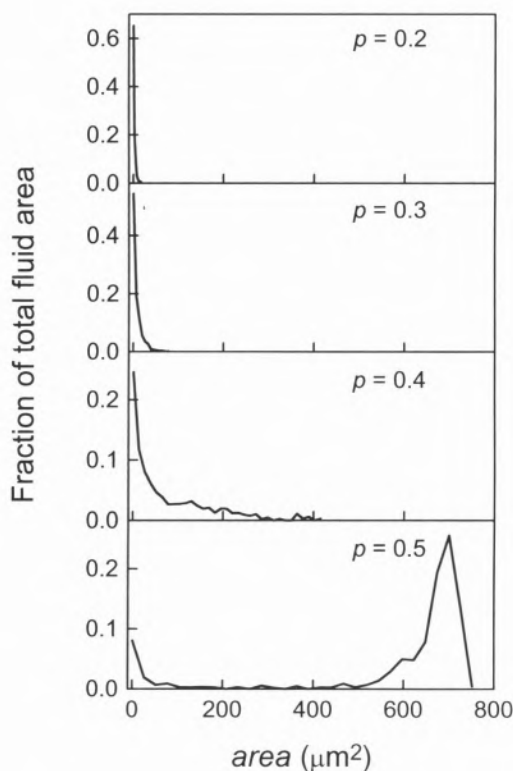
Figure 9 – Histograms of total fluid in domains with equal areas as a function of the domain areas for four different fluid fractions: p=0.2, 0.3, 0.4, and 0.5. It is to note that the plane, simulated as in previous figures, has a finite area of 1300 μm² which limits the largest fluid domain present.

and it is also obvious that the global rate coefficient of dimerization will appear time dependent with some non-zero value at the beginning, and reaching zero when only isolated single molecules are left in the compartments without the possibility of reacting. From what was said we may easily anticipate that, in the case of heterobimolecular reactions where one of the reactants is in much smaller amount than the other, the difference between homogeneous and microcompartmentalized systems will be still more evident. In the extreme case of an enzymatic reaction even a small degree of compartmentalization will result in a practical inhibition of the reaction.

To quantify the extent of the inhibition of a reaction due to the membrane phase separation we define the expected relative yield as:

$$\langle\phi\rangle = \frac{\langle\Phi_{ret}\rangle}{\langle\Phi_{cont}\rangle} \tag{4}$$

where $\langle\Phi_{ret}\rangle$ is the reaction yield expected to be achieved when the membranes are reticulated (microcompatmentallized), and $\langle\Phi_{cont}\rangle$, the yield in the homoge-

neous case. However, biological systems are *a priori* compartmentalized in physically separated units such as cells, and in model lipid bilayer systems in isolated liposomes. When the conditions are such that phase separation occurs, in each of these units, U, a number N_{dom} of non-connective fluid domains is formed. If we consider that these domains are of equal size and that their number is identical in each unit, it may be shown that [49] for a reaction of an enzyme **E** with a substrate **R** catalyzing the production of product **P**, according to the reaction scheme: $\mathbf{E} + \mathbf{R} \rightarrow \mathbf{E} + \mathbf{P}$, the relative yield of **P** will be given by

$$\langle\varphi\rangle = \frac{1 - \exp\left\{-\dfrac{[\mathbf{E}]}{[\mathbf{U}]N_{dom}}\right\}}{1 - \exp\left\{-\dfrac{[\mathbf{E}]}{[\mathbf{U}]}\right\}} \tag{5}$$

In Figure 10 the relative yield of product formation is represented as a function of N_{dom} for four different concentrations of the enzyme represented as [**E**]/[**U**]. It is immediately clear that the consequence of a phase separation, giving rise to non-connective fluid domains, has drastic consequences on the efficiency of the enzymatic reaction whenever the enzyme concentration is low which, in the biological system, is usually the case.

A common mechanism in cellular physiological processes is the formation of protein aggregates comprising a fixed number of monomer proteins. Also in this
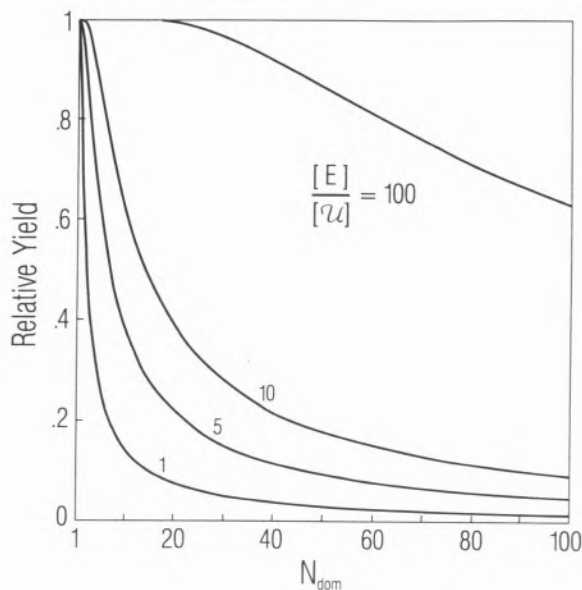

Figure 10 – Relative yield, <φ>, of product formation for a catalyzed reaction as a function of the number of domains per reaction unit, U, for different enzyme (catalyst) concentrations.

case there is a strong inhibition of the process due to isolation of the monomers in fluid non-connective domains. The relative yield for a general polymerization reaction producing aggregates of k molecules $k\mathbf{R} \rightarrow \mathbf{R}_k$ with $k = 2, 3, \ldots$ is [49]

$$\langle \varphi \rangle = \frac{1 - \exp(-\mu_{ret}) \sum_{i=0}^{\infty} \sum_{j=0}^{k-1} j \frac{\mu_{ret}^{(ki+j-1)}}{(ki+j)!}}{1 - \exp(-\mu_{cont}) \sum_{i=0}^{\infty} \sum_{j=0}^{k-1} j \frac{\mu_{cont}^{(ki+j-1)}}{(ki+j)!}} \qquad (6)$$

where the mean number of reactants per domain in the case of reticulated units is $\mu_{ret} = \frac{[R]}{[U] N_{dom}}$ which becomes μ_{cont} for $N_{dom} = 1$. For the quite common case of tetramer formation the reaction becomes inefficient even for a very small number of domains per unit, as can be seen in the representation of $\langle \phi \rangle$ as a function of N_{dom}, equation (6), for the cases of $k = 2, 3$ and 4, Figure 11.

It is clear that in the real case of a phospholipid mixture below the percolation threshold, all these physiologically relevant reactions will become highly improbable and by changing the physical-chemical state of their membrane a cell could, in principle, control many of its metabolic steps.

The effect on the yields is accompanied by a no less noticeable modification of the reaction kinetics. We have studied the kinetics of photodimerization of 12-(9-anthroyloxy) stearic acid, 12AS, in a model system constituted by a dispersion of cetyltrimethylamonium chloride, CTAC, and polyoxyethylene(10) lauryl ether, $C_{12}E_{10}$, micelles [50]. In these systems two different dimers are formed, one thermally unstable head-to-head dimer, $\mathbf{D_{hh}}$, and a stable head-to-tail dimer, $\mathbf{D_{ht}}$. The global kinetic scheme of the reaction in micelles, including the steps of exit and entrance of the monomer, A, in the micelles, is presented in the Scheme I. The exit steps are slow, as can be seen in Table I where the relevant rate constants involved in the process are presented, but for large irradiation times they lead to the randomization of the system [50]. The relative order of magnitude of the rate constants involved, is similar to what is to be expected for phospholipid bilayers with non-connective fluid domains: the reaction is nearly diffusion controlled, and the interchange of molecules between micelles model quite well the possible leakage of reagents between separated fluid domains observed in bilayers.
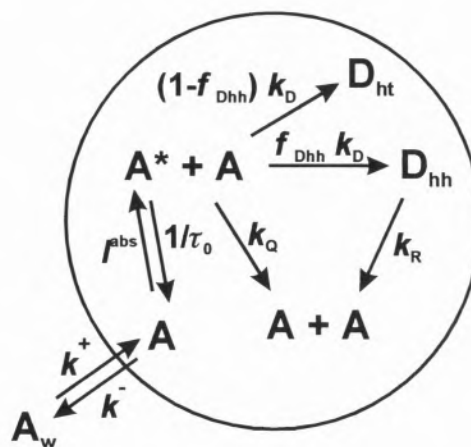
Scheme I

Table I - Steady-state photodimerization rate constant, k_D, association rate constant, k^+, and exit rate constant, k^-, for 12-(9-anthroyloxy) stearic acid, 12AS, in micelles of cetyltrimethylamonium chloride, CTAC, and polyoxyethylene(10) lauryl ether, $C_{12}E_{10}$, according to Scheme I.

Surfactant	k_D $(10^7 \, M^{-1}s^{-1})$	k^+ $(10^{10} \, M^{-1}s^{-1})$	k^- $(10^{-3} \, s^{-1})$
CTAC	2.2	1.2	0.7
$C_{12}E_{10}$	8.9	1.6	30.

In Figure 12 a simulation of our system in CTAC, irradiated with a typical light intensity and in the absence of water solubility of the reagents, displaying the time dependence of the apparent rate coefficient for the reaction defined as

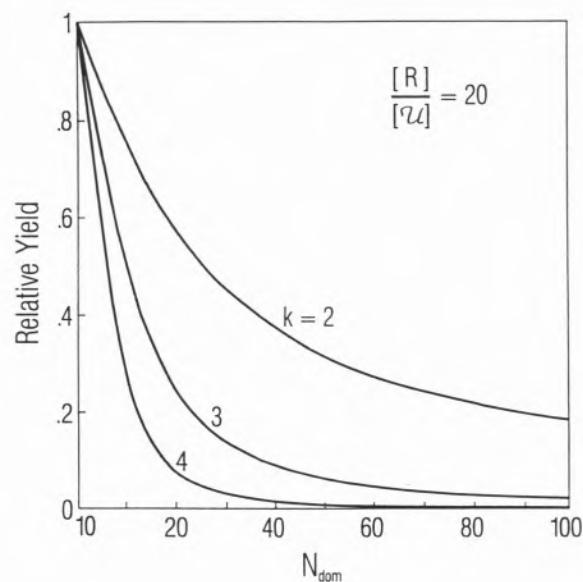$$k_{app} = \frac{\dfrac{d[A_2]}{dt}}{[A][A^*]} \qquad (7)$$

Figure 11 – Relative yield of a polimerization reaction for 20 monomers per unit as a function of the number of domains per unit. Plots are presented for the case of dimer ($k=2$), trimer ($k=3$), and tetramer ($k=4$).

is presented for several occupation numbers. The value of the time-independent rate constant for a homogeneous phase with the same characteristics of the micelle media is also shown for comparison. Due to the large number of molecules left unreacted when the occupation number is small, see insert of Figure 12 where the yield of the reaction is presented, the apparent rate coefficient attains values near zero immediately after the beginning of the irradiation.
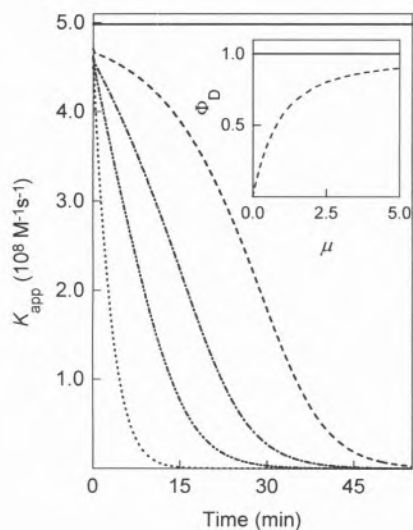

Figure 12 – Theoretical simulation of a non-reversible photodimerization reaction in a micelar system without exchange of monomers between micelles. Variation of k_{app}=(d[A_2]/dt)/[A][A*], with time of irradiation for mean occupation values of 0.3 (···), 1.0 (–··–), 2.0 (–·–), and 5.0 (– – –). The solid horizontal line, at the top, indicates the rate constant of the same reaction in a homogeneous media with identical characteristics. Inset: efficiency of dimerization in the homogeneous (——) and comparmentalized (– – –) system as a function of the mean occupation number, μ.

The effect of the rate of entrance and exit from the micelles, k^+ and k^-, is to reduce the difference between homogeneous and compartmentalized media but, as may be seen in Figure 13, only when the interchange is quite fast the behavior approaches the one observed for homogeneous media. It should, however, be noted that, once interchange is considered, the theoretical relative yield of the reaction is unity no matter how much time the system will need to approach this maximum yield [50].

The results obtained with this micellar system show how important the distribution of reactants in non-communicating compartments can be for the kinetics of a bimolecular reaction triggered by an external factor, light in our case.
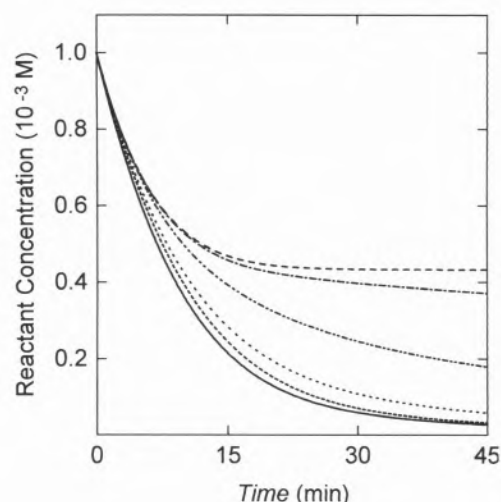

Figure 13 – Theoretical simulation of the disappearance of reactant concentration as a function of time in a photodimerization reaction in micelles when exchange between micelles is considered and compared with the reaction in homogeneous phase (——). Curves are plot for k- (s^{-1}) = 0.0 (– – –), 1×10^{-4} (–··–), 1×10^{-3} (–·–), 1×10^{-2} (···), 1×10^{-4} (–·–), 10.0 (---),

Relevance to Biological Systems

In a recent paper we have discussed several consequences of phase separations in membranes [9]. What follows will be a brief synopsis of those considerations.

Biological membranes are the interface of communication between the cell and its environment. Reception and processing of information from the environment will, therefore, be conditioned by the ability of the membrane to respond to external stimuli so that the consequences of heterogeneity in this structure could be quite significant. Processing of information involves membrane protein activity at the unimolecular (first order reaction) level and the ability of membrane components to react with each other at the multimolecular (second or higher order reactions) level.

Conformation and dynamics of proteins, and as a consequence their activity, is largely conditioned by the environment. When a membrane protein encounters itself in a given membrane phase, the physical (fluidity and lateral pressure) and chemical (ionic environment, charge and hydrogen-bonding ability) properties of that phase may condition the activity of the protein [31]. This concept can be applied to membrane-bound enzymes and receptors. The relationship between membrane lipid environment and membrane enzyme activity has been well studied and it is not uncommon in receptor biochemistry and pharmacology to encounter multiple affinities of a single receptor species in a membrane for its ligand.

42

Without excluding other plausible explanations, we propose that these multiple affinities may be a consequence of multiplicity of membrane environments for the receptor population in a given membrane as the consequence of phase coexistence in it.

As shown in the preceding sections, the effects of membrane heterogeneity on reaction yields and reaction kinetics can be quite significant. When reactants are micro-compartmentalized, reaction yields are, in the extreme case, limited to encounters at the phase boundaries which implies a slow reaction rate and very low reaction yields. In homogenous media the reactions proceed to completion at a considerably faster, often diffusion-controlled, rate. As a consequence, transitions between heterogeneous and homogenous states, induced by physical and/or chemical processes, will imply simultaneous transitions in the rate and yields of chemical reactions that occur in the system and could act as trigger processes that may be important in cell physiology.

Assuming that membrane components (proteins and lipids) show preferential partitioning (solubility) behavior in different coexistent membrane phases, the existence of heterogeneity raises questions with regard to long-range diffusivity of these components. The range and rate of diffusion is, as discussed earlier, a function of the percolative properties of the membrane lipid bilayer. A considerable body of evidence indicates that protein diffusion in cellular plasma membranes is generally hindered. This has been generally attributed to various types of associative interactions of these proteins both within and outside the membrane but can also be interpreted in terms of the percolative behavior in a heterogeneous membrane context [9].

Finally, microscopic and mesoscopic domains in a membrane may be diffusionally trapped by specific binding interactions of one or more of their components with structures that are external to the cell. Situations can be visualized in which such a diffusional trapping forces domains of an identical phase to come in contact with each other so that the phase boundary between them disappears and the domain size grows. This sort of growth can eventually lead to a macroscopic phase separation as is seen in many cells. Elsewhere [9] we have hypothetically described the formation of apical and basolateral domains and the formation of the tight junction in epithelia.

Bibliography

1. E. Gorter, F. Grendel (1925) *J. Exper. Med.* **41**, 439-443.

2. J.F. Danielli, H. Davson (1935) *J. Cell. Comp. Physiol.* **5**, 595-610.

3. J.D. Robertson (1959) *Biochem. Soc. Symp.* **16**, 3-43.

4. S.J. Singer, G.L. Nicolson (1972) *Science* **175**, 720-731.

5. S.H. Wu, H.M. McConnell (1975) *Biochemistry* **14**, 847-854.

6. D. Marsh (1990) CRC Handbook of Lipid Bilayers, pp. 234-263, CRC Press, Boca Raton, FL.

7. K. Simons, S.D. Fuller (1985) *Ann. Rev. Cell Biol.* **1**, 243-288.

8. W.H. Evans (1980) *Biochim. Biophys. Acta* **604**, 27-64.

9. W.L.C. Vaz (1996) In: Handbook of Non-Medical Applications of Liposomes, Vol. II: Models of Biological Phenomena (Y. Barenholz, D. Lasic, editors), Ch. 3, pp. 51-60, CRC Press, Boca Raton, FL.

10. K. Huang (1987) In: Statistical Mechanics, 2nd. edition, pp. 408-412, John Wiley, New York.

11. M.K. Jain (1983) In: Membrane Fluidity in Biology (R.C. Aloia, editor), pp. 1-37, Academic Press, New York.

12. W.L.C. Vaz, P.F.F. Almeida (1993) *Current Opinion Struct. Biol.* **3**, 482-488.

13. K. Jacobson, W.L.C. Vaz, editors (1992) Comments on Molecular and Cellular Biophysics Vol. 8: Domains in Biological Membranes, Gordon & Breach, London.

14. W.L.C. Vaz (1994) *Biophys. Chem.* **50**, 139-145.

15. G. Cevc, D. Marsh (1987) Phospholipid Bilayers: Physical Principles and Models, John Wiley, New York.

16. H. Träuble (1977) In: 34th. Nobel Symposium: Structure of Biological Membranes (S. Abrahamsson, I. Pascher, editors), pp. 509-550, Plenum Press, New York.

17. J.W. Gibbs (1877) *Trans. Connecticut Acad.* **3**, 108-248.

18. J.W. Gibbs (1877) *Trans. Connecticut Acad.* **3**, 343-524.

19. M.P. Lisanti, E. Rodriguez-Boulan (1990) *Trends Biochem. Sci.* **15**, 113-118.

20. K. Simons, G. van Meer (1988) *Biochemistry* **27**, 6197-6202.

21. R.M. Clegg, W.L.C. Vaz (1985) In: Progress in Protein-Lipid Interactions, Vol 1 (A. Watts, J.J.H.H.M. De Pont, editors), pp. 73-229, Elsevier, Amsterdam.

22. W.L.C. Vaz, F. Goodsaid-Zalduondo, K. Jacobson (1984) *FEBS Letters* **174**, 199-207.

23. K. Jacobson, A. Ishihara, R. Inman (1987) *Ann. Rev. Physiol.* **49**, 163-175.

24. T.M. Jovin, W.L.C. Vaz (1989) In: Methods in Enzymology, Vol. 172, (S. Fleischer, B. Fleischer, editors), pp. 471-513, Academic Press, New York.

25. L.A. Sklar, G.P. Miljianich, E.A. Dratz (1979) *Biochemistry* **18**, 1707-1716.

26. W.L.C. Vaz, E.C.C. Melo, T.E. Thompson (1989) *Biophys. J.* **56**, 869-876.

27. J.F. Tocanne (1992) *Comments Mol. Cell. Biophys.* **8**, 53-72.

28. W. Kleemann, H.M. McConnell (1974) *Biochim. Biophys. Acta* **345**, 220-230.

29. A.R.G. Dibble, M.D. Yeager, G.W. Feigenson (1993) *Biochim. Biophys. Acta* **1153**, 155-162.

30. D. Marsh (1987) *J. Bioenerg. Biomemb.* **19**, 677-689.

31. P.F. Devaux, M. Seigneuret (1985) *Biochim. Biophys. Acta* **822**, 63-125.

32. L. Bakás, H. Ostolaza, W.L.C. Vaz, F.M. Goñi (1996) *Biophys. J.* **71**, 1869-1876.

33. I. Mellman, editor (1996) *Current Opinion Cell Biol.* **8**(4), 497-574

34. W.L.C. Vaz, Z.I. Derzko, K. Jacobson (1982) In: Cell Surface Reviews, Vol. 8: Membrane Reconstitution (G. Poste, G.L. Nicolson, editors), pp. 83-136, Elsevier, Amsterdam.

35. D.M. Soumpasis (1983) *Biophys. J.* **41**, 95-97

36. Z. Derzko, K. Jacobson (1980) *Biochemistry* **19**, 6050-6057.

37. M.B. Schneider, W.K. Chan, W.W. Webb (1983) *Biophys. J.* **43**, 157-165.

38. W.L.C. Vaz, E.C.C. Melo, T.E. Thompson (1990) *Biophys. J.* **58**, 273-275.

39. T. Bultmann, W.L.C. Vaz, E.C.C. Melo, R.B. Sisk, T.E. Thompson (1991) *Biochemistry* **30**, 5573-5579.

40. P.F.F. Almeida, W.L.C. Vaz, T.E. Thompson (1992) *Biochemistry* **31**, 7198-7210.

41. P.F.F. Almeida, W.L.C. Vaz, T.E. Thompson (1993) *Biophys. J.* **64**, 399-412.

42. F.P. Coelho, W.L.C. Vaz, E. Melo (1997) *Biophys. J.* **72**, 1501-1511.

43. D.J. Keller, J.P. Korb, H.M. McConnell (1987) *J. Phys. Chem.* **91**, 6417-6422.

44. M.J. Saxton (1994) *Biophys. J.* **66**, 394-401

45. P.F.F. Almeida (1992) Ph.D. Dissertation, University of Virginia.

46. W. Xia, M.F. Thorpe (1988) *Phys. Rev. A* **38**, 2650-2656.

47. E.J. Garboczi, M.F. Thorpe, M.S. De Vries, A.R. Day (1991) *Phys. Rev. A* **43**, 6473-6482.

48. J. Martins, W.L.C. Vaz, E. Melo (1996) *J. Phys. Chem.* **100**, 1889-1895

49. E.C.C. Melo, I.M.G. Lourtie, M.B. Sankaram, T.E. Thompson, W.L.C. Vaz (1992) *Biophys. J.* **63**, 1506-1512.

50. M.J. Moreno, I.M.G. Lourtie, E. Melo (1996) *J. Phys. Chem.* **100**, 18192-18200.

Molecular Thermochemistry: 20 Years of Experiments and Estimates

Termoquímica Molecular: 20 Anos de Experiências e Estimativas

MANUEL E. MINAS DA PIEDADE[1] and JOSÉ A. MARTINHO SIMÕES[2]

[1] CENTRO DE QUÍMICA ESTRUTURAL, COMPLEXO I, INSTITUTO SUPERIOR TÉCNICO, 1096 LISBOA CODEX, PORTUGAL
[2] DEPARTAMENTO DE QUÍMICA E BIOQUÍMICA AND CITECMAT, FACULDADE DE CIÊNCIAS, UNIVERSIDADE DE LISBOA, 1700 LISBOA, PORTUGAL

The present paper provides a brief overview of Molecular Thermochemistry research made at Lisbon, throughout two decades. Those experimental studies, which have been concerned with the energetics of many organometallic, organic, and inorganic substances, led to the development of methods to estimate new data. A few recent examples, including β-elimination and DNA-repair reactions, and the bonding in alkaline metal alkoxides and fullerenes, were selected to illustrate the energetics-structure-reactivity relationship.

Apresenta-se, neste artigo, uma breve panorâmica dos estudos sobre Termoquímica Molecular realizados em Lisboa, nos últimos vinte anos. O trabalho experimental, que envolveu uma variedade de compostos organometálicos, orgânicos e inorgânicos, conduziu também ao desenvolvimento de métodos de estimativa de novos dados termoquímicos. Com o objectivo de ilustrar a relação entre energética, estrutura e reactividade moleculares, são apresentados alguns exemplos recentes, incluindo reacções de eliminação β e de reparação do ADN, bem como a investigação da natureza das ligações químicas em fullerenos e em alcóxidos de metais alcalinos.

1. Is Molecular Thermochemistry old-fashioned?

Molecular Thermochemistry aims to investigate the stability of individual molecules. *Stability* is, however, a fairly ambiguous concept. A water molecule, which meets our intuitive criteria of endurance, is promptly destroyed in the presence of sodium atoms. Methane, with its four strong carbon-hydrogen bonds, is easily consumed by reaction with oxygen. Hydrogen peroxide, having a rather weak oxygen-oxygen bond, may survive forever under appropriate conditions. Therefore, a given molecule exists only under certain physical and chemical environments. And when it is said to be *stable*, one should ask: "Stable, relative to what?".

Thermodynamics provides the tools to analyze the type of stability mentioned above, known as *thermodynamic stability*. For instance, the yield of a chemical reaction in the gas phase, at a given temperature and pressure, can be calculated from the equilibrium constant (K), which is related to the standard Gibbs energy of that reaction.

As indicated by the familiar equation 1, $\Delta_r G_m^\circ$ can be obtained from the standard enthalpy and entropy of the reaction. $\Delta_r H_m^\circ$ and $\Delta_r S_m^\circ$ can in turn be derived from the standard enthalpies of formation and the standard entropies of reactants and products [1].

$$- RT \ln K = \Delta_r G_m^\circ = \Delta_r H_m^\circ - T\Delta_r S_m^\circ \qquad (1)$$

A reaction Gibbs energy is therefore a measure of the thermodynamic stability of a given molecule, under given chemical and physical conditions. However, at room temperature, the term $T\Delta_r S_r^\circ$ is often small compared to $\Delta_r H_m^\circ$, implying that the reaction enthalpy is the dominant term in equation 1. As $\Delta_r H_m^\circ$ is calculated from the standard enthalpies of formation, these quantities can thus be regarded as gauges of thermodynamic stability.

A large number of Molecular Thermochemistry studies have been concerned with the thermodynamic stability of chemical bonds rather than with the thermodynamic stability of molecules as a whole. Both types of information - bond dissociation enthalpies

(see Appendix) and enthalpies of formation, respectively - enable the calculation of reaction enthalpies. In many occasions, however, the former are the only data available. Consider, for instance, vitamin E (α-tocopherol, TcOH; see Figure 1), which breaks the lipid peroxidation cycle by reacting with a lipid peroxyl radical (ROO•) [2]. Although the enthalpies of formation of reactants and products are unknown, the enthalpy of reaction 2 can be calculated from equation 3 because the enthalpies of the bonds cleaved and formed are accessible.

$$ROO^\bullet(sln) + TcOH(sln) \rightarrow ROOH(sln) + TcO^\bullet(sln) \quad (2)$$

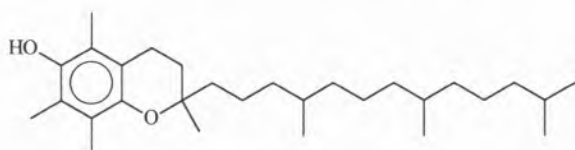$$\Delta_r H^\circ_m(2) = DH^\circ_{sln}(TcO-H) - DH^\circ_{sln}(ROO-H) \quad (3)$$

Figure 1 – Chemical structure of α-tocopherol.

The importance of bond dissociation enthalpies is not confined to the calculation of reaction enthalpies. They may also lead to insights into reaction kinetics and mechanisms. For example, Ingold and coworkers have found a correlation between the O–H bond dissociation enthalpies of several substituted phenols and the respective rate constants of the hydrogen abstraction reactions by peroxyl radicals [3]. The low O–H bond dissociation enthalpy in vitamin E is consistent with a high rate constant of reaction 2 and is in keeping with the good antioxidant properties of this substance.

A general treatment of the fascinating bridges between thermochemistry and kinetics is included in a famous book by Benson [4]. Unfortunately, the relationships are not always as simple as in the case of substituted phenols. It is often found that the *kinetic stabilities* of molecules belonging to a given family do not correlate with their thermodynamic stabilities. The former, being determined by the reaction mechanism, depend on the size of the activation barrier and on other details of the reaction profiles; the latter are simply determined by the thermodynamics of reactants and products. In other words, the instability of a molecule can have a "purely" kinetic origin.

The distinction between thermodynamic and kinetic stability of a compound or a chemical bond was the driving force to start the thermochemical studies in Lisbon, some 20 years ago. The groups of Wilkinson and Lappert had noted that the instability of some transition metal compounds containing metal-carbon bonds could have a kinetic root [5,6] and would not necessarily imply that those bonds were weak. It had been

recognized, for example, that a metal complex $M(L)^n(C_2H_5)$, where L represents a ligand like phosphine, cyclopentadienyl, etc., decomposes through a mechanism known as β-elimination. As observed in Scheme 1, the destabilization of the four-centered transition state, due to the stretching of the metal-carbon bond, is compensated by the formation of an incipient metal-hydrogen bond. The pathway does not require the simple cleavage of the M–C σ bond. Hence, the thermodynamic stability cannot be inferred from the decomposition temperature of the compound.
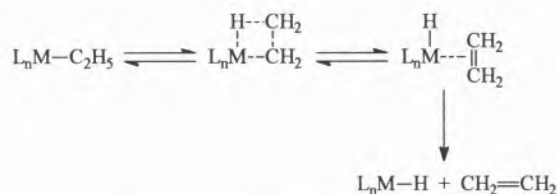
Scheme 1

In 1975, the controversy around the stability of transition metal-alkyl complexes stimulated the interest of Romão Dias, head of the Organometallic Chemistry group at IST, and Calado, head of the Experimental Thermodynamics group at the same Institute. One of the outcomes of joint discussions was the decision to hire a graduate student to work on the project. Another was to use some form of calorimetry to investigate the problem. As this technique was not in their area of expertise, in order to proceed more rapidly some outside help was sought. Two groups (from the University of Manchester, UK, and University of Porto, Portugal) gave a very significant contribution during the first steps. The British group (Skinner, Pilcher and Connor [7]) was the leading authority on thermochemistry of organometallic compounds and used several types of calorimetry, particularly Calvet (heat-flux) microcalorimetry. The interests of the Portuguese group, headed by Ribeiro da Silva, were in thermochemistry of coordination complexes. The main technique used in their studies was isoperibol reaction-solution calorimetry. To make a long story short, after an undetermined number of attempts to probe the thermochemistry of some molybdenum and tungsten bis(η5-cyclopentadienyl) complexes, $M(Cp)_2L_2$ (M = Mo, W; L = H, Me), anaerobic reaction-solution calorimetry (RSC) was finally recognized as the best method to investigate the thermodynamic stability of those compounds [8,9]. Since then, RSC has been used in Lisbon to study the thermochemistry of many organometallic compounds, aiming to examine the systematics of metal-ligand bond dissociation enthalpies and to explore new methods to predict the enthalpies of reactions involving transition metal compounds. Some of this work, now shared by people from three institutions (Instituto Superior Técnico, Faculdade de Ciências da Universidade de Lisboa, and Instituto Tecnológico e Nuclear), has been reviewed elsewhere [10,11].

Information about the stability of molecules and bonds has been steadily accumulating throughout the past two decades. The development of new experimental methodologies, in solution and in the gas phase, allowed the thermochemical study of neutral and ionic molecular species that are not amenable to classical calorimetry. A pictorial overview of the main methods - old and new - is shown in Figure 2. Here, it is deliberately stressed that bond energies (or bond enthalpies), rather than enthalpies of formation, are the goal of most studies in modern thermochemistry. As noted above, there are many molecules for which only bond dissociation enthalpy data are available, this being especially true for organometallic compounds [11,12]. But perhaps the most striking feature of Figure 2 is the large number of techniques that have contributed to the present knowledge in Molecular Thermochemistry. Actually, the number is even higher than indicated, because some gas phase techniques and some auxiliary methodologies have been omitted. Why then, such a variety? The answer is quite simple: the investigation of the stability of any molecule is a very specific task. The choice of a given technique is often dictated by the nature of atoms that constitute the molecule, by its physical state, and by its lifetime.

Despite all the efforts to increase the amount and the quality of thermochemical data, there are still many important gaps to be filled. Today, the databases of enthalpies of formation and bond dissociation enthalpies are fairly large [12-17], particularly for organic and inorganic substances, but there is (and there will always be) a large difference between the sizes of those databases and the virtually infinite number of known molecules. As a result, several empirical methods for estimating those data have been developed [4,13,17-20]. It can be anticipated that these research lines will have increased importance in the future, but their progress depends on the availability of experimental data, needed to test the reliability of the estimates and also to "calibrate" quantum chemical calculations. Computational Chemistry methods have been playing a rather significant role in Molecular Thermochemistry and some of them afford highly reliable results, for many species. The fast improvement of hardware and software will strengthen that role and Computational Chemistry will replace many experimental methodologies.

From what has been said in this short outline, which included a short digression through the origins of the "Lisbon group", it seems clear that Molecular Thermochemistry is not a science from the past. No doubt that some of the techniques in Figure 2 are over 100 years old. It is also true that the available empirical estimation schemes and Computational Chemistry methods are often reliable enough to replace laboratory work. But it is also a fact that many more enthalpies of formation and bond enthalpy data are needed to improve our understanding of chemical structure and reactivity, whose relationship is in the core of modern chemical research [21].

The present interest in Molecular Thermochemistry is best demonstrated by the variety of recent experimental techniques, depicted in Figure 2, which have extended our ability to study the energetics of species like short-lived ions and radicals. Furthermore, the selected examples addressed in the following paragraphs show that the use of "classical" methods, such as calorimetry, still have a significant and unreplaceable role. The most classical of them all, combustion calorimetry, is fundamental to probe the thermochemistry of molecules such as buckminsterfullerene. Finally, a single example of an
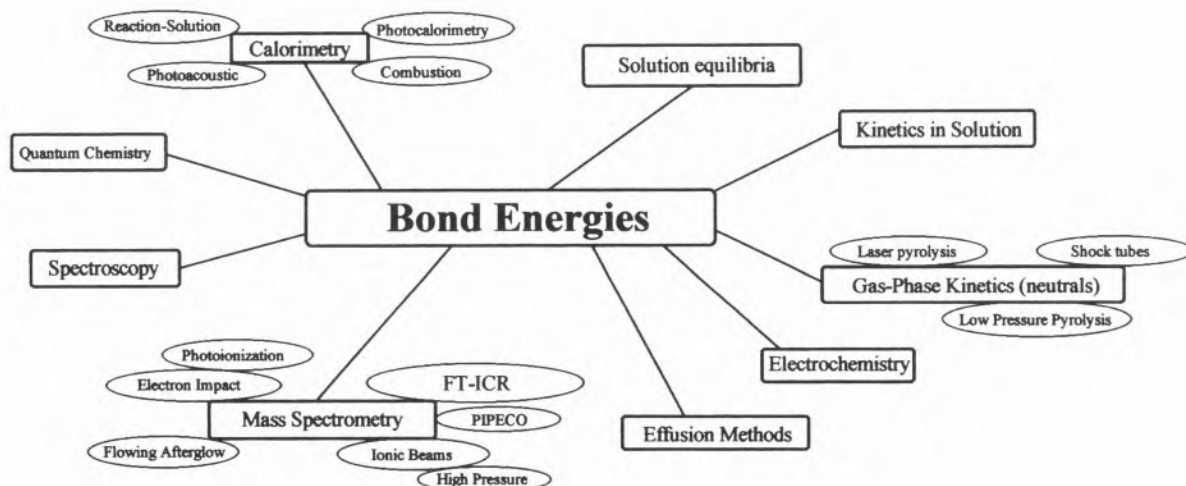

Figure 2 – Methods used to study the thermochemistry of chemical bonds.

area where the present thermochemical knowledge is rather scanty: the solvation of free radicals. The combination of gas-phase and solution data, obtained from some of the techniques displayed in Figure 2, will refine our understanding of the solvent effect on the chemical behavior of those species.

2. β-Hydride Elimination

As stated above, bond dissociation enthalpy data, $DH°$ (M−L) (M = metal center; L = ligand), obtained from reaction-solution calorimetry experiments, have been used, by us and others, to investigate trends in the chemical reactivity of organometallic complexes. The scope of these studies can be illustrated by the discussion of the β-hydride elimination reaction (Scheme 1), which is the most important decomposition pathway for transition metal, lanthanide and actinide alkyl complexes containing β-hydrogen substituents, and a key elementary step in many catalytic cycles [22]. For ethyl (Et) and butyl (Bu) derivatives the reaction can be represented by equations 4 and 5, respectively.

$$L_nM–Et \rightarrow L_nM–H + H_2C=CH_2 \quad (4)$$

$$L_nM–Bu \rightarrow L_nM–H + H_2C=CHC_2H_5 \quad (5)$$
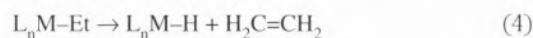
L_nM is a coordinatively unsaturated metal complex with n ancillary ligands, L. The enthalpies of reactions 4 and 5, $\Delta_r H_m°$ (4) and $\Delta_r H_m°$ (5), can be related to bond dissociation enthalpies by equations 6 and 7, respectively.

$$\Delta_r H_m° (4) = DH° (M–Et) + DH° (C_2H_{-4}H) – DH° (M–H) \quad (6)$$

$$\Delta_r H_m° (5) = DH° (M–Bu) + DH° (C_4H_{-8}H) – DH° (M–H) \quad (7)$$

Table 1 lists enthalpies of β-hydride elimination for various organometallic systems. These values were calculated from $DH° (C_2H_4–H) = 151.5±4.0$ kJ/mol [11,13] and $DH° (C_4H_8–H) = 144.1±8.0$ kJ/mol [11,13], and from the experimentally measured or estimated M–H, M–Et and M–Bu bond dissociation enthalpy data indicated in the Appendix [10,11,23-36]. Analysis of Table 1 suggests that, with the notable exception of the rhodium system, the reaction is more endothermic, and therefore less favorable, for actinides and early transition metal complexes, than for late transition metal complexes. In addition, β-hydride elimination from a butyl ligand to give 1-butene is more favorable than the corresponding reaction for an ethyl ligand.

In reactions 4 and 5 a terminal alkene is generated by β-hydride elimination. It is interesting to compare the thermochemistry of this type of reaction with that of a reaction in which a non-terminal alkene is formed, and also with the thermochemistry of a reaction that yields a

Table 1. Enthalpies of β-hydride elimination reaction for various transition metal and actinide systems (reactions 4 and 5; see text and Appendix). Data in kJ/mol.

Complex [a]	$\Delta_r H_m°$	
	L = Et	L = Bu
$Th(Cp^*)_2L_2$	82±11	63±14
$Th(Cp^*)_2(O\text{-}t\text{-Bu})L$	94±11	72±18
$Th(Cp^*)_2(Cl)L$	77±11	66±16
$Th(Cp^*)_2[OCH(t\text{-Bu})_2]L$	113±18	102±18
$U(Cp^*)_2[OSi(t\text{-Bu})(Me)_2]L$	109±10	98±14
$Zr(Cp^*)_2L_2$	79±7	68±12
$Hf(Cp^*)_2L_2$	94±11	72±15
$Mo(Cp)_2L_2$	51±13	41±17
$Mo(Cp)(CO)_3L$	55±13	44±15
$W(Cp)_2L_2$	44±8	33±13
$Mn(CO)_5L$	76±12	65±16
$Rh(tmp)L$	104	93
$Ir(Cl)(CO)(PMe_3)_2(I)L$	39±9	20±22
$Pt(PR_3)_2(Cl)L$	51±37	40±38

[a] $Cp^* = \eta^5\text{-}C_5Me_5$; tmp = 5,10,15,20-tetrakis(2,4,6-trimethylphenyl)porphyrinato dianion.

cyclic alkene from a cyclic alkyl. Recent reaction-solution calorimetry studies of $Zr(Cp)_2(Cl)R$ (R = H, alkyl) complexes allow us to make these comparisons (reactions 8-11) [37].
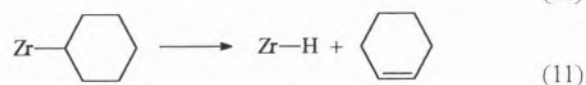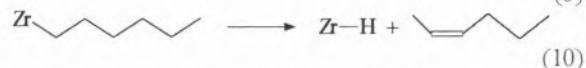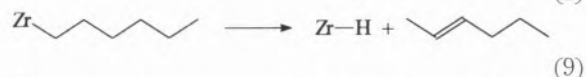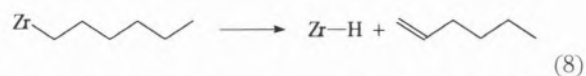
The enthalpies of reactions 8-11 are given by equations 12-15 where Hx = hexyl, Cy = cyclohexyl,

$$\Delta_r H_m° (8) = DH (Zr–Hx) + DH (1\text{-hexene–H}) – DH (Zr–H) \quad (12)$$

$$\Delta_r H_m° (9) = DH (Zr–Hx) + DH (E\text{-2-hexene–H}) – DH (Zr–H) \quad (13)$$

$$\Delta_r H_m° (10) = DH (Zr–Hx) + DH (Z\text{-2-hexene-H}) – DH (Zr–H) \quad (14)$$

$$\Delta_r H_m° (11) = DH (Zr–Cy) + DH (CY\text{-hexene-H}) – DH (Zr–H) \quad (15)$$

By using, $DH°$(Zr–H) = 364±5 kJ/mol [37], $DH°$ (Zr–Hx) = 317±10 kJ/mol [37], $DH°$ (Zr–Cy) = 319±7 kJ/mol [37], $DH°$ (1-hexene–H) = 141.4±8.2 kJ/mol [11,13], $DH°$ (E-2-hexene–H) = 131.0±8.1 kJ/mol [11,13], $DH°$ (Z-2-hexene–H) = 132.6±8.1 kJ/mol [11,13], $DH°$ (cy-hexene–H) = 155.1±4.0 kJ/mol [11,13], it is concluded that $\Delta_r H°_m$(8) = 94±14 kJ/mol, $\Delta_r H°_m$(9) = 84±14 kJ/mol, $\Delta_r H°_m$(10) = 86±14 kJ/mol, and $\Delta_r H°_m$(11) = 110±10 kJ/mol. These results indicate that, at least for this Zr system, it is less favorable to obtain a terminal alkene from a linear alkyl ligand coordinated to a metal center by β-hydride elimination, than a non-terminal alkene. It can also be concluded that it is less favorable to generate a cyclic alkene from the parent coordinated cyclic alkyl, than a linear (terminal or non-terminal) alkene from the parent alkyl ligand. Note that, since $DH°$ (Zr–Hx) ≈ $DH°$ (Zr–Cy), this last conclusion is mainly due to the fact that $DH°$ (cy-hexene–H) considerably exceeds $DH°$ (1-hexene–H), $DH°$ (E-2-hexene–H), and $DH°$(Z-2-hexene–H).

We have been discussing reactivity trends based on the exothermicity or endothermicity of a reaction, more exothermic meaning more favorable conversion of reactants into products. However, as stated above, the thermodynamic driving force of a chemical reaction is measured by the Gibbs energy of reaction, which, in addition to an enthalpic contribution also includes an entropic term (equation 1). A large and negative $\Delta_r H°_m$ (a very exothermic reaction) in conjunction with a large and positive $T\Delta_r S°_m$ will favor the yield of the reaction.

It has already been noted that the enthalpic term usually dominates the entropic term around room temperature. This explains why $\Delta_r S°_m$ is frequently ignored in the discussion of reaction thermochemistry. In some cases, however, $T\Delta_r S°_m$ makes an important contribution or even determines the sign of $\Delta_r G°_m$. For example, studies of reaction 16 in tetrahydrofuran, lead to $\Delta_r H°_m$ (16) = -30.5 kJ/mol and $T\Delta_r S°_m$ (16) = -31.9 kJ/mol, at 298.15 K [38]. This corresponds to $\Delta_r G°_m$ = 1.4 kJ/mol. In this case, ignoring the entropic contribution (i.e. making $\Delta_r G°_m ≈ \Delta_r H°_m$) results in an extremely large error in the value of the equilibrium constant ($K = 1.8×10^5$ instead of $K = 0.57$).

$$Cr(CO)_3(PCy_3)_2 \text{ (sln)} + H_2 \text{ (sln)} \rightarrow Cr(CO)_3(PCy_3)_2(\eta^2\text{-}H_2) \text{ (sln)} \quad (16)$$
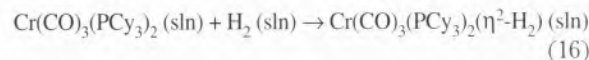
Fortunately, the entropy of a reaction essentially depends on the net change of the internal and external degrees of freedom between reactants and products and not on the types of bonds broken and formed. Therefore, $\Delta_r S°_m$ for organometallic reactions can frequently be identified with known $\Delta_r S°_m$ values for model organic or inorganic reactions that mimic the changes in degrees of freedom of the organometallic reaction [39]. For example, an estimate of the entropy of reaction 11 can be made by using reactions 17 or 18 as models. The values of $T\Delta_r S°_m$ at 298.15 K, for reactions

17 and 18, are 42.7 kJ/mol and 45.8 kJ/mol, respectively [16,40]. Note that, although different reactants and products are involved in reactions 17 and 18, the corresponding entropy changes are similar. It is therefore expected that the $T\Delta_r S°_m$, value for reaction 11 can be identified with the average of the two above values, ca. 44 kJ/mol, with a small error (less than 5 kJ/mol). The exercise can be repeated for reaction 8 by using reactions 19 and 20 as models. In these cases, $T\Delta_r S°_m$ = 37.9 kJ/mol and $T\Delta_r S°_m$ = 42.6 kJ/mol, respectively. The values are very similar to those obtained for reactions 17 and 18, showing that, in general, for β-hydride eliminations an entropic contribution of ca. 35-45 kJ/mol should be considered. This reaction is thus favored by a $T\Delta_r S°_m$ term which may offset $\Delta_r H°_m$ for late transition metal systems (Table 1).

(17)

(18)

(19)

(20)
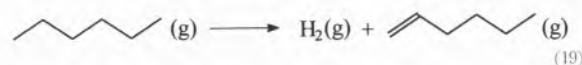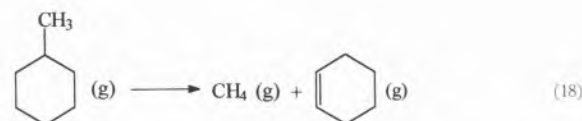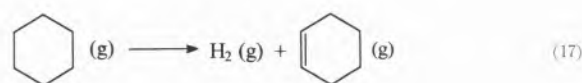
3. Alkaline Metal Alkoxides

The thermochemistry of sodium and lithium alkoxides has been the subject of two publications from our group [41,42]. This work, which has now been extended to other metals (K, Rb, Cs, Mg, Ca) [43], is recalled here to illustrate a typical application of reaction-solution calorimetry results in the area of solid-state Inorganic Chemistry. The data will also be used to make a very brief description of a procedure for estimating standard enthalpies of formation of inorganic and organometallic compounds, which we like to call Tina's method, after our colleague (Clementina Teixeira, IST) who first suggested it.

The standard enthalpies of formation of the crystalline compounds MOR, where M = Li or Na, and R is an alkyl group, have been derived from the enthalpies of their reactions with water or with aqueous hydrochloric acid solutions. As shown in Figure 3, when $\Delta_f H°_m$ (MOR, cr) are plotted against the standard enthalpies of forma-

tion of the respective liquid alcohols, $\Delta_f H^\circ_m$ (ROH, 1), good linear correlations are observed in the case of R = *n*-alkyl. The relationships are described by equation 21, which can then be used to estimate enthalpies of formation of other *n*-alkoxides by using literature data for $\Delta_f H^\circ_m$ (ROH, 1).
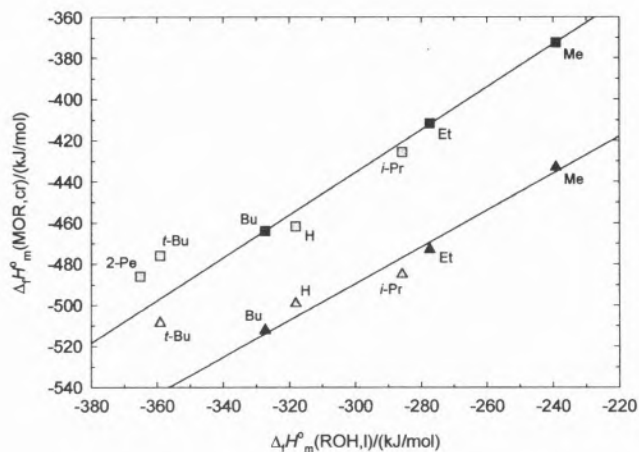

Figure 3 – Standard enthalpies of formation of sodium (squares) and lithium (triangles) alkoxides versus the standard enthalpies of formation of the corresponding alcohols.

$$\Delta_f H^\circ_m (MOR, cr) = a\Delta_f H^\circ_m (ROH, 1) + b \qquad (21)$$

The method illustrated by this equation has been applied to numerous organic, inorganic and organometallic families of molecules and subject to a detailed analysis [18,37,41,42,44-54]. Here only a few aspects will be emphasized. First, note that the points for R = *t*-Bu lie clearly above the line, i.e. their enthalpies of formation are higher than expected from the enthalpy of formation of *t*-butyl alcohol. It has been suggested that these destabilizations may be related to different solid state structures of the alkoxides rather than to steric effects [42]. However, it has also been shown that a simple modification of equation 21, which includes the group electronegativities of RO in the molecules MOR (M = Li, Na) and ROH, allows to fit all the experimental data within a few kilojoules, indicating that the "high" values have - at least in part - an electronic origin [42].

Another interesting use of equation 21 is that it enables to estimate gas-phase MO-R bond dissociation enthalpies. For the alkoxides that fit the correlation, it is possible to conclude that the differences DH°(M-OR) – DH°(RO-H) are approximately constant [41,42]. As the O-H bond dissociation enthalpies in alcohols fall in a narrow range, with an average of ca. 499 kJ/mol, $< DH^\circ$(Li-OR) $> = 394$ kJ/mol and $< DH^\circ$(Na-OR) $> = 280$ kJ/mol could be derived [41,42].

The strongly ionic nature of the MOR bond has been confirmed by calculating the lattice energies, U°,

of the alkoxides, through the Born-Haber cycle shown in Figure 4, or, alternatively, by deriving the heterolytic MOR bond dissociation enthalpies, DH°(M$^+$- OR$^-$), through the cycle in Figure 5. It was found that the lattice energies of the alkoxides are only less than ca. 10% lower than the lattice energies of the hydroxides, U°(NaOH) = 886.4 kJ/mol and U°(LiOH) =1028.4 kJ/mol, which have a rather ionic M–OR bond. A similar variation has been observed for the heterolytic bond dissociation enthalpies.

The thermochemical cycle in Figure 5 also affords estimates of the sublimation enthalpies of the alkoxides, by using the DH°(M–OR) and U°(MOR) data. This is particularly useful because these quantities are not easy to obtain experimentally for many ionic-type compounds. It has been concluded that $\Delta^g_{cr} H^\circ_m$(MOR) for the *n*-alkoxides are in the range of 215-230 kJ/mol [41, 42]. Incidentally, the value calculated for LiOMe, 216 kJ/mol, together with the experimental value for $\Delta_f H^\circ_m$ (LiOMe, cr) = -433.0±2.4 kJ/mol, leads to $\Delta_f H^\circ_m$ (LiOMe,g) = -217 kJ/mol, which is in excellent agreement with a theoretical result derived by Sana *et al.*, -214 kJ/mol [55].
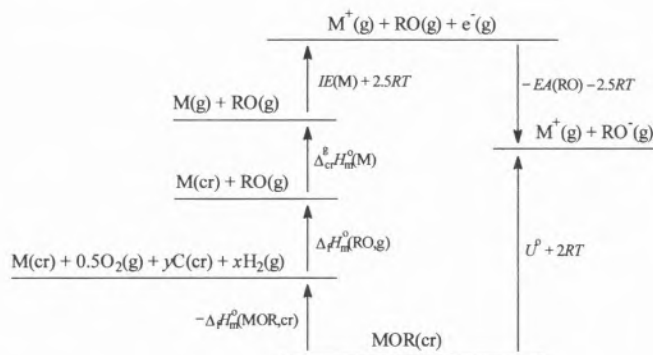

Figure 4 –Born-Haber cycle for alkaline metal alkoxides. *IE*(M) and *EA*(RO) are the ionization energy of the alkaline metal and the adiabatic electron affinity of the alkoxy radical, respectively.
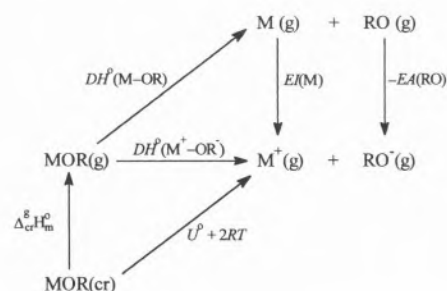

Figure 5 – Thermochemical cycle for estimating the enthalpies of sublimation of alkaline metal alkoxides.

4. They came from outer space!

The search for complex molecules in the shell of gas and dust surrounding red giant stars, and for the origin of the diffuse interstellar bands, led to what is probably the most revolutionary discovery in chemistry in the latest years - the fullerenes [56]. Until 1985, only six crystalline forms of carbon were known: two forms of graphite, two forms of diamond, chaoit and carbon(VI). But in September 1985, a new form of carbon, C_{60}, shaped like a soccer ball (Figure 6), was
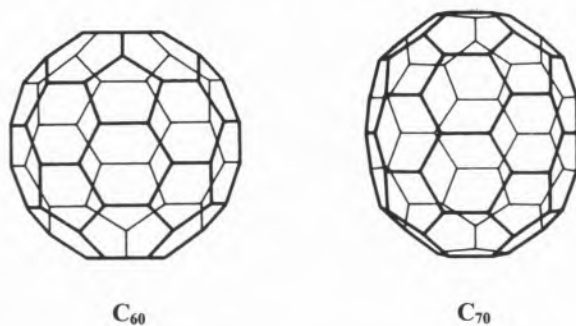

C_{60} C_{70}

Figure 6 – The structures of the two most famous fullerenes: C_{60} and C_{70}.

postulated by a group led by Kroto from Sussex University, U. K., and Smalley and Curl, from Rice University, U. S. A. [57]. The existence of this species was proposed from mass spectral evidence obtained in experiments involving laser vaporization of graphite in a laser-supersonic cluster beam apparatus. The C_{60} molecule and the related C_{70} (Figure 6) were finally isolated in 1990 by a team composed of Krätschmer and Fostiropoulos from the Max Planck Institute of Nuclear Physics in Heidelberg, Germany, and Lamb and Huffman, from the University of Arizona, U. S. A. [58]. There is now a whole galaxy of fullerenes, extending well beyond C_{100}, as well as other carbon structures such as carbon nanotubes. The chemistry of the fullerenes is also undergoing rapid development and many organic, inorganic, and organometallic derivatives have been prepared [59]. For the discovery of the fullerenes Kroto, Curl and Smalley were awarded the 1996 Nobel Prize in Chemistry.

The enthalpies of formation of C_{60} and C_{70} are key values to establish the thermodynamic stability of these molecules, and also to assess the results of Computational Chemistry methods that are used to predict the properties of the fullerenes and their mechanisms of formation. Microcombustion calorimetric experiments in our laboratory led to $\Delta_f H^\circ_m$ (C_{60}, cr) = 2278.1±14.4 kJ/mol and $\Delta_f H^\circ_m$ (C_{70}, cr) = 2577.8±16.2 kJ/mol, at 298.15 K [60,61]. Statistical mechanical calculations of

the heat capacities of gaseous C_{60} and C_{70} as a function of the temperature, in conjunction with a critical survey of the literature data for their heat capacities in the crystalline state and their enthalpies of sublimation, enabled to derive the enthalpies of formation of gaseous C_{60} and C_{70}, at 298.15 K [60-62]. The obtained results are compared in Table 2 with other experimental [60,61,63-68] and theoretically predicted [69-88] values, reported in the literature.

The agreement between the experimental results in Table 2 is far from satisfactory. It is however sufficient to set reliable upper and lower limits for $\Delta_f H^\circ_m$ (C_{60}, g) and $\Delta_f H^\circ_m$ (C_{70}, g). These limits can be used to assess the theoretical predictions, which show much larger discrepancies (Table 2). In general, the results of the *ab initio* methods, or of semi-empirical calculations specifically parameterized for fullerenes, are closer to the experimental values. It is also interesting to note that the empirical group additivity method of Armitage and Bird [78], which is based on enthalpy of formation data for polycyclic aromatic hydrocarbons, predicts the enthalpies of formation of C_{60} and C_{70} with remarkable accuracy.

The data in Table 2 also indicate that the enthalpy of formation per carbon atom, $\Delta_f H^\circ_m / n$ (n = number of carbon atoms in the fullerene), is smaller for C_{70} than for C_{60}. This conclusion supports the theoretical prediction that a general tendency exists for a decrease of $\Delta_f H^\circ_m / n$, towards zero, with the increasing size of the fullerenes [89] - the bigger the fullerene the closer its structure becomes to that of graphite, which has $\Delta_f H^\circ_m / n = 0$. It also indicates that, at room temperature, C_{70} is thermodynamically more stable than C_{60}.

The carbon-carbon mean bond dissociation enthalpies, $\overline{DH^\circ}$ ($C_f - C_f$), for C_{60} and C_{70}, can be derived from equation 22. Here, m is the number of bonds in the fullerene (m = 90 for C_{60} and m = 105 for C_{70}) and $\Delta_f H^\circ_m$ is the enthalpy of atomization of the fullerene, i. e. the enthalpy of reaction 23.

$$\overline{DH^\circ}(C_f - C_f) = \frac{\Delta_a H^\circ_m}{m} \tag{22}$$

$$C_n (g) \rightarrow nC (g) \tag{23}$$

The enthalpies of atomization of C_{60} and C_{70} can be calculated from $\Delta_f H^\circ_m$ (C, g) = 716.68±0.45 kJ/mol [90] and the enthalpies of formation of the fullerenes in Table 2. When these data are used with equation 22 it is possible to conclude that $\overline{DH^\circ}$ ($C_f - C_f$) is in the range 448.9–450.5 kJ/mol for C_{60} and in the range 451.2–453.2 kJ/mol for C_{70}. Thus, $\overline{DH^\circ}$ ($C_f - C_f$) is slightly larger in C_{70} than in C_{60}, as expected from the above conclusion that, at room temperature, C_{70} is thermodynamically more stable than C_{60}. For comparison, the bond enthalpy terms for single, double, and aromatic C–C bonds are E(C–C) = 357.6 kJ·mol, E(C=C) = 556.5 kJ·mol, and $E(C_b–C_b)$ = 498.6 kJ/mol [17].

Table 2. Comparison between experimental and theoretical results for the enthalpies of formation of C_{60} and C_{70} in the gas phase.
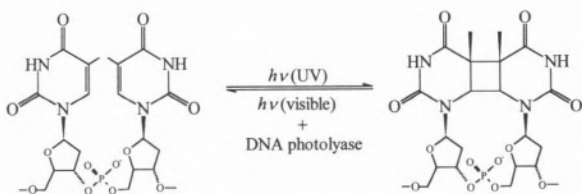
$\Delta_f H^\circ_m(g)$ / (kJ/mol)		Method	Reference
C_{60}	C_{70}		
1197	1443	MMP2	69
2175	2438	MM2	70
2217		*ab initio* SCF	71
	2611	MNDO calibrated using experimental data for C_{60}	72
2322	2465	Tight-binding hamiltonian	73
2398	2676	MM3	74
2401	2665	MM3	64, 75
2435		*ab initio* STO-3G and extrapolation method	76
2510	2661	*ab initio* HF-LYP/DZP//MNDO	77
2653	2714	Group additivity method	78
	2785	MNDO calibrated using experimental data for C_{60}	79
2615	2790	*ab initio* HF/STO-3G	74
2812		*ab initio* HF/6-31G*//STO-3G and group additivity method	80
2884	3051	MNDO calibrated using data for graphite	69, 81
3012		*ab initio* STO-3G and group additivity method	82
3392	3699	PM3	72, 79, 83
	3700	PM3	84
3633	3930	MNDO, standard parameters	72, 79
3637	3954	MNDO, standard parameters	81, 83, 85- 87,
4069	4443	AM1	72, 79
4072	4485	AM1	69
4092		PRDDO	88
2459±14[a]	2788±21[b]	Experimental	60,61
2454±15[a]	2585±22[b]	Experimental	63
2508±17[a]	2765±22[b]	Experimental	64
2463±10[a]		Experimental	65
2603±14[a]		Experimental	66
2536±15[a]		Experimental	67
2540±10[a]		Experimental	68

[a] Calculated using $\Delta^g_{cr}H^\circ_m (C_{60})$ = 181±2 kJ/mol, at 298.15 K [62].

[b] Calculated using $\Delta^g_{cr}H^\circ_m (C_{70})$ = 210±13 kJ/mol, at 298.15 K, selected in reference 61.

5. Energetics of DNA Repair by DNA Photolyases

Exposure of DNA to ultraviolet radiation results in the formation of pyrimidine dimers, as a consequence of a cycloaddition reaction between two neighbor pyrimidines in the double helix (Scheme 2) [91]. This reaction constitutes the highest quantum yield damage caused to DNA by UV-light [91]. In a wide variety of living organisms, the lesion can be reversed, in a light-assisted process, by enzymes called DNA photolyases (Scheme 2) [92].

As can be seen in Scheme 2, the repair process involves the cleavage of a cyclobutane ring. For reaction 24, at 298.15 K, $\Delta_r H^\circ_m$ = 76.5±0.8 kJ/mol [13] and $T\Delta_r S^\circ_m$ = 51.4 kJ/mol [40], implying that $\Delta_r G^\circ_m$ = 25.1 kJ/mol. This result could suggest that the repair process might be endergonic. In order to test this hypothesis and to understand the driving force of the enzyme action, the enthalpies of formation of compounds **1** and **2** (equation 25) were determined by microcombustion calorimetry. The obtained values, $\Delta_f H^\circ_m(\mathbf{1}, cr)$ = -1006.6±3.7 kJ/mol and $\Delta_f H^\circ_m(\mathbf{2}, cr)$ = -1116.6±3.7 kJ/mol, lead to an enthalpy of −110.0±5.2 kJ/mol for the clea-

Scheme 2

vage of the model photodimer **1** (reaction 25) [93]. This reaction should also have a positive entropy contribution, and therefore, contrary to reaction 24, is exergonic. In conclusion, although photoenzymes can induce strongly endergonic reactions through the formation of a high energy enzyme substrate complex, this is not the case of DNA photolyases, as suggested by our study: according to the model used, the role of the enzyme is purely kinetic.

It is also interesting to note that the exothermicity of reaction 25, when compared to the endothermicity of reaction 24, reflects the additional strain in the pyrimidine photodimer, when compared to the simple cyclobutane ring, and the formation of the more stable delocalized double bond in the pyrimidine ring.

$$\square \ (g) \longrightarrow \ \| \ (g) + \| \ (g) \qquad (24)$$

(25)
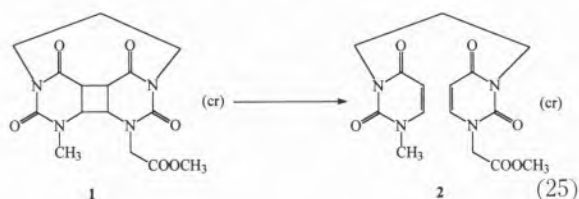
6. Conclusion

The four examples described in the previous paragraphs, which stemmed from our own research interests or were the result of fruitful collaborations with other groups, illustrate how we have been using thermochemical methodologies to examine several issues in different areas of Chemistry. As hinted by the discussions above, some of these problems are still being addressed by more laboratory work. The thermodynamic stability of organometallic substances and metal-ligand bonds, for instance, which has been at the center of our research interests for many years, still plays a significant role in our group's activity. Besides new experiments and the development of estimation methods, the work in this area now includes a general critical analysis of all the data available in the literature [12].

The above case-studies involved only the two main techniques that so far have been used in our research – reaction-solution calorimetry and microcombustion calorimetry. More recently, other experimental methods (photocalorimetry, photoacoustic calorimetry, and ion-cyclotron resonance mass spectrometry) have been added to our thermochemical tools, allowing to extend the range of problems we wish to address. Photocalorimetry has enabled to probe the thermochemistry of some light-induced reactions [94]. Photoacoustic calorimetry, and ion-cyclotron resonance mass spectrometry will enable, for example, to investigate the solvation energetics of transient species.

Appendix

The definition of the most common thermochemical quantities, such as *standard enthalpy of formation*, can be found in Physical Chemistry textbooks [1]. Other, more specific, thermochemical quantities, referred to in this paper, are discussed, for example, by Cox and Pilcher [17]. Nevertheless, for the sake of clarity, some definitions are given below.

Consider the methane molecule. The C–H *bond dissociation enthalpy*, $DH°(CH_3 - H)$, is the enthalpy of the following reaction:

$$CH_4(g) \rightarrow CH_3(g) + H(g)$$
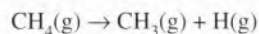
The *mean* C–H *bond dissociation enthalpy*, $DH°(C-H)$, is one fourth of the *enthalpy of atomization* of methane:

$$CH_4(g) \rightarrow C(g) + 4H(g)$$
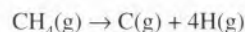
The concept of *bond enthalpy term, E*, can be better illustrated by using ethane as an example. The C–C and C–H bond enthalpy terms in this molecule are the quantities whose sum reproduces the enthalpy of atomization of C_2H_6. In this atomization reaction, one C–C bond and six primary C–H bonds are cleaved:

$$C_2H_6(g) \rightarrow 2C(g) + 6H(g)$$
$$\Delta_a H_m° = E(C-C) + 6E(C-H)_p$$
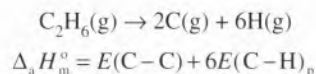
All species above are in their standard states and at 298.15 K.

Bond dissociation enthalpies (and bond enthalpy terms) should only be defined in the ideal gas phase because otherwise they would be affected by intermolecular interactions. However, from a practical point of view, *solution-phase bond dissociation enthalpies, $DH°_{sln}$*, are often used, since many important reactions occur in solution. Also, reliable solvation enthalpy data are very scarce, hindering the calculation of gas phase values from solution experiments. The C–H bond dissociation enthalpy of methane in solution, $DH°_{sln}(CH_3 - H)$, would be defined as above, with all the species (reactant and products) in solution, at infinite dilution.

Appendix – Bond dissociation enthalpies for various transition metal and actinide complexes [10,11,23-36]. Data in kJ/mol.[a]

Complex	$DH°$(M – L) or $\overline{DH°}$(M – L)		
	L = H	L = Et	L = Bu
Th(Cp*)$_2$L$_2$	(388±6)[b]	318±8	307±9
Th(Cp*)$_2$(O-t-Bu)L	(388±6)[b]	330±8	316±15
Th(Cp*)$_2$(Cl)L	(388±6)[b]	313±8	(310±12)[c]
Th(Cp*)$_2$[OCH(t-Bu)$_2$]L	389±6	(3501±7)[d]	347±15
U(Cp*)$_2$[OSi(t-Bu)(Me)$_2$]L	342±5	(299±7)[e]	(296±10)[e]
Zr(Cp*)$_2$L$_2$	339±2	(266±5)[f]	(263±8)[f]
Hf(Cp*)$_2$L$_2$	346±7	(288±8)[g]	274±10
Mo(Cp)$_2$L$_2$	257±8	156±9	154±12
Mo(Cp)(CO)$_3$L	282±6	(185±11)[h]	(182±11)[h]
W(Cp)$_2$L$_2$	311±4	(203±5)[i]	(200±9)[i]
Mn(CO)$_5$L	245±10	(169±6)[j]	(166±9)[j]
Rh(tmp)L	251	203	(200)[k]
Ir(Cl)(CO)(PMe$_3$)$_2$(I)L	C + (109±15)[l]	C – (41±0)	[C – (15±14)][m]
trans-Pt(PR$_3$)$_2$(Cl)H	307±37 (R = Ph)	206 (R = Et)	(203)[n]

[a] Values in parentheses are estimates.

[b] Average of $DH°$(Th – H) = 384±6 kJ/mol in Th(Cp*)$_2$[O-2,6-(t-Bu)$_2$C$_6$H$_3$]H, $DH°$(Th – H) = 389±6 kJ/mol in Th(Cp*)$_2$[O-CH(t-Bu)$_2$]H, and $\overline{DH°}$(Th–H) = 390 kJ/mol in [Th(Cp*)$_2$H]$_2$.

[c] Estimated from $DH°$(Th–Et) = 313±8 kJ/mol, $DH°$(Et–H) = 421±4 kJ/mol, and $DH°$(Bu–H) = 418±8 kJ/mol, by assuming that $DH°$(Th–Et) $DH°$(Th–Bu) = $DH°$ –(Et–H) $DH°$(Bu–H).

[d] Estimated from $DH°$(Th–Bu) = 347±15 kJ/mol, by using the assumption in note c.

[e] Estimated from $DH°$(U–Me) = 317±6 kJ/mol, in U(Cp*)$_2$[OSi(t-Bu)(Me)$_2$]Me, $DH°$(Me–H) = 439.4±0.8 kJ/mol, $DH°$(Et–H) = 421±4 kJ/mol, and $DH°$(Bu–H) = 418±8 kJ/mol, by assuming that $DH°$(U–Me) – $DH°$(U–Et) = $DH°$(Me–H) $DH°$ – (Et–H) and $DH°$(U–Me) – $DH°$(U–Bu) = $DH°$(Me–H) – $DH°$(Bu–H).

[f] Estimated from $\overline{DH°}$(Zr–Me) = 284±2 kJ/mol, in Zr(Cp*)$_2$Me$_2$, by using the method described in note e.

[g] Estimated from $\overline{DH°}$(Hf–Me) = 306±7 kJ/mol, in Hf(Cp*)$_2$Me$_2$, by using the method described in note e.

[h] Estimated from $\overline{DH°}$(Mo–Me) = 203±8 kJ/mol, in Mo(Cp)(CO)$_3$Me, by using the method described in note e.

[i] Estimated from $\overline{DH°}$(W–Me) = 221±3 kJ/mol, in W(Cp)$_2$Me$_2$, by using the method described in note e.

[j] Estimated from $\overline{DH°}$(Mn–Me) = 187±4 kJ/mol, in Mn(CO)$_5$Me, by using the method described in note e.

[k] Estimated from $\overline{DH°}$(Rh–Et) = 203 kJ/mol, in Rh(tmp)Et, by using the assumption in note c.

[l] C is an arbitrary constant.

[m] Estimated from $DH°$(Ir–Me) = C + (6±11) kJ/mol in Ir(Cl)(CO)(PMe$_3$)$_2$(I)Me, using the assumption indicated in note e.

[n] Estimated from $DH°$(Pt–Et) = 206 kJ/mol in *trans*-Pt(PEt$_3$)$_2$(Cl)Et, using the method indicated in note c.

References

1. P. W. Atkins, *Physical Chemistry* (5th ed.); Oxford University Press: Oxford, 1994.

2. G. W. Burton, K. U. Ingold, *Acc. Chem. Res.* **19** (1986) 194.

3. G. W. Burton, T. Doba, E. J. Gabe, L. Hughes, F. L. Lee, L. Prasad, K. U. Ingold, *J. Am. Chem. Soc.* **107** (1985) 7053.

4. S. W. Benson, *Thermochemical Kinetics*; Wiley: New York, 1976.

5. G. Wilkinson In *Proceedings of the 5th International Conference on Organometallic Chemistry*, Moscow, 1971; Butterworths: London, 1972.

6. P. J. Davidson, M. F. Lappert, R. Pearce, *Chem. Rev.* **76** (1976) 219.

7. G. Pilcher, *J. Chem. Thermodynamics* **28** (1996) 1195; *Chem. Brit.* **32**, No. 9 (1996) 76.

8. J. C. G. Calado, A. R. Dias, J. A. Martinho Simões, M. A. V. Ribeiro da Silva, *J. Chem. Soc., Chem. Commun.* (1978) 737.

9. J. C. G. Calado, A. R. Dias, J. A. Martinho Simões, M. A. V. Ribeiro da Silva, *J. Organometal. Chem.* **174** (1979) 77.

10. A. R. Dias, J. A. Martinho Simões, *Polyhedron* **7** (1988) 1531.

11. J. A. Martinho Simões, J. L. Beauchamp, *Chem. Rev.* **90** (1990) 629.

12. J. A. Martinho Simões, *NIST Organometallic Database*, to be released.

13. J. B. Pedley, *Thermochemical Data and Structures of Organic Compounds*; TRC Data Series, Vol. I; Thermodynamics Research Center: College Station, 1994.

14. W. G. Mallard, General Editor *NIST Chemistry WebBook* (http://webbook.nist.gov/chemistry); NIST Standard Reference Database 69 - February 1997 Release.

15. W. Chase, Jr., C. A. Davies, J. R. Downey, Jr., D. J. Frurip, R. A. McDonald, A. N. Syverud, *JANAF Thermochemical Tables* (3rd ed.); *J. Phys. Chem. Ref. Data* **14** (1985), Suppl. No. 1.

16. D. D. Wagman, W. H. Evans, V. B. Parker, R. H. Schumm, I. Halow, S. M. Bailey, K. L. Churney, R. L. Nuttall, *The NBS Tables of Chemical Thermodynamic Properties*; *J. Phys. Chem. Ref. Data* **11** (1982), Suppl. No. 2.

17. J. D. Cox, G. Pilcher, *Thermochemistry of Organic and Organometallic Compounds*; Academic Press: London, 1970.

18. J. A. Martinho Simões, M. E. Minas da Piedade, In *Energetics of Organic Radicals*; J. A. Martinho Simões, A. Greenberg, J. F. Liebman, Eds.; SEARCH Series, Vol. 4; Blackie: London, 1996; Chapter 6.

19. G. C. Vogel, R. S. Drago, *J. Chem. Ed.* **73** (1996) 701, and references cited therein.

20. Y.-R. Luo, S. W. Benson, *Acc. Chem. Res.* **25** (1992) 375, and references cited therein.

21. See, for example, *The Chemical Bond, Structure and Dynamics*; A. Zewail, Ed.; Academic Press: San Diego, 1992.

22. See, for example, R. H. Crabtree, *The Organometallic Chemistry of the Transition Metals* (2nd ed.); Wiley: New York, 1994.

23. J. W. Bruno, T. J. Marks, L. R. Morss, *J. Am. Chem. Soc.* **105** (1983) 6824.

24. J. W. Bruno, H. A. Stecher, L. R. Morss, D. C. Sonnenberger, T. J. Marks, *J. Am. Chem. Soc.* **108** (1986) 7275.

25. L. E. Schock, T. J. Marks, *J. Am. Chem. Soc.* **110** (1988) 7701.

26. M. J. Calhorda, A. R. Dias, M. E. Minas da Piedade, M. S. Salema, J. A. Martinho Simões, *Organometallics* **6** (1987) 734.

27. M. J. Calhorda, M. A. A. F. de C. T. Carrondo, A. R. Dias, A. M. Galvão, M. H. Garcia, A. M. Martins, M. E. Minas da Piedade, C. I. Pinheiro, C. C. Romão, J. A. Martinho Simões, L. F. Veiros, *Organometallics* **10** (1991) 483.

28. S. P. Nolan, R. Lopez de la Vega, C. D. Hoff, *J. Organometal. Chem.* **315** (1986) 187.

29. S. P. Nolan, R. Lopez de la Vega, S. L. Mukerjee, A. A. Gonzalez, K. Zhang, C. D. Hoff, *Polyhedron* **7** (1988) 1491.

30. S. P. Nolan, R. Lopez de la Vega, S. L. Mukerjee, C. D. Hoff, *Inorg. Chem.* **25** (1986) 1160.

31. J. A. Connor, M. T. Zafarani-Moattar, J. Bickerton, N. I. El Saied, S. Suradi, R. Carson, G. Al-Takhin, H. A. Skinner, *Organometallics* **1** (1982) 1166.

32. B. B. Wayland, in *Energetics of Organometallic Species*; J. A. Martinho Simões, Ed.; Kluwer: Dordrecht, 1992; p 69.

33. G. Yoneda, D. M. Blake, *J. Organometal. Chem.* **190** (1980) C71.

34. G. Yoneda, D. M. Blake, *Inorg. Chem.* **20** (1981) 67.

35. C. T. Mortimer, *Rev. Inorg. Chem.* **6** (1984) 233.

36. R. L. Brainard, G. M. Whitesides, *Organometallics* **4** (1985) 1550.

37. H. P. Diogo, J. A. Simoni, M. E. Minas da Piedade, A. R. Dias, J. A. Martinho Simões, *J. Am. Chem. Soc.* **115** (1993) 2764.

38. A. A. Gonzalez, C. D. Hoff, *Inorg. Chem.* **28** (1989) 4295.

39. M. E. Minas da Piedade, J. A. Martinho Simões, *J. Organometal. Chem.* **518** (1996) 167.

40. D. R. Stull, E. F. Westrum, Jr., G. C. Sinke, *The Chemical Thermodynamics of Organic Compounds*; Wiley: New York, 1969.

41. J. P. Leal, A. Pires de Matos, J. A. Martinho Simões, *J. Organometal. Chem.* **403** (1991) 1.

42. J. P. Leal, J. A. Martinho Simões, *J. Organometal. Chem.* **460** (1993) 131.

43. a) J. P. Leal, P. M. Nunes, M. E. Minas da Piedade, to be published. b) T. Barreira, J.P. Leal, to be published.

44. A. R. Dias, J. A. Martinho Simões, C. Teixeira, C. Airoldi, A. P. Chagas, *J. Organometal. Chem.* **335** (1987) 71.

45. A. R. Dias, J. A. Martinho Simões, C. Teixeira, C. Airoldi, A. P. Chagas, *J. Organometal. Chem.* **361** (1989) 319.

46. D. Griller, J. A. Martinho Simões, D. D. M. Wayner, In *Sulfur-Centered Reactive Intermediates in Chemistry and Biology*; C. Chatgilialoglu, K.-D. Asmus, Eds.; Plenum: New York, 1991.

47. A. R. Dias, J. A. Martinho Simões, C. Teixeira, C. Airoldi, A. P. Chagas, *Polyhedron* **10** (1991) 1433.

48. J. A. Martinho Simões, In *Energetics of Organometallic Species*; J. A. Martinho Simões, Ed.; NATO ASI Series C No. 367; Kluwer: Dordrecht, 1992.

49. J. P. Leal, J. A. Martinho Simões, *Organometallics* **12** (1993) 1442.

50. P. B. Dias, M. E. Minas da Piedade, J. A. Martinho Simões, *Coord. Chem. Rev.* **135/136** (1994) 737.

51. J. F. Liebman, J. A. Martinho Simões, S. W. Slayden, In *Lithium Chemistry: Principles and Applications*; P. von R. Schleyer, A.-M. Sapse, Eds.; Wiley: New York, 1995.

52. J. F. Liebman, J. A. Martinho Simões, S. W. Slayden, In *The Chemistry of Organic Arsenic, Antimony and Bismuth Compounds*; S. Patai, Ed.; Wiley: New York, 1994.

53. J. F. Liebman, J. A. Martinho Simões, S. W. Slayden, In *The Chemistry of Organic Germanium, Tin, and Lead Compounds*; S. Patai, Ed.; Wiley: New York, 1995.

54. J. F. Liebman, J. A. Martinho Simões, S. W. Slayden, *Struct. Chem.* **6** (1995) 65.

55. M. Sana, G. Leroy, C. Wilante, *Organometallics* **10** (1991) 264.

56. See, for example, J. Baggot, *Perfect Symmetry*; Oxford University Press: Oxford, 1996.

57. H. W. Kroto, J. R. Heath, J. R. O'Brien, S. C. Curl, R. Smalley, *Nature* **318** (1985) 162.

58. W. Krätschmer, L. D. Lamb, K. Fostiropoulos, D. R. Huffman, *Nature* **347** (1990) 354.

59. For a leading reference see M. S. Dresselhaus, G. Dresselhaus, P. C. Eklund, *Science of Fullerenes and Carbon Nanotubes*; Academic Press: San Diego, 1996.

60. H. P. Diogo, M. E. Minas da Piedade, T. J. S. Dennis, J. P. Hare, H. W. Kroto, R. Taylor, D. R. M. Walton, *J. Chem. Soc., Faraday Trans* **89** (1993) 3541.

61. H. P. Diogo, M. E. Minas da Piedade, A. D. Darwish, T. J. S. Dennis, *J. Phys. Chem* **58** (1997) 1465.

62. V. Piacente, G. Gigli, P. Scardala, A. Giustini, D. Ferro, *J. Phys. Chem.* **99** (1995) 14052.

63. (a) T. Kiyobayashi, M. Sakiyama, *Annual Report of Microcalorimetry Research Center, Faculty of Science, Osaka University*, **13** (1992) 58; (b) T. Kiyobayashi, M. Sakiyama, *Fullerene Sci. Technol.* **1** (1993) 269.

64. H.-D. Beckhaus, S. Verevkin, C. Rüchardt, F. Diederich, C. Thilgen, U.-H. ter Meer, H. Mohn, W. Müller, C. S. Foote, *Angew. Chem. Int. Ed. Engl.* **33** (1994) 996.

65. H.-D. Beckhaus, C. Rüchardt, M. Kao, F. Diederich, C. S. Foote, *Angew. Chem. Int. Ed. Engl.* **31** (1992) 63. We have recalculated the uncertainty reported by these authors in order to include the error from the enthalpy of formation of gaseous CO_2.

66. W. V. Steele, R. D. Chirico, N. K. Smith, W. E. Billups, P. R. Elmore, A. E. Wheeler, *J. Phys. Chem.* **96** (1992) 4731.

67. V. P. Kolesov, S. M. Pimenova, V. K. Pavlovich, N. B. Tamm, A. A. Kurskaya, *J. Chem. Thermodynamics* **28** (1996) 1121.

68. A. Xu-wu, H. Jun, B. Zheng, *J. Chem. Thermodynamics* **28** (1996) 1115.

69. J. M. Rudzinski, Z. Slanina, M. Togasi, E. Ōsawa, T. Iizuka, *Thermochim. Acta* **125** (1988) 155.

70. M. Froimowitz, *J. Comp. Chem.* **12** (1991) 1129.

71. J. Almlöf, H. P. Lüthi, *Supercomputer Research in Chemistry and Chemical Engineering*; ACS Symposium Series 353; American Chemical Society: Washington, 1987.

72. S. Tseng, M.-Y. Shen, C.-H. Yu, *Theoret. Chim. Acta* **92** (1995) 269.

73. (a) B. L. Zhang, C. Z. Wang, K. M. Ho, *Chem. Phys. Lett.* **193** (1992)

225. (b) B. L. Zhang, C. Z. Wang, K. M. Ho, C. H. Xu, C. T. Chan, *J. Chem. Phys.* **97** (1992) 5007.

74. R. L. Murry, J. R. Colt, G. E. Scuseria, *J. Phys. Chem.* **97** (1993) 4954.

75. F. Diederich, R. L. Whetten, C. Thilgen, R. Ettl, I. Chao, M. M. Alvarez, *Science* **254** (1991) 1768.

76. J. M. Schulman, R. L. Disch, M. A. Miller, R. C. Peck, *Chem. Phys. Lett.* **141** (1987) 45.

77. J. Cioslowski, *Chem. Phys. Lett.* **216** (1993) 389.

78. D. A. Armitage, C. W. Bird, *Tetrahedron Lett.* **34** (1993) 5811.

79. S. Tseng, C.-H. Yu, *Chem. Phys. Lett.* **231** (1994) 331.

80. J. M. Schulman, R. L. Disch, *J. Chem. Soc., Chem. Commun.* (1991) 411.

81. D. Bakowies, W. Thiel, *J. Am. Chem. Soc.* **113** (1991) 3704.

82. J. M. Schulman, R. C. Peck, R. L. Disch, *J. Am. Chem. Soc.* **111** (1989) 5675.

83. N. Matsuzawa, D. A. Dixon, *J. Phys. Chem.* **96** (1992) 6241.

84. E. Roduner, I. D. Reid, *Chem. Phys. Lett.* **223** (1994) 149.

85. M. D. Newton, R. E. Stanton, *J. Am. Chem. Soc.* **108** (1986) 2469.

86. M. Manoharan, M. M. Balakrishnarajan, P. Venuvanalingam, K. Balasubramanian, *Chem. Phys. Lett.* **222** (1994) 95.

87. M. Kolb, W. Thiel, *J. Comp. Chem.* **14** (1993) 37.

88. D. S. Marynick, S. K. Estreicher, *Chem. Phys. Lett.* **132** (1986) 383.

89. J. Cioslowski, *Electronic Structure and Calculations on Fullerenes and their Derivatives*; Oxford University Press: Oxford, 1995.

90. *CODATA Key Values for Thermodynamics*; J. D. Cox, D. D. Wagman, V. A. Medvedev, Eds.; Hemisphere: New York, 1989.

91. For a leading reference see, J. Cadet, P. Vigny, *Bioorganic Photochemistry*; H. Morrison Ed.; Wiley: New York, 1990; Vol. 1, p 1.

92. See, for example, G. M. Myles, A. Sancar, *Chem. Res. Toxicol.* **2** (1989) 197.

93. H. P. Diogo, A. R. Dias, A. Dhalla, M. E. Minas da Piedade, T. P. Begley, *J. Org. Chem.* **56** (1991) 7340.

94. P.B. Dias, C. Teixeira, A.R. Dias, J.A. Simoni, J.A. Martinho Simões, *J. Organometal. Chem.* **482** (1994) 111.

Influence of Organic Matter in Natural Water Mechanisms

Influência da Matéria Orgânica em Mecanismos nas Águas Naturais

M.L.S. SIMÕES GONÇALVES*, A.M. MOTA, M.M. CORREIA DOS SANTOS

*CENTRO DE QUÍMICA ESTRUTURAL - COMPLEXO I - INSTITUTO SUPERIOR TÉCNICO, AV. ROVISCO PAIS, 1096 LISBOA CODEX

In order to elucidate the role of organic matter in possible mechanisms in natural waters the following points have been studied, mainly using electrochemical methods: 1) Complexation reactions of humi and fulvic acids of different origins with Ph(II) and Cd(II), being noticed that complexation behavioar is not much dependent of humic organics. 2) Competition with major constituents such as Ca(II) and Al(III). 3) Characterization and lead complexation with alga exudates. 4) Stabilization of oxidation states of generally less stable elements, in environmental conditions.

Para se compreender o papel da matéria orgânica em mecanismos existentes nas águas naturais estudaram-se os seguintes aspectos, usando principalmente métodos electroquímicos: 1) Reacções de complexação de ácidos húmicos e fúlvicos de origens diferentes como Pb(II) e Cd(II), tendo-se verifiado que a matéria húmica não tem uma grande influência nas reacções de complexação. 2) Competição com os macroconstituintes como Ca(II) e Al(III). 3) Caracterização de exudados libertados por um tipo de alga inicelular e complexação com Pb(II). 4) Estabilização de estados de oxidação menos estáveis de elementos em condições ambientais.

1. Introduction

Organics in natural waters are of different types including *simple ligands* such as aminoacids, amines and carboxylic acids *and not well characterized mixtures*, e.g. compounds released by biota and humic mater due to slow degradation of bioorganisms.

The quantity and composition of exudates released by phytoplancton vary drastically, depending on the growth phase, nutritional state and of the biological composition, being formed by low molecular weight compounds, namely aminoacids and amines and/or high molecular weight compounds such as proteins [1].

Humic matter (HM) specially fulvic and humic acids (FA and HA) are one of the major sources of organics in aquatic media, forming a polymeric mixture of ill defined compounds. They constitute (0.05 - 1.0) mg l^{-1} of dissolved organic carbon (DOC) in seawater and (1-30) mg l^{-1} in wetland waters, corresponding 1 mg l^{-1} approximately to (1-5) μmol l^{-1} of complexing sites [2]. Humic matter plays an important role in metal comple-

xation and redox processes in natural waters, strongly affecting bioavailability, toxicity and mobility of metal ions [3,4]. In general the binding of heavy metals by humic and fulvic acids decrease the availability of metal ion for the bioorganisms, whereas increasing the mobility of metal, because the natural complexing agents may act as solubilizers in aquatic systems.

However in seawater the importance of organics, in particular HM for controlling speciation of heavy metals is decreased due to the large excess of alkaline and alkaline earth cations that compete for complexation [13, 14].

On the other hand high levels of aluminium are present in interstitial water of soils and groundwater [15], decreasing complexation of transition elements with natural organic ligands and therefore their transport, toxicity and availability [16].

In this context and in order to elucidate examples of possible mechanisms in natural waters, complexation reactions of humic and fulvic acids of different origin with cations such as Pb(II) and Cd(II) are going to be considered [21, 26, 38], as well as competition with

major constituints such as Ca(II) and Al(III) [14,16]. It has been noticed that the complexation behaviour of humics and fulvics with heavy metals is not much dependent of their origin [26].

Characterization of exudates released by a particular type of unicelular alga, Selenastrum capricornutum Printz, (considered as a standard for assaying alga growth by U.S. Environmental Agency) in the presence and absence of Pb(II) is also presented, checking the possibility that the algae can contribute to their own detoxification [17,18].

Finally organics in natural waters represent a reactive media in which numerous chemical reactions can occur, not only of acid base and complexation types, but also redox processes. So, for example, it has been noticed that copper (I) although not thermodynamicaly stable in oxigenated waters controled by O_2/H_2O couple, has been detected in fogwater [5] and seawater [6]. The photooxidation of dissolved organic carbon, in particular of compounds with groups of aldehyde, sugar, hydroquinone and phenolic types in the photic zone may form radicals such as $RO_2^{\bullet}$, $HO_2^{\bullet}$, $O_2^{\bullet}$ that can reduce copper(II) to copper (I) [7, 8, 9], eventually stabilized by sulfite in fogwater, [5], by chloride in seawater [6,10,11] and probably by amines in productive waters [12], preventing its rapid reoxidation. According to this mechanism 5 to 10% of copper(I) has been detected in Atlantic and Gulf of Mexico with depth profiles characterized by surface maxima, decreasing to the bottom, which is consistent with a photochemical mechanism [6] and values 25% have been detected in fogwater with DOC values of (10-100) mg l^{-1} [5].

2. Basic concepts

Humic substances are heterogeneous ligands with different functional groups; the major ones being of carboxylic and phenolic type (about 80% and 20% respectively) and some minor groups e.g. amines. They present two sets of pK^H values, one between 4.5 and 5.5 and the other with values between 8.5 and 9.5, range that is due to different vicinities of phenolic groups. Although the structure of humic compounds depends on its origin this type of variation is typical of most humic samples.

To study complexation reactions in natural water conditions (low concentration of organics and very low concentration of trace metals) anodic stripping voltammetry (ASV) in d.c. mode and in pulse modes - differential pulse (DPASV) or square wave (SWASV) with hanging mercury drop electrode (HMDE), or mercury film electrode (MFE) are the most appropriate techniques, since concentrations as low as 10^{-10}M can be determined, depending on deposition time and type of electrode [3, 19].

To determine speciation parameters of labile complexes from the voltammetric signal a large excess of ligand should be present compared to the total metal concentration $[M]_t$, so that $[L]_t \sim [L']$ where $[L]_t$ and $[L']$ stand respectively for total concentration and ligand concentration not bound to metal ion [20]. One must point out that if the ligand concentration is not in excess the voltammetric peak becomes distorted [21]. In stripping techniques the condition $[L]_t \gg [M]_t$ is more demanding than in direct voltammetry, because metal concentration at the electrode surface during the stripping step $[M]^o_t$ is higher than in the bulk of the solution. Adsorption of the ligand on the electrode can also distort the voltammogram.

In this work factors that affect the voltammograms will be discussed such as 1) the influence of ligand to metal concentration ratio at the electrode surface on ASV signal, particularly in the presence of adsorption 2) the rate of complexation and dissociation reactions i.e. lability of the complexes, 3) the diffusion coefficient of species in solution and 4) the heterogeneity of organics.

2.1 Lability and Reversibility

Lability in ASV is associated with the kinetics of complex dissociation and formation during the time scale of each step, when the metal ion is consumed or released at the electrode surface [19, 22, 23]. The complexes ML will be labile if there is thermodynamic equilibrium at electrode surface during the redox processes.

For labile complexes the peak current (i_p) will be related to lability during the deposition step and the shift observed in the peak potential in the absence and presence of ligand, ΔEp, takes into account the complexation affinity during the stripping step.

The term "lability" is going to be used related to the kinetics of chemical reactions coupled to electrochemical processes and "reversibility" takes into account kinetics of redox mechanism, (the couple being reversible if equilibrium is obtained for all potentials) [19, 22, 23]. Lability during deposition step in ASV can be checked if at different stirring rates the normalized current $\emptyset = i_p^{M+L}/i_p^M$ (i_p^{M+L} and i_p^M stand respectively to the current in the presence and absence of ligand) is the same within experimental errors, and the peak potential obtained by differential pulse polarography (DPP) shifts to more cathodic values with increase of ligand concentration for the same time scale of the the technique. Lability in stripping step can be detected in a similar way as in direct voltammetry, following the shift of the peak potential with ligand concentration [23].

It should be noticed that deviations from lability behaviour in the dissociation process strongly affect the peak currents, decreasing their values (higher stability parameters are then obtained if speciation is determined from i_p without taking into account the kinetic effect), but they do not influence significantly the potential values in the presence of large excess of ligand.

Since for labile complexes the free metal ion is being reduced directly on the electrode we assumed a reversible reaction for Cd(II) and Pb(II) complexes in KNO_3 medium.

2.2 Heterogeneity

The thermodynamic meaning of the stability constant K_{ML} defined for a simple ligand is lost for heterogeneous ligands, when a large number of complexing sites exist (different functional groups and vicinities of each group), being necessary to consider conformational and electrostatic effects too. So, in this case, the determination of K_{ML} leads to a mean stability parameter ($\overline{K}$) of all occupied sites over all site concentrations. Since metal ion binds first to the strongest complexing sites of the ligand, $\overline{K}$ decreases when increasing total metal concentration; the same happening in terms of the competition with the protons. Assuming 1:1 complexes $\overline{K}$ is defined as:

$$\overline{K} = \frac{\Sigma\,[ML_i]}{[M]\,\Sigma\,[L_i]} \qquad (1)$$

In order to interpret accurately complexation with humic matter using a discret model at least 6-8 sites are necessary to be considered [51].

For the interpretation using continuous models different distribution functions can be used, such as the differential equilibrium function [3], or the NICA - Donnan model [52]. The two types of models can interpret speciation in a similar way, being eventually one more appropriate than the other to study complexation reactions in natural environment, where mixtures of ligands in solution (homogeneous and heterogeneous), particles (inorganic and biogenic covered or not by organics) and metal ions exist in a complex network. To interpret complexation in terms of the differential equilibrium function, K_{DEF}, obtained from equation (2) is plotted versus = [ML] / [L]$_t$ for each point of the titration curve [3, 24]. In fact K_{DEF} includes a small range of sites around the corresponding titration point and therefore is more selective than $\overline{K}$. In the presence of a constant [L]$_t$, K_{DEF} is expressed by:

$$K_{DEF} = -\frac{\alpha^2}{[M]_t}\,(\frac{1}{1 +(\alpha-1)\,d\ln[M]_t\,/\,d\ln\alpha}) \qquad (2)$$

where $\alpha = [M]_t\,/[M]$

Another way of interpreting heterogeneity of humic matter it is to assume NICA - Donnan model with two classes of groups: carboxylic (1) and phenolic (2). The following equation can be used to describe protonation [25, 26]:

$$Q = M_1\,(1 - \frac{(K_1^1[H])^{m_1}}{1+(K_1^1[H])^{m_1}}) + M_2\quad(1-\frac{(K_2^1[H])^{m_2}}{1+(K_2^1[H])^{m_2}}) \qquad (3)$$

where Q (charge of humic matter) and [H] are known from potentiometric data. From the fitting of this expression to the experimental values, the unknown parameters M_1 and M_2 (the total charge of carboxylic and phenolic groups), K_1^1 and K_2^1 (average values of protonation constants for the two different classes of groups) and m_1 and m_2 related to the width of the distribution, can be determined.

The variation of charge per unit of mass ΔQ (Coulombs Kg^{-1}) can be obtained from potenciometric data according to:

$$\Delta Q = N'_{OH}\,F\,/\,m_{HM} \qquad (4)$$

Where m_{HM} is the mass of humic matter in solution, N'_{OH}, is the concentration of OH consumed by the organics and F = 96500 Coulombs $equivalent^{-1}$. From comparison of acid-base potentiometric titrations of humic matter and of the supporting electrolyte the value N'_{OH}, can be obtained. In order to know the absolute charges for each point of the titration, the value for one specific point must be known, generally the one corresponding to the zero of charge.

The heterogeneous binding of cations (proton and metal ion) by the ligand can be represented by:

$$Q_{M,t} = \left\{\frac{(K_{Mi}^1)^{nM_i}}{(K_{Mi}^1)^{nM_i} + (K_{Hi}^1)^{nH_i}}\right\} \times \left\{\frac{\sum_i [(K_{Mi}^1)^{nM_i} + (K_{Hi}^1)^{nH_i})]^{p_i}}{1+\sum_i \left[(K_{Mi}^1)^{nM_i} + (K_{Hi}^1)^{nH_i}\right]^{p_i}}\right\}^{nH_i}_{nM_i}$$

$$(5)$$

where i stands for the type of sites (1-carboxylic and 2-phenolic) $Q_{M,t}$ is the total charge, $K_{Mi}^1 = K_{Mi}$ [M] and $K_{Hi}^1 = K_{Hi}$ [H], n-accounts for the non-ideal behaviour of each type of site (0<n<1), p is related to the width of the distribution due to the intrinsic chemical heterogeneity of the ligand, which is the same for any metal ion and / or proton (0<p<l with p = 1 for homogeneous ligands) [27].

2.3 Surface concentration effect

To evaluate complexing parameters from voltammetric measurements the concentration of the ligand not bound to the metal ion, at the electrode surface [L']° should be the same as in the bulk of the solution i.e. [L']° ≈ [L'] ≈ [L]$_t$. To satisfy this condition within 5%, the following relation should be verified [L]$_t$ / [ML] ≥ 20 for direct voltammetry (e.g. d.c. voltammetry, pulse voltammetry, square wave voltammetry) and [L]$_t$/[ML]° ≥ 20 for stripping technique (eg. ASV, DPASV), which implies that in the presence of strong complexation [L]$_t$/ / [M]$_t$ ≥ 20 and [L]$_t$ / [M]$_t^\circ$ ≥ 20 respectively.

According to reference [2] the value of $[M]_t^o$ can be approximately estimated from

$$[M]_t^o = 2.3 \frac{(D_{ox} D_{red})^{1/2}}{\delta r} t_d [M]_t \qquad (6)$$

For typical values $D_{ox} = D_{red} = 10^{-5}$ cm^2 s^{-1}, drop radium of the electrodes, $r = 0.04$ cm, thickness of diffusion layer $\delta = 2 \times 10^{-3}$ cm and deposition time $t_d = 180$ s, the expression $[L]_t / [M]_t^o \geq 20$ implies $[L]_t / [M]_t \geq 1000$ which is a very severe restriction.

2.4 Asorption of organic matter on the electrode

Adsorption can affect the voltammetric signal and so it should be avoided in order to study complexation in solution, although sometimes complexation in solution and of adsorbed species can be separated. Adsorption by itself can be studied by a.c. voltammetry determining the capacitive current at the angle phase of 90°.

In order to minimize adsorption, modified electrodes can be used. In this context the electrode can be covered by Nafion, a polymer of perfluorosulfonate type (cation - exchange resin) which is non-electroactive and insoluble in water. These polymers are formed by hydrophilic ionic clusters (with negative sulfonic groups, their counter ions and water molecules) randomly distributed throughout the backbone of hydrophobic tetrafluoroethylene. These two factors contribute to the selectivity of Nafion for cations, specially hydrophobic organic cations and to minimize adsorption of anions in solution [29, 30]. One important reason for the widespread application of Nafion modified electrodes in electroanalytical chemistry is their ability to preconcentrate cations, which increases the sensitivity of the method [30, 31, 32, 33, 55].

For the experimental conditions generally used the diffusion layer is about one hundred times the thickness of the Nafion layer, which allows rapid electrode response and does not hinder mass transport of metal ion (limited by the convective diffusion transport in solution [34]).

3. Complexation with humic matter

In complexation studies of Pb(II) and Cd(II) with HM it has been checked that the complexes are labile for both steps in ASV during the time scale of the technique ($t = t_p = 50$ ms for stripping and $t = 45$ ms for deposition, from $\delta = \sqrt{\pi D t}$ where δ is the thickness of diffusion layer and D the diffusion coefficient). However $i_p^{M+L} < i_p^M$ for all the points of the titration curve which imply that $D_{ML} < D_M$.

A value of $D_{ML} = 5.5 \times 10^{-7}$ cm^2 s^{-1} has been determined from the peak currents obtained in the presence of sufficient excess of ligand, so that there is a linear relation-ship between i_p and $[M]_t$ for HM commercially obtained from Roth. For a humic sample coming from a peat [37] the value of D_{ML} determined experimentally is $(2-5) \times 10^{-8}$ cm^2 s^{-1}, depending the value of D_{ML} on the aggregation of the compound, that is influenced by the experimental conditions, namely salt concentration and pH.

For D_{ML} 2×10^{-8} cm^{-2} s^{-1} it is worthwhile to emphasize that the expression $[L]_t / [M]_t^o \geq 20$ implies according to equation (6') $[L]_t / [M]_t \geq 350$, so a not so demanding excess of ligand is necessary.

For a labile, reversible and homogeneous system with $D_{ML} \approx D_M$ during a titration of the ligand with the metal ion $[M]_t$ and / or t_d it was shown that [20, 21]:

a) when $[M]_t \times t_d$ is so small that $[M]_t^o \ll [L]_t$, the peak height (ip) and width ($W_{1/2}$) are the same as those obtained in the absence of ligand and Ep, although constant, has a shift relatively to the peak of the metal ion.

b) when $[M]_t^o < [L]_t$, but is not negligible, the peak height decreases, the width increases, compared to the value in the absence of ligand and Ep shifts anodically with increase of $[M]_t \times t_d$ due to the surface concentration effect. In fact $[M]_t^o$ increases during the rising part of ASV voltammogram, leading to a decrease in the concentration of sites not bound to M, the shift of potential to more positive values increasing with increase of $[M]_t^o$, which leads to a broader and lower peak [36].

c) increasing $[M]_t \times t_d$ further the ligand becomes fully saturated at the electrode surface ($[M]_t^o \approx [L]_t$ for a 1:1 complex) giving a peak at the potential E_{sat}. If $[M]_t^o > [L]_t$ the remaining metal not bound to the ligand is present in the free form and so the voltammogram may present a shoulder, that accounts for the metal bound to the ligand, (whose height and potential depends namely on $[L]_t$ and does not vary with $[M]_t \times t_d$) and a peak due to the metal reoxidized to free cation which potential tends to Ep^M obtained in the absence of ligand. It should be emphasized that the shoulder can be noticed only it $E_p^M - E^{sh} > 60$ mV (E^{sh} is the potential of the shoulder).

If the ligand is heterogeneous ip and $W_{1/2}$ are respectively smaller and higher in the presence of the ligand, than in its absence even in condition a) [36]. The above behaviour can be seen in Fig. 1 for commercially Roth humic acid, where for the experimental conditions of the work the shoulder only can be detected for ip/i$^{sh} \approx 10$ and $\Delta Ep \approx 80$mV.

From the time dependence of capacitive current, i_{ac}, obtained by a.c. voltammetry for different concentrations of humic matter, it has been noticed that there is adsorption of humic acid on the electrode, in particular of Roth commercial sample, and for ligand concentrations of $(40-80) \times 10^{-6}$ eq l^{-1} used in DPASV measurements, the electrode is fully saturated for E = -0.75 V and time intervals higher than (60-30) s respectively. Therefore saturation of the electrode by adsorbed molecules is attained during the deposition step of DPASV at this value of deposition potential.
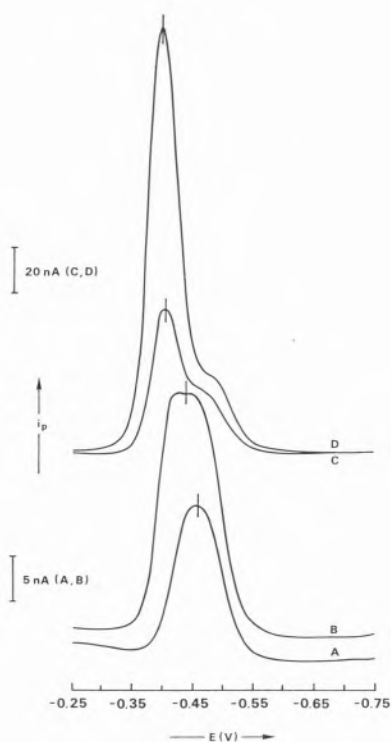
Figure 1 – Anodic stripping voltammograms obtained with "Roth humic acid" for $[L]_t$ = 42 eq l^{-1} in 0.02 M KNO_3, t=22 °C, pH = 5.0, t_d = 1 min, $[Pb]_t$ (μM) = 1 (A); 2(B); 4(C); 8(D).
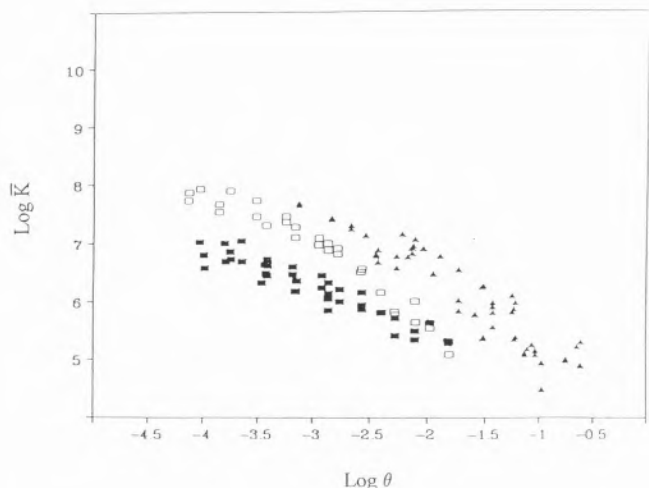
Figure 2 – Log $\overline{K}$ vs log θ from Pb(II) titration of humic acid from a peat with three different electrodes. Experimental conditions pH =5,0 0.02 M KNO_3, $[HM]_t$ = 3.5×10^{-5} M and $[Pb]_t$ = 3×10^{-9} - 6×10^{-8} M, $[HM]_t$ = 7.53×10^{-5} M and 15×10^{-5} M with $[Pb]_t$ = 1×10^{-8} - 1×10^{-6} M, ■ NCMFE, □ MFE and ▲ HMDE.

The effect of adsorption on the voltammetric signal increases with ligand content for low concentration of humic acid, but decreases after complete saturation of the electrode since in this case complexation in the adsorbed layer tends to become constant, while complexation in solution continues to increase [20].

On the other hand, both values of log K obtained from either ip or Ep, may be affected by adsorption of humics on the electrode. A higher complexation affinity is measured from potential values during the stripping step due to the molecules adsorbed on the electrode, while during the deposition step adsorption of humic acid may induce reduction of more metal ion, increasing the peak current (ip) and therefore decreasing log K i.e. log $\overline{K}_{ip}$ < log $\overline{K}_{Ep}$. When a reverse trend is obtained adsorption effect should be masked by heterogeneity, since it also affects log K obtained from Ep and ip, but in the opposite direction.

In Fig. 2 the values of the average formation constants of Pb(II) with HA from a peat (from ΔE_p) versus the degree of occupation of sites (θ) obtained for different types of working electrodes: Nafion coated mercury film electrode (NCMFE), MFE and HMFE are presented, in order to see the influence of adsorption in complexation results. The higher values of log $\overline{K}$ from MFE and HMDE compared to NCMFE for the same θ value, are due to the additional complexation of the metal ion with the ligand on the adsorbed layer during the stripping step [38]. Adsorption effect is similar in voltammetric results obtained by HMDE and MFE, but for NCMFE adsorption is less important due to repulsion of HM negative charges at the electrode surface. From Fig. 2 it can be seen that the difference between the values of log $\overline{K}$ obtained for NCMFE and MFE decreases with increasing $[M]_t$ and decreasing $[L]_t$ which is due to the decrease in the repulsion of HM from NCMFE when the ligand becomes closer of neutrality situation.

So in order to decrease the adsorption effect on complexometric studies in natural waters (large ligand to metal ratios) the MFE should be coated with Nafion in such a way that repulsion of negatively charged groups by the film will be effective [38]. However when adsorption is not so important or, can be avoided electrochemically HMDE should be used since the results are more reproducible. Sometimes complexation is solution and of adsorbed species can be studied separately.

3.1 Determination of complexometric parameters in solution and at the interface

In order to exemplify how to determine complexometric parameters in solution or in the adsorbed layer, we are going to present in more detail the results obtained for the systems Pb(II) and commercial humic acid from Roth (D_{ML} = 5.5 × 10^{-7} cm^2 s^{-1}) at pH=5.0, ionic strength 2 × 10^{-2} M (KNO_3), and t = 20°C. [20]. In this case HM adsorbed on working electrode leads to a surface concentration effect similar to the described

above, due to a gradual saturation of adsorbed sites by the metal ion [35].

For labile systems during both steps of ASV and with $D_{ML} < D_M$ the conditional stability parameters $\overline{K}$ can be determined, either from current or from potential values according to:

$$i_p^{M+L} / i_p^M = (\overline{D}/D_M)^{1/2} \tag{7}$$

$$\overline{D} = (D_M [M] + D_{ML} [ML]) / [M]_t \tag{8}$$

$$\Delta Ep = E_p^{M+L} - E_p^M = \frac{RT}{nF} \ln \left(\frac{D_M}{\overline{D}} \right)^{1/2} - \frac{RT}{nF} \ln \alpha \tag{9}$$

where $\alpha = 1 + \overline{K} [L]_t [M]_t / [M]$ \tag{10}

$\overline{K}$ values (obtained either from i_p or from Ep_j vs the degree of occupation of sites θ are presented in Fig. 3. Since Ep is related to the complexing strength in the stripping step, the parameter $\overline{K}_{Ep}$ is associated to $[M]_t^o$ (total metal concentration at the electrode surface during stripping step) and $\overline{K}_{ip}$ is associated to the bulk concentration $[M]_t$. Therefore $\overline{K}_{Ep}$ should be plotted versus θ ($=[ML]^o / [L]_t$) and K_{ip} versus θ ($=[ML] / [L]_t$) for comparison. The concentration of $[ML]^o$ is determined from equation [9] and $[M]_t^o$ is estimated from:

$$[M]_t^o = 2.3 \frac{(\overline{D} D_r)^{1/2}}{\delta r} t_d [M]_t \tag{6'}$$

This equation that can only be used as an approximation to heterogeneous systems, is formally identical to equation (6) but D_M has been substituted by $\overline{D}$, in order to take into account all the labile species that arrive to the electrode surface to be reduced during the deposition step.

Fig. 3 shows that $\overline{K}_{Ep}$ is higher than $\overline{K}_{ip}$ for the same θ value, probably due to the adsorption of the ligand on mercury, which strongly affects the values of peak potential. In the presence of adsorption equation 9 should be redefined adding the term $K_{ad}[L']_{ad}$ to $\overline{K}$ $[L]_t$ in order to take into account the contribution of adsorbed sites [35]. The concentrations of L'_{ad} (adsorbed ligand sites not bound to the metal ion) is similar to $[L]_t^{ad}$ for $[M]_t^o \ll [L]_t^{ad}$. On the other hand $[L]_t^{ad}$ (the total concentration of adsorbed ligand sites) will be constant and independent of the ligand concentration in solution, if the electrode is saturated since in this case the term $\overline{K}_{ad} [L]_t^{ad} \ll \overline{K} [L]_t$. From Fig. 3 it can be seen that $\overline{K}_{ip}$ is less influenced by adsorption, since is less dependent on $[L]_t$ concentration, as happens also for K_{DEF}.

The stability parameter $\overline{K}_{ad}$ for complexation in the adsorbed layer can be determined from equation 9 replacing in this equation α by $\alpha_t = 1 + \overline{K}_{ad} [L']_{ad} + \overline{K}$ $[L]_t$ (valid for $[L'] \approx [L]_t$). From this expression and the
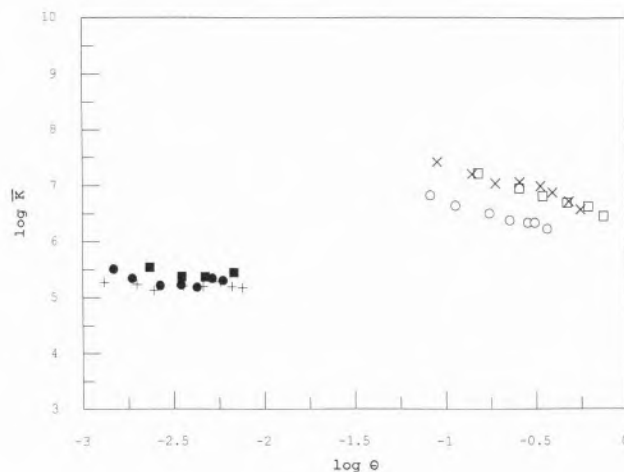

Figure 3 – Log $\overline{K}$ vs log θ for Pb(II) titration with "Roth humic acid" in 0.02 M KNO_3 at pH = 5.0, t=22 °C $[Pb]_t < 0.53$ µM and $[L]_t = 84$ eq l^{-1}, data from i_p (●) or E_p(o), $[L]_t = 64$ eq l^{-1} data from i_p(+) or E_p(x); $[L]_t = 42$ eq l^{-1}, data from i_p(■) or E_p (□).

mass balance for adsorbed ligand, $[L]_t^{ad} = [L']_{ad} (1 + \overline{K}_{ad}$ $[M]^o)$ where $[M]^o$ is given by $[M]_t^o / \alpha_t$, it was found that:

$$\overline{K}_{ad} = \frac{\alpha_t - 1 - \overline{K} [L]_t}{[L]_t^{ad} + [M]_t^o (\frac{1 + \overline{K} [L]_t}{\alpha_t} - 1)} \tag{11}$$

The parameter $\overline{K}_{ad}$ is then determined from this equation using: α_t from ΔE_p according to equation 9, $\overline{K}$ determined from i_p measurements, $[L]_t^{ad} = 1.6 \times 10^{-4}$ eql^{-1} calculated below and $[M]_t^o$ given by eq. (6').

It has been noticed that the curves i_p versus t_d for different $[M]_t$ values present a break point for a certain time, t_c that is inversely proportional to $[M]_t$ (eq. 6'). Then t_c should represent the critical time for the saturation of complexing sites by metal ion at the electrode surface ($\overline{D}$ and $[M]_t^o$ approximately constants in eq 6' corresponding to $[M]_t^o = [L]_t^{ad} + [L]_t^{sol}$). From eq. (6') a value of $[L]_t^{ad} = (1.6 \pm 0.3) \times 10^{-4}$ eq. $l^{-1} > [L]_t^{sol} = 4.2 \times 10^{-5}$ eq.l^{-1} has been determined, which means that the number of moles of adsorbed sites per litre of adsorbed layer, is higher than the concentration in the bulk of solution. A similar value of $[L]_t^{ad}$ has also been calculated from i^{sh}, confirming the previous hypothesis.

The variation of $\overline{K}_{ad}$ with the degree of occupation of adsorbed sites θ_d ($= [ML]_{ad} / [L]_t^{ad}$) is presented in Fig. 4 where the values of $(K_{DEF})_{ad}$ are also plotted. The value of θ_d is calculated from $[M]_t^o = [M]^o + [ML]_{ad} + [ML]^o$ where $[ML]^o = \overline{K} [L]_t [M]^o$ and $[M]^o = [M]_t^o / \alpha_t$.
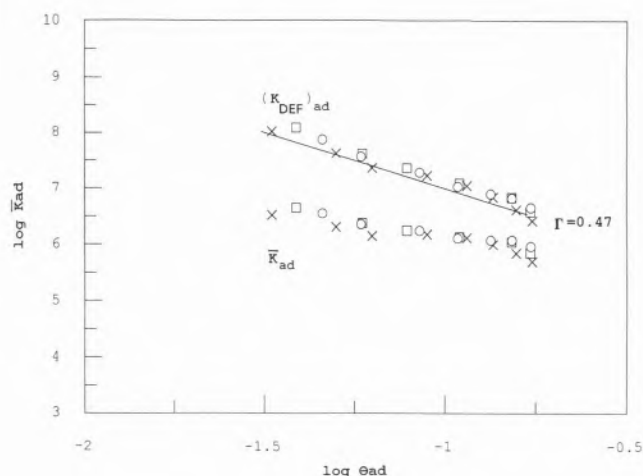
Figure 4 – Log $\overline{K}_{ad}$ and log $(K_{DEF})_{ad}$ vs log θ_{ad} for Pb(II) titration with "Roth humic acid", where ad stands for adsorbed layer. Same experimental conditions as Fig. 3; $[L]_t$ (eq l^{-1}) = 84(o), 64($\times$); 42($\square$).

Comparing K_{DEF} of the lead complexes in the bulk of the solution and in adsorbed layer, it can be seen that complexation of lead with adsorbed humic matter is stronger than in solution for the same degree of occupation of sites. This might be due either to the higher affinity of the adsorbed sites influenced by the spatial rearrangement of the molecule, or to a higher ratio of stronger sites to total sites, influenced by the different affinity of each site and the vicinity of mercury negatively charged.

It is worthwhile to point out that if the difference between log $\overline{K}$ $[L]_t^{sol}$ and log $\overline{K}_{ad}$ $[L]_t^{ad}$ was higher than 3, two separate inflection points should be expected. On the other hand if $[L]_t^{ad} \gg [L]_t^{sol}$ the same t_c value should be obtained independently of $[L]_t^{sol}$, if the electrode is fully saturated, as observed experimentally and which confirms the previous results [39].

Often the appearance of a shoulder is not observed in complexation reactions with other heterogeneous macromolecules, although $w_{12}^{M+L} > w_{12}^{M}$ and asymmetric peaks are obtained when $[L] / [M]_t^\circ$ decreases (increase of $[M]_t$ and/or t_d), probably due to lower ΔE_p values (lower complexing affinity) and/or lower D_{ML} which decreases the term RT/nF ln $(\overline{D}/D_M)^{1/2}$ in eq. 9.

Using Nica model [52] according to equations (3) and (5) it was possible to conclude that at pH=5.0, ionic strength 0.02M KNO_3 and t=20°C:

1) Humics and fulvics of different origin present pK values of the order of 4.5-5.5 and 8.5-9.5, attributed to heterogeneous carboxylic (hydrogen bonds involved) and phenolic groups respectively.

2) In complexes with humic acid from a peat

Pb(II) is preferentially bound to phenolic groups and Cd(II) to carboxylic groups, as can be seen in Fig. 5 where the distribution function F is plotted versus log K_{ML} [26].

3) Pb(II) has higher affinity to humics than for fulvics in general, showing that the complexity of the structure of the ligand favours complexation.

4) The intrinsic heterogeneity of phenolic groups (p=0.65) is similar for humic and fulvic acids, although smaller than for carboxylic groups (p=0.47).

5) Complexation with carboxylic groups seems to be independent of the type of humic matter and the metal ion, probably due to the predominantly ionic character of the binding.
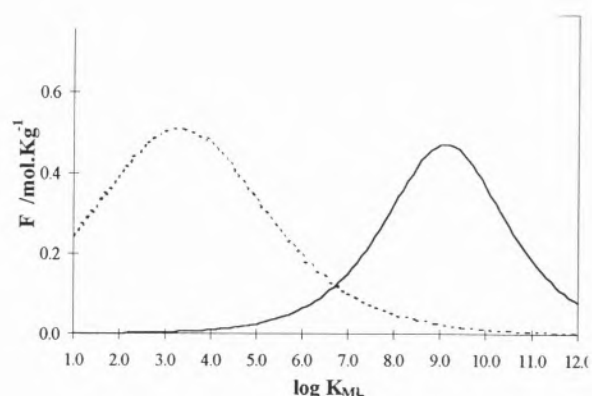
Figure 5 – F vs log kML for tritration of humic acid from a peat with Cd(II): carboxylic groups (– – –) and with Pb(II): phenolic groups (–) according to NICA model.

4. Competition reactions of major and minor cations for humic matter

In the environment, competition between major and minor cations for ligands in solution is of great importance, not only in a thermodynamic point of view, but also in terms of kinetics, since exchange reactions between alkaline earth cations and transition elements are in general slower than complexation reactions with heavy metals, in natural water conditions [13]. This point will be illustrated by competition studies of Cd(II), Pb(II) or Zn(II) with Ca(II) or Al(III).

4.1 Speciation in the presence of calcium

Competition between metal ions and calcium for binding sites on HM has been interpreted according to the exchange reaction [14]:

$$CaL + M = Ca + ML$$
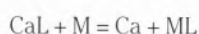
being the mass balances:

$$[M]_t = [M] + [ML] \tag{12}$$

$$[L]_t = [L] + [ML] + [CaL] \tag{13}$$

$$[Ca]_t = [Ca] + [CaL] \tag{14}$$

Experimental values of $\overline{K}$ have been obtained from the titration of humic material, in the presence and absence of calcium, with cadmium(II). In each titration the total concentration of humic material and calcium is maintained constant and the free ion concentration was determined from the mean diffusion coefficients, being the mean parameter $\overline{K}$ easily obtained for each titration point if calcium is absent.

The determination of $\overline{K}$ in the presence of calcium is more complicated, since the ligand concentration depends on the amount of calcium bound to the humic material, that it is not possible to estimate beforehand because the stability constant of the calcium complex K_{CaL} is not known. In order to determine $\overline{K}$ in the presence of calcium the following equation was used:

$$\frac{1}{\overline{K}'} = \left[\frac{[M]}{[ML]} \left([L]_t - [ML]\right) \right] = \frac{1}{\overline{K}} + \frac{\overline{K}_{CaL}}{\overline{K}} [Ca^{2+}] \tag{15}$$

where $\overline{K}'$ is the apparent stability ($\overline{K}$) conditional with respect to calcium. If for a fixed cadmium concentration and different calcium concentrations $\overline{K}$ and K_{CaL} are almost constant, then $1/\overline{K}'$ versus $[Ca^{2+}]$ should have a linear correlation from which $\overline{K}$ and K_{CaL} can be determined. Since the free calcium is unknown an iterative procedure has been used with $[Ca^{2+}] = [Ca^{2+}]_t$ for the first approximation. The experimental results fit reasonably a linear plot supporting the proposed model as can be seen from table 1.

Table 1 – Log $\overline{K}$ for Cd(II) humic acid complexes considering and not Ca^{2+} competition as a function of concentration of $[Ca]_t$ and $[Cd]_t$.

[Ca]$_t$ [M]	[Cd]t [M]				
	3.0×10^{-8}	5.9×10^{-8}	9.9×10^{-8}	3.0×10^{-7}	9.8×10^{-7}
0	5.1	5.1	4.8	4.5	4.3
3×10^{-5}	4.9	4.7	4.5	4.4	4.2
1×10^{-4}	4.7	4.6	4.5	4.1	4.0
3×10^{-4}	4.4	4.3	4.2	3.9	3.8
log $\overline{K}$ *	5.0	4.9	4.8	4.4	4.3
log K_{CaL}	4.05	4.00	4.00	4.00	3.98

* Considering competition of Ca^{2+} (eq.15)

From this table one can conclude that 1) at constant $[Cd]_t$ the values of log K_{CdL} decrease with increasing $[Ca]_t$ 2) at constant $[Ca]_t$ the values of log K_{CdL} decrease with increasing $[Cd]_t$, which reflects the heterogeneity of humic sample to cadmium 3) there is no significant heterogeneity for calcium 4) the parameter $\overline{K}_{CdL}$ calcu-

lated for equation (15) agrees with the value obtained in the absence of calcium, according to the above mechanism 5) log $\overline{K}_{CaL} \sim$ log $\overline{K}_{CdL}$, similar to complexes formed with carboxylic groups, as happens *e.g.* with citric acid [40].

So, in competition between Ca^{2+} and Cd^{2+} for the binding sites of HM the same value of $\overline{K}$ is obtained in the absence or presence of calcium if [L] is redefined as $[L]_t - [CaL] - [CdL]$; therefore calcium influences cadmium speciation, decreasing the number of available sites for complexation, but in the concentration range used, Ca^{2+} does not compete directly to ligand groups bound to Cd. The same type of behaviour has been found for Zn(II) [14].

4.2 Speciation in the presence of aluminium

The competition between Pb(II) and Al(III) however is different. Even when [L] is redefined as above a decrease in log $\overline{K}$ is observed with the increase of $[Al]_t$ [16], considering the value of log $K_{AlL} = 6.8$ for humic matter [41,42].

Therefore the competition of aluminium in the presence of lead is not only due to the decrease of available ligand sites, but an additional interaction between Al(III) and Pb(II) should occur, probably due to an electrostatic effect of Al(III), which affects the charged complexing sites of the molecule.

To take into account the electrostatic effect, the following expression has been used for the mean stability parameter $\overline{K}$:

$$\overline{K} = [ML]/[M].[L] \, e^{\gamma \, [Al]t/[L]t} \tag{16}$$

where γ is a constant parameter, independent of the concentration.

This expression agrees with the fact that the reaction depends not only on the energy of the covalent bond, but is also influenced by the surface electrostatic field, which is considered the only secondary effect in the reaction:

$$M (HM) + Al^{3+} = M(HM)Al$$

In fact in this condition it will be:

$$K = K_{int} \exp[(1-z) \, F\Psi/RT] \tag{17}$$

where K_{int} is the complexation constant of Pb(II) with HM in the absence of Al(III), z is the charge of aluminium and Ψ is the difference of potential between the complex and the solution.

For the constant capacity model the difference of potential should be proportional to the aluminium concentration per group of ligand, and so equation (17) leads to equation (16); the best fitting between experimental points and eq. (16) is obtained for $\gamma = 15\pm2$ (Fig. 6). The agreement of log K versus log θ, for the different
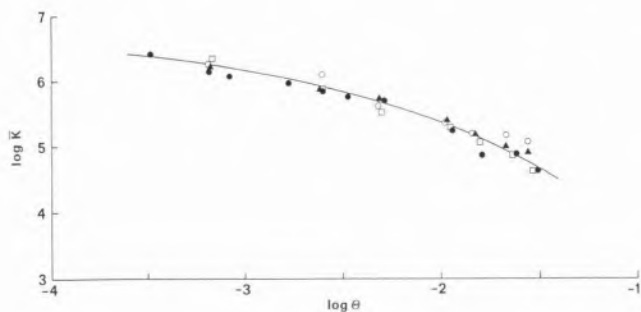
Figure 6 – log $\overline{K}$ vs log θ obtained from a titration of humic acid from a peat with Pb(II) with determined from eq. 16 (–) (▲)
$[Al]_t$ (M) = 0.0 (□), 1×10^{-5} D, 3×10^{-5} (●), 4×10^{-5} (q) $[L]_t = 1.5\times10^{-4}$ M.

aluminium concentrations, confirms the assumption that the affinity of Pb(II) to humic matter is influenced by an electrostatic interaction of aluminium(III).

5. Complexation reactions with exudates

In order to illustrate this type of reactions, complexation of lead with the exudates released by unicellular algae Selenastrum capricornutum Printz in different growth phases (exponential and beginning of stationary phase) in the absence (control) and presence of 2.3×10^{-7} M in Pb(II) (contaminated), has been studied. [18]

So, titrations of the exudates (after filtration of the algae) with Pb(II) have been followed by DPASV using three types of working electrodes: HMDE, MFE and NCMFE.

Before voltammetric measurements the exudates have been characterized in terms of DOC, acid-base properties and adsorption on the electrode. By potentiometry two types of pk^H values have been determined, one of them around 6 and the other around 10, so of the same order of those determined for HM, being the total concentration of sites $C_H = 2\times10^{-3}$ M. In terms of adsorption it has been noticed by a.c. voltammetry (90° ongle phase) that there is adsorption on the HMDE and MFE, but not on NCMFE, since the capacitive curves are identical for the supporting electrolyte and the sample, as we should expect attending to the fact this type of organics should present a negative charge in solution.

During the titration of the exudates with Pb(II) followed by DPASV using NCMFE it is clear that the current is smaller in the presence than in the absence of the organics (as also happens for MFE and HMDE) and presents a constant shift of potential during the whole titration, ($[Pb]_t < 10^{-6}$ M). The experimental results have been interpreted in terms of a mixture of inert and labile complexes (both in deposition and stripping steps). [18]

It has also been assumed that the diffusion coefficient of the labile complexes D_{ML} is equal to D_M, since although with an excess of ligand ($C_H = 2\times10^{-3}$ M) the last part of the titration curve ($[Pb]_t > 1.5\times10^{-7}$ M) is parallel to the calibration. On the other hand the complexes should be homogeneous since $w_{1/2}^M = w_{1/2}^{M+L}$.

5.1 Control samples

The total concentration of the inert fraction $[L]_t^{in}$ can be obtained from the interception of the straight line through the last points with the axis of $[M]_t$.

A conditional parameter for inert sites K_{in} has been estimated from the first part of the titration curve where these sites are not saturated

$$K_{in} = \frac{[ML]_{in}}{[M]_{lab}[L']_{in}} \tag{18}$$

being $[L']_{in}$ the inert complexing sites not bound to the metal ion and $[M]_{lab}$ the labile metal concentration determined from i_p and the mass balances:

$$[M]_t = [M]_{lab} + [ML]_{in} \tag{19}$$

$$[L]_t^{in} = [L']_{in} + [ML]_{in} \tag{20}$$

From these calculations the value of log $K_{in}^* = 7.4\pm0.2$ has been calculated from all electrodes and no difference was obtained between stationary and exponential phases (table 2).

The apparent weaker complexation of inert sites measured with HMDE and MFE reflected in the smaller values of $[L]_t^{in} K_{in}$ compared with the results of NCMFE, is due to the induced adsorption of lead on the two former electrodes.

Considering the values $\Delta E_p = (-8\pm3)$mV for exponential phase and (-15 ± 3)mV for stationary phase obtained with NCMFE and $[L]^{lab} = [L]_t = C_H = 2 10^{-3}$M (since $[L]_t^{in} \sim 10^{-8}$ M) we can determine log $K_{lab} \sim 2.7$ and 3.0 for the exponential and stationary phases respectively.

5.2 Contaminated samples. Comparison with controls

For contaminated samples, labile lead concentration in the medium before titration $[Pb]_{lab}^{initial}$ can be determined from i_p. From the total concentration of Pb(II) in solution before titration (60% of added lead) the concentration of initial inert ligands has been estimated.

On the other hand the concentration of total available inert sites, $[L]_{t,av}^{in}$, being occupied during the titration with Pb(II) can also be estimated and so the concentration of total inert sites (table 2). From this table it is clear that the total concentration of inert sites in contaminated sample is $\sim10^{-7}$ M, higher than in control although in this last medium there is a higher number of cells.

Table 2 – Complexing parameters determined for inert complexes from ip for control and contaminated samples in the exponential (exp) and stationary (st) phases

	$[L]_t^{in}(10^{-8} M)$	$\log K_{in}^{*}$	$\log K'_{in}$	$\log K_{in}$
HMDE				
Control				
exp	2.5	7.2	–	–
st	3.0	7.3	–	–
Contaminated				
exp	8	6.8	–	
st	11	7.0	–	–
MFE				
Control				
exp	1.0	7.5	–	–
st	1.0	7.5	–	–
Contaminated				
exp	7	7.2	–	–
st	10	7.2	–	–
NCMFE				
Control				
exp	4	7.6	7.9	14.9
st	4	7.5	8.0	15.1
Contaminated				
exp	10	7.2	7.5	14.1
st	11	7.5	8.0	14.7

Comparing the values of K_{in}^{*} for control and contaminated samples we can see that this constant is of the same order of magnitude, indicating that mainly the same groups are involved.

From table 2 it can also be seen, for all electrodes, a slightly higher complexing effect $(K_{in}^{*}[L]_t^{in})$ for the beginning of stationary phase, when compared to exponential phase. If inert complexes (with slower rates of dissociation), are less toxic and attending to the fact that the uptake of Pb(II) by algae between the exponential phase and beginning of stationary phase of batch experiment is negligible, the above behaviour may be attributed to a defense mechanism in presence of Pb(II). These results also show that adsorption does not affect much i_p values contrarily to what was observed for E_p [18].

In terms of ΔE_p measured in the stripping step when using NCMFE no difference has been observed between control and contaminated samples and so the labile complexes have similar stability constants.

From $[Pb]_{lab}^{initial}$ measured by i_p and the ratio $[Pb]_{lab}/[Pb]$ determined from ΔE_p with NCMFE, we can conclude that in alga's contaminated medium the concentration of $[Pb]_{lab}/[Pb]_t = 72\%$ and $[Pb]/[Pb]_t = 36\%$ ($[M]_t = 1.4 \times 10^{-7}$ M) for the exponential phase, being 48% and 16% respectively for stationary phase.

Another conditional parameter K'_{in} at pH = 5.0 was determined assuming that labile complexes are the same for both steps, deposition and stripping, (due to the same time scale of both steps) whose values can be compared with complexation of HM with Pb(II):

$$K'_{in} = \frac{[ML]_{in}}{[M][L']_{in}} \qquad (19)$$

Since pk^H values are known steocheometric stability constants have also been determined from the values of NCMFE:

$$K_{in} = \frac{[ML]_{in}}{[M][L]_{in}} \qquad (20)$$

These results are important in terms of toxicity, because free lead and the complexes that are able to dissociate during the time scale of uptake by algae are in general the most toxic species.

6. Comparison of complexation reactions with humic matter and exudates

Comparing the types of lead complexes formed with HM and exudates we can conclude that:

1) Exudates are homogeneous ligands of low molecular weight, since $D_{ML} = D_M \sim 7. \ 10^{-6}$ cm^2 s^{-1} for labile complexes. On the other hand humic matter is heterogeneous in terms of groups and their vicinities and has higher molecular weight (depending of the type of aggregation), since 2×10^{-8} cm^2 s^{-1} < D_{ML} < 5×10^{-7} cm^2 s^{-1}, so much smaller values than D_M.

2) Labile complexes of Pb(II) with exudates are less stable, with $\log K_{lab} \sim 3$, (contaminated and control samples in exponential and stationary phases) than with HM with $5 < \log \overline{K} < 7$ for $-4.0 < \log \theta < -2.0$ (conditional stability constants at pH = 5.0).

3) Although lead complexes with humic matter are generally labile (only eventually inert for $\theta \log < -4.0$), this cation forms well characterized inert complexes with exudates released by unicellular algae Selenastrum capricornutum Printz with $\log K' \sim 8.0$ (K' is the conditional stability constant at pH = 5.0) for all the experimental conditions: control and contaminated medium, in exponential and stationary phases (Table 2).

4) The exudates released by the above alga have inert sites in a much smaller concentration than labile sites.

5) The concentration of labile ligands released by this unicellular alga is independent of the presence or absence of Pb(II) and of the growing phase, but the concentration of inert sites is higher in the contaminated sample probably due to a defense mechanism. However inert sites for control and contaminated samples are of the same type, since stability constants are of the same order of magnitude.

According to kinetic and thermodynamic parameters and the time scale of DPASV the labile and inert behaviour of the complexes, has been checked attending to the fact that the sites will be labile if diffusion

flux << reaction flux and inert in the inverse situation. So according to reference [43]:

$$\frac{K_d^{1/2} \varepsilon^{-1/2} (\varepsilon^{-1} + K')}{K'(1+K')^{1/2}} \; t^{1/2} = t^{1/2} \gg 1 \text{ for labile complexes}$$

with $\varepsilon = D_{ML}/D_M$

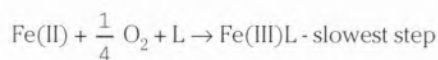$$K = \frac{[ML]}{[M][L]} = \frac{k_a}{k_d}$$

$$K' = k'_a \, k_d = \frac{[ML]}{[M]}$$

where k_a and k_d are the rate constants of the direct and inverse complexation reactions. The value $k_a = 7.5 \times 10^9$ M^{-1} s^{-1} was used considering that the slowest step in complex formation is the dehydration of Pb(II).

7. Redox reactions

Our current understanding of the reductive and oxidative transformation of organics in aquatic ecosystems is very limited. Although the functional groups that are susceptible to redox reactions in environmental systems have been identified, we often do not yet have the ability to predict accurate reactions [53]. This is due primarily to the complexity of environmental systems, which makes it very difficult to identify the electron donors and acceptors in aquatic ecosystems. For example, transition metals (particularly iron(II) or copper(I) complexes) sulphides, humic matter and polyphenols have been suggested as potential redutants. This is a topic of great interest, because reductive transformations can result in the formation of reactive products that may be more detrimental to aquatic ecosystems than the parent compound. Furthermore organics may undergo facile reductions in anoxic systems.

So organic matter in the environment can be involved in a complex network of acid-base, complexation, precipitation, adsorption and redox reductions, being the transition metal couples Fe(III)/Fe(II), Mn(IV)/ Mn(II) and also Cu(II)/Cu(I) of the major importance. Namely Fe(III)/Fe(II) system is involved in catalytic oxidation of hydroxocarboxylic acids, such as polyphenolic, gallic and tanic acids (L) according to the reactions [44]:

$$\text{Fe(II)} + \frac{1}{4} O_2 + L \rightarrow \text{Fe(III)L - slowest step}$$

$$\text{Fe(III)L} \rightarrow \text{Fe(II)} + L(ox) \text{ - step accelerated by sunlight}$$

which explains the presence of Fe(II) during the day in oxic waters in the presence of humic type organics. In this context it is important to distinguish between Fe(II) and Fe(III) using fast analytical techniques, such as flow injection (FIA) as can be seen for example in reference [54] and in those summarized in this work.

7.1 Cu(II)/Cu(I) system

In this context we are going to present in more detail a study about the types of amines that can stabilize copper (I), so increasing the redox potential of the couple Cu(II)/Cu(I) and favouring the oxidation of other species, as for example organic matter, being involved in the complex network of reactions in the environment [12,45].

In this study voltammetric methods such as differential pulse polarography (DPP), platinum rotative disc electrode (RDE) and ASV have been used to reduce electrochemically copper(II) in the presence of several monoamines such as ethanolamine, 5-amino penthanol, ethylamine, diethylamine and triethylamine, as well as purine bases that constitutes the building blocks of DNA and RNA: adenine, hydroxantine and xantine.

The reduction of Cu(II) on the mercury electrode can occur in two ways [23]:

1. Direct reduction Cu(II) + 2e = Cu(0)
2. Reduction in two steps: Cu(II) + e = Cu(I)
   Cu(I) + e = Cu(0)

The ability of the ionic medium to stabilize Cu(I) by complex formation determines which of these pathways is to be preferred in a particular case.

However in complexation studies of copper(II) with amines by voltammetric methods three main problems must be taken into account: the adsorption on the electrode (particularly mercury electrode) of the amines and/or metal induced by them, the strong basicity of amines which may lead to the formation of hydroxy complexes (and possibly to the precipitation of copper(II) hydrolyzed products) and finally the oxidation of mercury favoured by the increase of pH (e.g. at pH ~10 it occurs at $E \approx 0V$ relatively to saturated calomel electrode) that can hinder global or partial Cu(II) reduction.

In order to avoid adsorption as much as possible, a large excess of amines comparatively to the metal ion should be added to the medium and techniques such as DPP and ASV with low detection limits have to be used.

7.1.1. Adsorption of amines

Before complexometric studies can be well interpreted it is important first of all to study adsorption of the ligands using a.c. voltammetry. From this type of measurements it has been noticed for purines that as long as the concentration of these ligands remains low ($< 10^{-4}$ M) adsorption at both extremes of the capacitive

curves is less important, especially at the specific potentials where the curves of capacitive current versus potential for different concentrations cross, both each other and the curve for the supporting electrolyte; *i.e.* for potentials close to -0.1 and -0.8 V. So ASV has been used with a deposition potential E_d = -0.8 V.

For ethanolamine, 5-aminopenthanol, ethyldiamine, diethylamine and triethylamine there is no adsorption as long as the pH and the concentration of amine remain low, the exact values for these variables depending on their nature, but corresponding to $[L]_t \sim 10^{-2}$ M-10^{-3} M and pH ~9. For each amine adsorption becomes more important with increasing pH and/or its concentration, and among the amines it increases with the number of substituent methyl groups. At the potential of zero charge (E_{pzc}) if we have an -OH substituent and the same hydrocarbon chain (ethenolamine versus ethylamine) adsorption is decreased and if the hydrocarbon chain is longer adsorption becomes more important (aminopenthanol versus ethanolamine and ethylamine).

The behaviour described indicates that the ligands are adsorbed as neutral species, hence are preferentially adsorbed in the range of potential in which the charge on the electrode is small [46]. As the potential becomes more positive or negative, peaks of adsorption - desadsorption are observed and outside this range there is no adsorption.

Finally it is important to point out that adsorption studies on a mercury electrode with different charges is important in environmental terms, because can simulate adsorption in different types of environmental particles, a mechanism of great importance in terms of autodepuration of ecosystems.

7.1.2 Copper Complexation with amines

Complexation studies can be done using voltammetric techniques, after choosing the best experimental conditions to avoid adsorption and being aware that adsorption-desosption peaks can be detected and cannot be confused with faradaic peaks in DPP or DPASV measurements.

For purine bases, in all cases stabilization of Cu(I) occurred in ASV experiments performed in acetate buffer and therefore electrooxidation of amalgamated copper(0) must proceed in two separate steps [10]. In most situations Hg oxidation overlaps the peak due to the reaction Cu(I) = Cu(II) + e. Only at lower pH values and for the lowest ligand concentration used, two peaks were detected [45]. This behaviour has already been observed for copper in the presence of adenine [47].

Evidence for the occurrence of a two-step mechanism when only one oxidation peak is observed is given by the variation of i_p versus the scan rate of the stripping step in the presence and absence of ligand, according to Randles Sevcik equation [48].
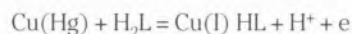
In fact not only does the peak current increases linearly with $\sqrt{v}$ but the peak potential Ep also remains

constant over the entire range of v. Additionally E_p-$E_{p/2}$ ($E_{p/2}$ being the half peak potential) is close to 56 mV within the experimental errors. So the redox process is reversible with a change of one electron (n=1), diffusion being the rate determining step. The good linear relationship for i_p versus $\sqrt{v}$ (r > 0.99) in the presence of the purines precludes a significant adsorption effect.
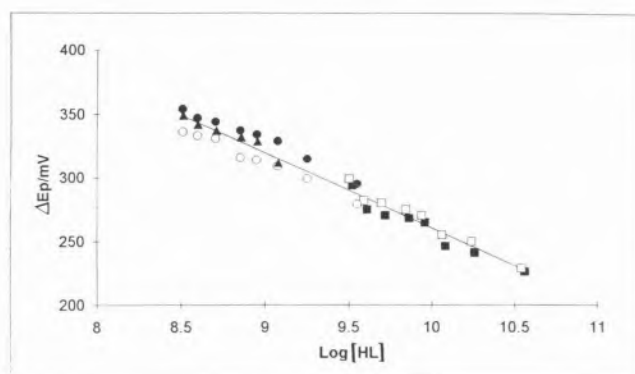
In order to determine the formation constants of copper(I) complexes with purines $\Delta E_p = E_p^c$-E_p^s has to be determined. However E_p^s value due to the redox reaction Cu(I) + e = Cu(0) in the absence of ligand is not accessible experimentally, being necessary to compute from the standard potentials E^o (Cu(I)/Cu(0)) and E^o(Cu(II)/Cu(0)), the experimental Ep value for the reaction Cu(II) + 2e = Cu(0) in the same supporting electrolyte and using an estimation of the activity coefficients according to Davies equation [10].

Adsorption of purines is minimized, since there is no adsorption at the deposition potential in ASV, and fast scan rates as well as an acidic medium (pH ~3.0-5.5) are being used.

Good linear correlations of ΔE_p versus pH (slopes of 591 mV) and for ΔE_p versus log [HL] (slopes of 60±2 mV) were obtained for xanthine and hypoxanthine (see Fig.7 as an example). Since the dominant species in the bulk solution is H_2L the mechanism for the oxidation of amalgamated copper Cu(Hg), in solutions containing hypoxanthine or xanthine and in the pH ranges 3.0-5.3 can be expressed by:

$$Cu(Hg) + H_2L = Cu(I) \ HL + H^+ + e$$

Accordingly formation constants determined according to Lingane's method [23]:

Figure 7 – Copper + hypoxanthine: variation of peak potential, (▲)Ep with log (HL) for [M]t =1.09×10-7 M at various pH values (■) 3.25; (□) 3.27; (●) 4.24; (○) 4.24; (▲) 5.23 0.10 M KNO₃, t=20°C.

$$E_p = - \frac{RT}{F} \times 2.30 \ (\log K_{Cu(I)HL} + \log[HL^-])$$

from what $K_{Cu(I)HL}$, the global stoichiometric formation constant, (defined as $[Cu(I)HL]/[Cu(I)][HL]$) can be determined.

For copper(I) adenine complexes it seems that for pH 4.5-5.5 a mixture of two complexes exist $Cu(I)HL^+$ and $Cu(I)L$. In the stripping step the following equilibria may occur, since the dominant species in the bulk of solution is HL:

$$Cu(Hg) + HL = Cu(I) HL^+ + e$$

$$Cu(Hg) + HL = Cu(I)L + H^+ + e$$
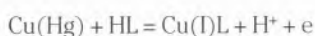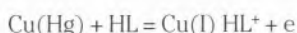
Calculation of the stoichiometric formation constants $K_{Cu(I)HL}$ and $K_{Cu(I)L}$ can be achieved using an extension of DeFord Hume's original formulation [49].

$$Fo = 1 + K_{Cu(I)L} \ [L] + K_{Cu(I)HL} \ [HL]$$

No literature values are available for comparison of copper(I) complexes with adenine, hypoxanthine and xanthine, probably due to the difficulty of preparation of Cu(I) complexes, which is overcomed here by the electrochemical synthesis of these complexes at the electrode surface.

Since a good linear correlation is obtained between pk^H values corresponding to the dissociation of the imidazole N-H group and the corresponding stabilities of the 1:1 complexes, i.e. Cu(I)HL for xanthine and hypoxanthine and Cu(I)L for adenine, the coordination to copper(I) in these complexes occurs to the nitrogen atoms N(9) of the imidazole ring and probably also to the N(3) atom of pyrimidine ring.

The complex Cu(I)HL formed with adenine has a smaller log K_{MHL} in comparison with log K_{ML}, at least partly due to the repulsion of H^+ in imidazole ring.

For copper(I) complexes with monoamines referred before and for the experimental conditions used [12] only one reduction peak has been obtained in DPP once more, whose potential moves cathodically with increasing ligand concentration. The peak obtained can be due to Cu(II) → Cu(0) or to Cu(I) → Cu(0) reduction, the oxidation of mercury overlapping the reduction Cu(II) → Cu(I) in the last case.

In order to check the mechanism, voltammetry with a platinum rotating disk electrode has been used, since a more anodic potential range can be used, being obtained from ethylamine, diethylamine and triethylamine systems two copper waves, one corresponding to the reduction Cu(II) → Cu(I) and the other to the reduction Cu(I) → Cu(0). With the increase of ligand concentration the first wave shifts anodically and the second one cathodically, as should happen for the system Cu(II) → Cu(I) → Cu(0) if the complexes with Cu(I) are more stable than with Cu(II).

In the case of 5-aminopenthanol and ethanolamine only a reduction wave corresponding to the change of two electrons has been detected, that moves cathodicaly with increasing ligand concentration.

Using E_p values obtained by DPP and considering the shift of peak potentials with increasing ligand concentration according to Lingane's method [23] applied to this pulse technique because $Ep = E_{1/2} - \frac{\Delta E}{2}$ ($E_{1/2}$ is the half wave potential in d.c polarograph and ΔE the pulse amplitude [50]) the type of complexes and the respective formation constants have been calculated (table 3), assuming the reaction is reversible according to half-width of the peak. So it has been concluded that ethyl, diethyl and triethylamine stabilize copper(I), but not ethanolamine and 5-aminopenthanol, due to the higher dipole moment of the molecules. Copper(I) forms ML_2 species with ethylamine and ML complexes with diethyl and triethylamine, probably due to stecheometric reasons related with the size of the ligand molecule.

Table 3 – Formation constants of Cu(I) - amine complexes obtained by voltammetric methods

Ligand	Complex	log K
Hypoxanthine	CuHL	14.8
Xanthine	CuHL	13.2
Adenine	CuHL+	11.6
Adenine	CuL	16 7
Ethylamine	CuL2	10.5
Diethylamine	CuL	6.6
Triethylamine	CuL	~7

So the presence of monoamines without significant polar groups or amines with special configuration may stabilize copper(I) in productive natural waters, increasing the redox potential of Cu(II)/Cu(I) couple and so influencing other redox reactions, namely oxidizing different types of dissolved organics groups.

8. Final conclusions

This work exemplifies how voltammetric methods can be used to study chemical processes in natural waters, namely complexation (in the bulk and at interfaces) and redox reactions, trying to understand the role of different types of organics (humic matter, organics released by algae and amines) in ecological mechanisms. In this context voltammetric methods are useful because they can differentiate between labile and inert species within the time-scale of the techniques and can produce electrochemically less stable oxidation states of an element, allowing the study of possible chemical reactions in the environment such as with Cu(I).

Competition reactions of major Ca(II), Al(III) and minor cations (Pb(II), Cd(II), Zn(II)) for humic matter

(generally a very significant part of organics in natural waters) have also been studied in a thermodynamic point of view, giving an insight within the complex nature of reactions that can happen in environmental conditions.

References

1. R.B. Gagosian and C. Lee in *Marine Organic Chemistry*, E.K. Duursma and R. Dawson (eds.), Elsevier, Amsterdam 1981 p.91.

2. R.F. Cleven, H.P. Van Leeuwen, *Int. J. Environ. Anal. Chem.* **27** (1986) 11.

3. J. Buffle, in H. Sigel (ed), Natural Organic Matter and Metal-Organic Interactions in Aquatic Systems (Metal Ions in Biological Systems vol. 18) Marcell Dekker New York 1984.

4. A. Bekveridge and W.F. Pickering, Water, Air, *Soil Pollut.,* **14** (1980) 171.

5. H. Xue, M.L. Simões Gonçalves, M. Reutlinger, L. Sigg, W. Stumm, *Env. Science Technology* **25** (1991) 1716.

6. J.W. Moffet, R.G. Zika Geochim., *Cosmochim. Acta* **52** (1988) 1849.

7. D. Jacob, E. Gottlieb, M. Prather, J. Geophys Res **94** (1988) 12975.

8. C. Weschler, M. Mandich, T. Gaedel, J. Geophys Res, **91** (1996) 5189.

9. T. Graedel, M. Mandich, C. Werchler, J. Geophys. Res **91** (1986) 5215.

10. M.L. Simões Gonçalves, L. Sigg, W. Stumm, Electroanalysis **3** (1991) 553.

11. M.L. Simões Gonçalves, M.M. Correia dos Santos, *J. Electroanal. Chem.* **143** (1983) 397.

12. M.M. Correia dos Santos, M.L. Simões Gonçalves, *Electroanalysis* **3** (1991) 131.

13. J.G. Herring, F.M. Morel, *Environ Sci. Technol.* **22** (1988) 1234.

14. M.A.T van den Hoop, H.P. van Leeuwen, J.P. Pinheiro, A.M. Mota, M.L. Simões Gonçalves, Colloids and Surfaces **95** (1995) 305.

15. G.H. Bolt, M.G. Brugenwert, A. Kamphorst, Adsorption of Cations in Soil Chemistry, Basic Elements, G.H. Bolt and M.G.M. Burggenwest (ed) Elsevier, (1978).

16. A.M. Mota, A. Rato, C. Brazia, M.L. Simões Gonçalves *Env. Sci. Technology,* **30** (1996) 1970.

17. P.J.B. Williams, Biological and Chemical Aspects of Dissolved Organic Material in Seawater, in Chemical Oceanography, J.P. Riley, G. Skirrow (eds) Academic Press N.Y. (1975).

18. S. Capelo, A.M. Mota, M.L. Simões Gonçalves, Anal. Chim. Acta (submitted).

19. A.M. Mota, M.M. Correia dos Santos in Interaction Between Trace Metals and Organisms (eds. A. Tessier, D. Turner), Wiley, N.Y. 1995 chap.5.

20. M.G. Bugarin, A.M. Mota, J.P. Pinheiro, M.L. Simões Gonçalves, *Anal. Chim. Acta* **294** (1994) 271.

21. A.M. Mota, J. Buffle, S.P. Kounaves, M.L. Simões Gonçalves, *Anal. Chim. Acta* **172** (1985) 13.

22. J. Buffle, Complexation Reactions in Aquatic Chemistry, Ellis Horwood Chichester 1988.

23. J. Heyrovsky, J. Kuta, Principles of Polarography, Chech Academy of Sciences Prague 1965.

24. D.S. Gamble, A.W. Underdown, C.H. Langford, *Anal. Chem.* **52** (1980) 1901.

25. W.H. van Riemsdijk, L.K. Koopal in J. Buffle and H.P. van Leeuwen (ed) Environmental Particles, vol. 1, Lewis, Chelsea, MI 1992, chap.12.

26. J.P. Pinheiro, Ph.D. Thesis, Instituto Superior Técnico (Lisboa) 1996.

27. M.F. Benedetti, C.J. Milne, D.G. Kinniburgh, W.H. van Riemsdijk, L.K. Koopal, *Env. Sci. Technol.* **29** (1991) 446.

28. J. Buffle, *J. Electroanal Chem.* **125** (1991) 273.

29. C.R. Martin, *H. Fresier, Anal. Chem.* **53** (1991) 904.

30. M.N. Szentirmay, *C.R. Martin, Anal. Chem* **56** (1984) 1818.

31. I. Rubinsten, A.J. Bard, *J.Am. Chem. Soc.* **103** (1981) 5007.

32. P. Ugo, B. Ballarin, S. Danicle, G.A. Mazzocchin, *J. Electroanal. Chem.* **291** (1990), 187.

33. P. Ugo, B. Ballarin, J. Denicle, G.A. Mazzocchin, *Anal. Chim. Acta* **244** (1991) 29.

34. B. Hoyer, T.M. Florence, *Anal. Chem.* **59** (1987) 2839.

35. J. Buffle, J.J. Vuilleumier, M.L. Tercier, N. Parthasarathy, *Sci. Total Environment* **60**(1987) 75.

36. M. Filella, J. Buffle, H.P. van Leeuwen, *Anal. Chim. Acta* **232** (1990) 209.

37. D. Kinniburgh, C. Milne, unpublished.

38. S. Capelo, A.M. Mota, M.L.S. Simões Gonçalves, Electroanalysis **7** (1995) 563.

39. J. Buffle, JJ. Vuilleumier, M.L. Tercier, N. Parthavarathy, *Sci. Total Environment* **60** (1987) 75.

40. A.E. Martell, R.E. Smith, Critical Stability Constants vol. 3. Plenum Press N.Y. 1977.

41. M. Jekel, Vom Waser **61** (1983) 349.

42. D.B. Pott, J.J. Alberts, A.W. Elzumen, *J. Chem. Geol* **48** (1985) 283.

43. H.G. de Jong, H. van Leeuwen, *J. Electroanal. Chem.* **234** (1987) 1.

44. W. Stumm, J.J. Morgan, Aquatic Chemistry 3rd ed. John Wiley & Sons (1996).

45. M.M. Correia dos Santos, C.M. Freire Lopes, M.L. Simões Gonçalves, *Bioelectrochem. Bioenerg.* **39** (1996) 55.

46. C.N. Reiley, W. Stumm in Progress & Polarography, P.Zuman and I.M. Koltoff (eds.) Wiley Interscience, N.Y. 1962 chap. 5.

47. R. Bilewicz, S. Glodowski, Z. Kublik, *J. Electroanal. Chem.* **274** (1989) 201.

48. A.J. Bard, R. Faulkner, Electrochemical Methods. Fundaments and Applications, Wiley, N.Y. (1980).

49. D. DeFord, D.H. Hume, *J. Am. Chem. Soc.* **73** (1951) 5321.

50. J. Osteryoung and K. Harabe, *Rev. Polarog. Japan* **22** (1976) 1.

51. E. Tipping, M.A. Hurley, *Geochim. Cosmochim Acta* **56** (1992) 3627.

52. M.F. Benedetti, W.H. van Riemsdijk, L.K. Koopal, D.G. Kinniburgh, D.C. Goody, C.J. Milne, *Geochim. Cosmochim. Acta* **60** (1996) 2503.

53. E.J. Weber, Abiotic Pathways of Organic Chemicals in Aquatic Ecosystems in Chemistry of Aquatic Systems: Local and Global Perspectives, G. Bidoglio and W. Stumm (eds.) Kluwer Academic, (1994).

54. A.L. Conceição, M.T. Pena, M.M. Correia dos Santos, M.L. Simões Gonçalves, M.D. Luque de Castro, *Anal. Chim. Acat* **343** (1997) 191.

55. M.M. Correia dos Santos, S. Capelo, M.L.S. Simões Gonçalves, *J. Electroanal. Chem.* **364** (1994) 171.